Engineered antigen-presenting hydrogels: model platforms for studies of T cell mechanotransduction

Dissertation

zur Erlangung des Grades

des Doktors der Naturwissenschaften

der Naturwissenschaftlich-Technischen Fakultät

der Universität des Saarlandes

von

Jingnan Zhang

Saarbrücken

2019

Tag des Kolloquiums: 14.05.2020

Dekan: Prof. Dr. Guido Kickelbick

Berichterstatter: Prof. Dr. Aránzazu del Campo Bécares

                         Prof. Dr. Markus Hoth

Vorsitz: Prof. Dr. Albrecht Ott

Akad. Mitarbeiter: Dr. Indra Navina Dahmke

Engineered antigen-presenting hydrogels: model platforms for studies of T cell mechanotransduction

Jingnan Zhang

geb. in Linyi, China

DISSERTATION

INM-Leibniz Institut für neue Materialien, Saarbrücken

I don't know what my morning jog would be like, if I didn't just once passed a bakery, filling my nose with the most amazing scent of freshly baked breads.

_____ for Brot und Seele, from Honestcooking

我首先热爱自然，其次是艺术。自然让我观察，艺术使我思考。

Acknowledgements

Without the kind help from many people, strong support by Deutsche Forschungsgemeinschaft funding (SFB1027 collective research center), and hosting by INM-Leibniz Institute for New Materials, it is not possible to finish my doctoral study here. If I was a tree, there is no doubt to say that I got a pleasant, enjoyable, and successful grown-up in a forest that was built up by all of them together in last 4 years. Therefore, I want to take this opportunity to convey my deepest and sincerest gratitude to them all here.

Above all, Arancha (Prof. Dr. Aránzazu del Campo), I would like to thank you for giving me the opportunity to pursue my academic career here. What you have done for me really give me the basic "soil" on which to live and grow up in the past 4 years. I still remember the first time we talked on the phone you mentioned we were moving to a new institute and planning to do something different, and maybe more challenging compared with previous research topic. As we can see now, you have successfully built up and developed this multi-disciplinary group (Dynamic Biomaterial, INM) with friendly, enthusiastic, collaborative and professional people from all over the world, which has made working here a pretty enjoyable experience. Personally, you have lead me to a new and exciting research area, guided me carefully whenever I need it, and offered many opportunities for me to take part in a variety of international conferences to enrich my knowledge, which have truly benefited me a lot. Of course, there are also so many things I've learnt from you about how balance life and work, which I think will be along with me through my lifetime. Thanks a lot Arancha.

Dr. Bin Li, you have always been my spiritual mentor, which is like how the sunshine nourish a young tree. It was really a good memory to work with you on the same

bench, eat with you on the same table, ride the same bike and even sleep on the same bed (of course not together). I would like to express my sincere gratitude to you for encouraging me whenever I got lost, helping me whenever I need to do AFM experiments, accompanying me whenever I felt sad. I hope and believe you have a successful and joyful scientific career in Munich and also China in the near future.

Dr. Renping Zhao, you are really a friendly, helpful, and patient collaborator. Whenever I took samples from INM to your place (CIPMM, Homburg), we could always sit face to face to discuss new plans for next experiments and data analysis with all the possible methods. I have learned so many scientific things from your side, which I hope to carry with me in my future career.

Dr. Aleeza Farrukh, thanks a lot for teaching me everything about hydrogel at the beginning of my doctoral study. Obviously, you are one of the most knowledgeable, diligent, helpful, and successful scientists in our group. Whenever we have any problems, whether it is about chemistry, material, or biology, you are always the first person to be thought of. I really wish you could have an enjoyable experience in USA and successful career in Pakistan later.

Dr. Terriac, Emmanuel, there is no exaggeration to say that you are probably the most helpful and enthusiastic scientist I know here. Thanks a lot for training me with microscope techniques, photolithography, and image analysis. France is a great place worth to go for thousands time, LOL!

Many thanks to Stefan for your kind help with German Abstract translation. Whenever I got problems in the labs, you are always the first person that can offer the best solution. I respect you so much because you are a so professional and responsible research scientist and lab manager.

I would like to say thank you so much Lulu Xue and Xinhong Xiong, it is you that make my life full of laughs and happiness, encouragement, inspiration. I hope both of

Acknowledgements

Acknowledgements

Abstract

T cells apply forces and eventually sense and then respond to the mechanical properties of their surroundings, including those of antigen presenting cells (APC) when they form the immunological synapse (IS). The identification of the mechanosensitive receptors and time scales at which they sense and actuate is experimentally difficult at the natural cell-cell interface. Inspired by the tools used in cell-matrix mechanobiology, this thesis presents synthetic, hydrogel-based models of APCs to study T cell mechanotransduction, focusing on the early T cell activation. Polyacrylamide (PAAm) hydrogels (1-50 kPa) were micropatterned with streptavidin and APC ligands (antibody against CD3 co-receptor (anti-CD3) and intercellular cell adhesion molecule-1 (ICAM-1)) at controlled ligand density and in geometries with defined dimensions. The anti-CD3 patterned hydrogels were used to study the interplay between hydrogel stiffness and CD3-mediated early T cell activation markers. In the last chapter, the regulatory role of ICAM-1 coupled to anti-CD3 and hydrogel stiffness in early T cell activation was studied on hydrogels with patterned anti-CD3 microdots surrounded by a background of ICAM-1. The results contribute to the understanding of the factors involved in T cell mechanotransduction, providing useful information for the future design of immunomodulatory materials.

Zusammenfassung

T-Zellen üben auf ihre Umgebung Kräfte aus und erfassen und reagieren auf die mechanischen Eigenschaften ihrer Umgebung, insbesondere auf Antigen-präsentierende Zellen (APC), wenn sie die immunologische Synapse (IS) bilden. Die Identifizierung der mechanosensitiven Rezeptoren und der Zeitskalen, in denen sie aktiviert werden, ist an der natürlichen Zell-Zell-Grenzfläche experimentell schwierig. Inspiriert von Werkzeugen aus der Zellmatrix-Mechanobiologie werden in dieser Arbeit synthetische hydrogelbasierte Modelle der IS entwickelt, um die T-Zell-Mechanotransduktion zu untersuchen, wobei der Schwerpunkt auf der frühen T-Zell-Aktivierung liegt. Dazu wurden Polyacrylamid (PAAm)-Hydrogele (1-50 kPa) hergestellt und mit Streptavidin- und APC-Liganden (Antikörper gegen CD3-Co-Rezeptor (Anti-CD3) und interzelluläres Zelladhäsionsmolekül-1 (ICAM-1)) mikrostrukturiert. Anhand von Hydrogelen mit Anti-CD3-Mustern wurde die Korrelation zwischen der CD3-vermittelten frühen T-Zell-Aktivierung und der Steifigkeit des Hydrogels untersucht. Anschließend wurde die zusätzliche regulatorische Rolle von ICAM-1 an Hydrogelen mit strukturierten Anti-CD3-Mikropunkten auf einem ICAM-1 Hintergrund untersucht. Die Ergebnisse tragen zum Verständnis der Faktoren bei, die an der T-Zell-Mechanotransduktion beteiligt sind, und liefern nützliche Informationen für das zukünftige Design immunmodulatorischer Materialien.

List of Abbreviations

3-APS	3-Aminopropyl-triethoxysilane
AA	Acrylic acid
AAm	Acrylamide
AFM	Atomic force microscopy
APCs	Antigen-presenting cells
APS	Ammonium persulfate
BCR	B cell receptor
bis-AAm	N,N'-methylene-bis-acrylamide
BSA	Bovine serum albumin
CD	Cluster of differentiation
CRAC	Ca^{2+} release-activated Ca^{2+} channels
cSMAC	Central SMAC
CTLA4	Cytotoxic T-lymphocyte-associated protein 4
CTLs	Cytotoxic T lymphocytes
DAG	Diacylglycerol
DAPI	4',6-Diamidino-2-phenylindole, dihydrochloride
DCs	Dendritic cells
DMEM	Dulbecco's Modified Eagle Medium
DMSO	Dimethylsulfoxide
dSMAC	Distal SMAC
ECM	Extracellular matrix
EDC	1-ethyl-3-(3-dimethylaminopropyl)carbodiimide
ER	Endoplasmic reticulum
F-actin	Filamentous actin
fBFP	Fluorescence bio-membrane force probe

List of Abbreviations

FBS	Fetal bovine serum
FcR	Fragment, crystallizable region receptor
FcR	Fragment, crystallizable region receptor
HA	Hyaluronic acid
HEPES	4-(2-hydroxyethyl)-1-piperazineethanesulfonic acid)
ICAM-1	Intercellular cell adhesion molecule-1
ICOS	Inducible T-cell costimulator
IFN-γ	Interferon-γ
IL-2	Interleukin-2
IP3	Inositol trisphosphate
IP3R	Inositol trisphosphate receptors
IS	Immunological synapse
ITAM	Immunoreceptor tyrosine-based activation motifs
LAT	Linker of activated T cells
Lck	Lymphocyte-specific protein tyrosine kinase
LFA-1	Lymphocyte function–associated antigen-1
MeOH	Methanol
MES	2-(N-morpholino)ethanesulfonic acid
MHC	Major histocompatibility complex
Milli-Q	Deionized, filtered ultrapure water
MMPs	Matrix metalloproteinases
MTOC	Microtubule-organizing center
MW	Molecular weight
NaCl	Sodium chloride
NaHCO$_3$	Sodium bicarbonate
NaOH	Sodium hydroxide

List of Abbreviations

NFAT	Nuclear factor of activated T cells
NF-kB	Nuclear factor kappa-light-chain-enhancer of activated B cells
NH_2	Amino group
NHS	N-hydroxysuccinimide
NK	Natural killer
NL	Nano-sphere lithography
OH	Hydroxyl
OVA	Ovalbumin
PAAm	Polyacrylamide
PAAm-co-AA	Polyacrylamide-co-polyacrylic acid
PAC	PhotoActiv Component
PBS	Phosphate buffered saline
PD-1	Programmed death-1
PDMS	Polydimethylsiloxane
PKC	Protein kinase C
PLCγ1	Phosphoinositide-specific phospholipase Cγ1
PMA	Phorbolmyristate acetate
pMHC	Peptide antigen presented on MHC complexes
pPEGMA	Poly(sodium 4-styrenesulfonate-co-poly(ethylene glycol) methacrylate)
PRRs	Pattern recognition receptors
pSMAC	Peripheral SMAC
PTK	Protein tyrosine kinase
pY	Phosphorylated ZAP70
SH2	Src homology 2
SLP-76	SH2 domain-containing leukocyte protein of 76 kDa

List of Abbreviations

x

SMAC	Supra-molecular activation cluster
SOCE	Store-operated Ca^{2+} entry
Syk	Spleen tyrosine kinase
TCGF	T cell growth factor
TCR	T cell receptor
TEMED	Tetramethylethylenediamine
Th cell	Helper T cell
THF	Tetrahydrofuran
Treg	T regulatory
ZAP-70	Zeta-chain-associated protein kinase 70

Whenever it is not stated here, all other abbreviations have their usual default meaning.

Contents

Contents

Contents

Motivation and scope of this thesis

T cell activation takes a leading role in adaptive immune response. Understanding the molecular basis of this process is necessary to develop effective therapeutic approaches for immune-related diseases. Currently, T cells are known to respond to both biochemical and mechanical information on the surface of antigen presenting cells (APCs), and experimental evidence has demonstrated that many cell surface [1-4] and intracellular molecules [5] are mechanosensitive. However, understanding of the mechanism by which mechanical cues regulate T cell activation remains to be explored.

Hydrogels modified with APC ligands have been increasingly used as mimics of the APC surface to explore the interplay between biochemical and biomechanical factors in T cell response when it contacts the APC to form the immunological synapse (IS). Most of these studies have focused on how APC ligands or APC stiffness affects cell spreading, migration, differentiation, proliferation and other late T cell activation steps, such as IL-2 and IFN-γ secretion. How the early T cell signaling events are affected by the mechanical engagement of individual receptor(s) is less studied.[6] Furthermore, most reported studies used model platforms with poor control over cell spreading area, which makes it difficult to decouple the effect of mechanics on T cell response from that induced by cell spreading area, which in turn can also be influenced by the mechanical information. In addition, most reported studies have not considered the highly regulated spatial organization of ligands at the T cell-APC interface during IS formation and T cell activation as additional factor that influences T cell responses.[7] Therefore, advanced APC model surfaces considering those issues are needed. In this context, this PhD thesis presents a hydrogel-based platform to study how the early T cell signaling events (i.e. Zap70 phosphorylation

and T cell receptor (TCR) accumulation) are regulated by the stiffness of the APC mimic at controlled density and spatial arrangement of the APC ligands at the artificial IS. For this purpose, a methodology to obtain patterned APC ligands (anti-CD3 and/or intercellular cell adhesion molecule-1 (ICAM-1)) on soft polyacrylamide (PAAm) hydrogels (Young's Modulus of 1-50 kPa) at defined geometries and densities was established using an automated microcontact printing system. This strategy allowed the preparation of micropatterned protein arrays with independent control of substrate stiffness, APC ligands spatial arrangement and ligand type and density. These model platforms were used to decipher the causal relationships between substrate stiffness and T cell early signaling. In addition, more complex IS designs containing multiple ligands in a patterned arrangement can also be obtained by a multistep microcontact printing. These engineered platforms were used to study how the engagement of LFA-1/ ICAM-1 receptor complex at the IS influences early T cell signaling in Jurkat T-cell within the different ranges of hydrogel stiffness.

This thesis work is presented as follows:

1) **Chapter 1** elaborates on the general background of this PhD thesis, in which it separately introduces the mammalian immune system, T cell activation, and also biochemical and biophysical models that have been used to explore T cell activation so far.

2) **Chapter 2** describes the methodology to obtain homogeneous protein micropatterns with defined protein density on hydrogels of different stiffness by automated microcontact printing system. Specifically, the preparation of PAAm hydrogels and PDMS stamps for automated microcontact printing is elaborated first, followed by the description of the characterization methods to evaluate and compare the surface density of protein on the hydrogels of different stiffness. Finally, the bioactivity of the micropatterned protein (anti-CD3) on the hydrogels

was quantified. The results in this chapter demonstrate that homogeneous, functional and reproducible protein patterns on soft hydrogels can be obtained. The methods were used for T cell mechanotransduction studies in the next chapters.

3)   In **Chapter 3,** I evaluated the suitability of anti-CD3 patterned hydrogels to act as APC mimics and interact with T cells, and to form IS-like interfaces for fundamental studies of CD3-mediated T cell signaling. The response of T cells to anti-CD3 antibody mechanical engagement within a defined IS contact area and with controlled protein density was assessed in terms of ZAP70 phosphorylation as an early T cell activation marker. This system unequivocally demonstrates that T cell activation level depends on the stiffness of the APC mimic.

4)   In **Chapter 4**, the APC model was further developed to include a second ligand relevant in the IS formation and T cell activation. Anti-CD3/ICAM-1 patterned hydrogels, recapitulating key features of a physiological IS structure, were developed to unravel the role of ICAM-1 in early T cell signaling (ZAP70 phosphorylation and TCR clustering) on substrates with different stiffness. With these advanced APC models the time scales for receptor organization and signal activation, and their dependence on hydrogel stiffness were studied. Thus the regulatory role of the ICAM-1 ligand coupled to mechanical cues was described in an APC model simply mimicking the physiological structure of IS.

5)   Finally, a conclusion about T cell mechanotransduction based on our engineered platforms and outlook section describing envisioned applications and further development of material-based models to interact with T cells are expounded in **Chapter 5**.

All the engineered biomaterial platforms as APC mimics for studies of T cell

mechanotransduction in this thesis are summarized in Scheme 1B.
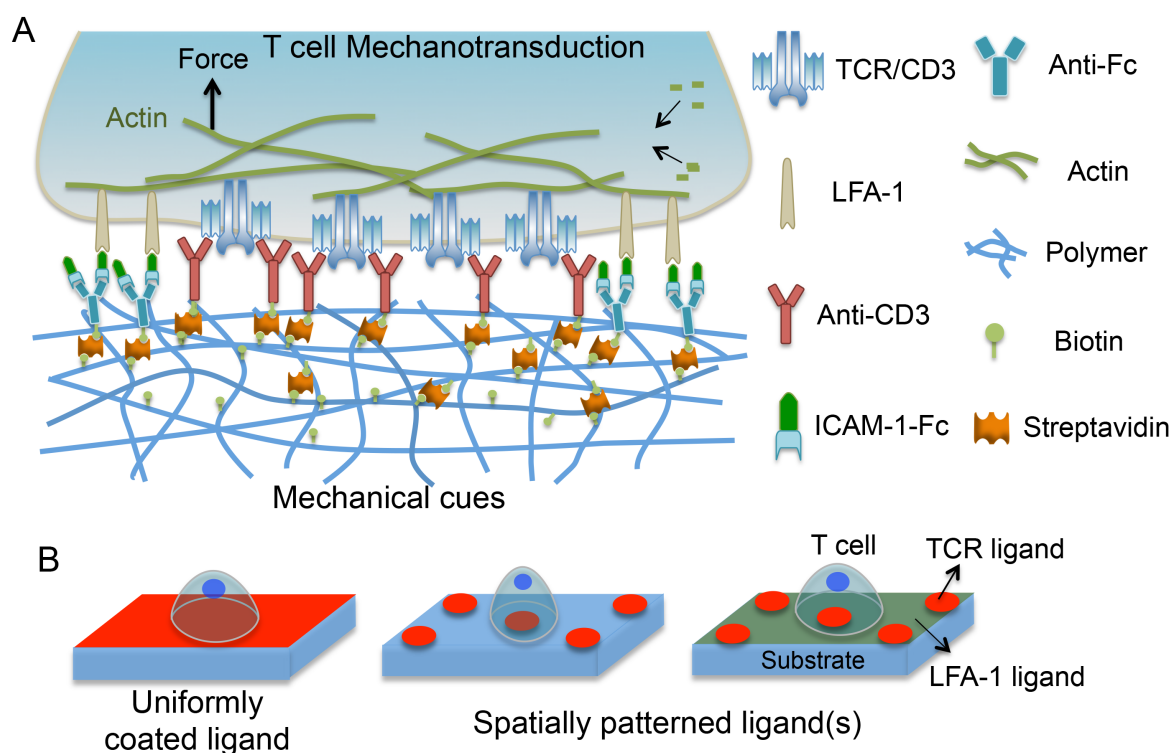
Scheme 1. Scheme representing the engineered biomaterial platform to mimic the surface of an APC for studies of T cell mechanotransduction. (A) Cross-section of an artificial model of IS including the TCR-CD3/anti-CD3 and the LFA1/ICAM-1 receptor complexes organized in a concentric manner. (B) Representation of the APC mimics developed in this thesis with uniformly coated or spatially patterned APC ligands.

Chapter 1

1 Introduction

1.1 Mammalian immune system

The immune system consists of a collection of biological structures and processes within an organism to defend against disease or other potential foreign invasions. The immune system consists of many parts including special proteins (antibodies), cells (white blood cells), tissues (bone marrow) and organs (skin, tonsils, spleen and thymus). This network attacks pathogens, such as bacteria, viruses or parasites, and is able to distinguish them from the organism's own healthy tissue through a series of steps, the immune response.[8, 9]

The immune response protects host from infection by layered defenses of increasing specificity. The immune responses can be fundamentally classified into 2 types: innate (natural) response, and acquired (adaptive) responses. The innate response renders an immediate, but non-specific response to pathogen attack and comprises all the immune defenses that lack immunologic memory. The acquired response occurs only when the surface receptors of antigen-specific B and T cells bind to their cognate antigens.[8] Innate and acquired responses cooperate together to protect its host. Disorders in these responses can lead to inflammatory diseases, autoimmune diseases (it means the body's own tissue is attacked by itself immune system as foreign matter), allergic disorders (the body's immune system overreacts   to defend against antigens) or even cancer.[10]

1.1.1 Innate immunity

The first line of defense of our body against pathogen attack includes physical, mechanical, and biological barriers that protect the body from foreign invasion. These consist of our skin, tight junctions between epithelial cells, tears, mucus, cilia, stomach acid, urine flow, beneficial bacteria and some white blood cells.[11] When one of these barriers is breached, the second line of the innate defense system performs its function through an immediate and non-specific immune response to prevent from an infection (innate immunity). Innate responses are featured by their steady mode of action, no matter how often the antigen is encountered. Upon activation of the innate immune system by antigens, specific chemical signals (bacterial peptides, cytokines released by white blood cells etc.) can guide a variety of immune cells, involving dendritic cells, macrophages, neutrophils, natural killer (NK) cells and dendritic cells (DCs) to the infected site (Figure 1).[12-14]

- Phagocytes, such as macrophages and neutrophils, use pattern recognition receptors (PRRs, like Toll like receptors, C-type lectin receptors etc.) to recognize invading antigens.[15, 16] Then they carry out phagocytosis to achieve target-killing effect, which is mediated by making pseudopodia (projections of cytoplasmic membrane) to form a vesicle (phagosome) around the pathogens.[17]

- NK cells are a type of cytotoxic lymphocytes that do not have a specific antigen receptor. Instead, they can induce antibody-dependent cellular cytotoxicity by using immunoglobulin receptors (fragment, crystallizable region receptor, FcR) to bind targets that coated with antibody. Secondly, they also use membrane receptors for the major histocompatibility complex (MHC) class I to recognize abnormal cells.[9] In case of failure to binding to MHC class I, NK cells can secrete perforins on the surface of their target cells, which will finally leads to lysis of the target.

- DCs constantly survey the surrounding environment to find out the pathogens. Upon contact with a presentable antigen, DCs are activated and then migrate to the lymph nodes. They interact with T cells and B cells severing as antigen-presenting cells (APCs) by presenting antigens on the cell surface. DCs also act as a critical link between innate and adaptive immunity.[18]
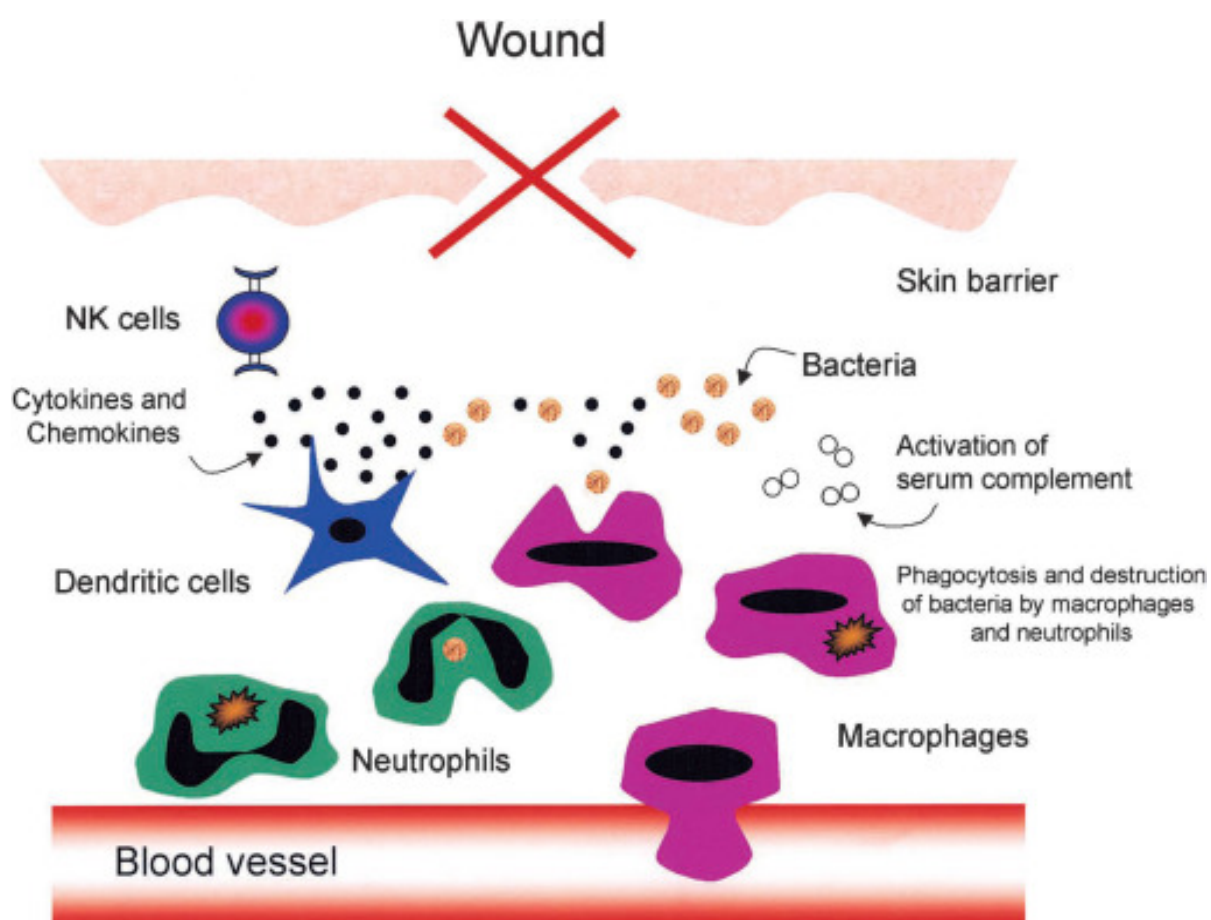
Figure 1. The innate immune system provides the initial defense against infection and injury. The primary components of innate immunity are: (1) physical and chemical barriers; (2) phagocytic cells (neutrophils and macro- phages), NK cells and DCs; (3) blood proteins, including members of the complement system and other mediators of inflammation; and (4) cytokines that regulate and co-ordinate many of the activities of the cells of innate immunity. Copyrights Elsevier.[14]

1.1.2 Adaptive immunity

Contrary to the innate immune system, the adaptive (acquired) immune system shows a high specificity to a particular pathogen. To carry out this specific immune response, two types of lymphocytes with different roles are involved: B cells and T cells (Figure 2).[14]

B cells develop from progenitor cells within the bone marrow. They constitutes the dominated cells that responsible for generating antibodies circulating in our blood plasma and lymph, which forms so-called humoral immunity.[19] B cell activation begins when the B cell binds to antigens through unique B cell receptors (BCRs). Then the antigen is engulfed, digested, and the antigen fragments are displayed on the cell surface through MHC molecule.[20] The antigen-MHC complex can be further recognized by helper T cell (Th cell) to induce secretion of cytokines and help B cells to multiply and mature to become effector cells, also named plasma cells. Plasma cells can make them become easier targets for clearance by macrophages, eosinophils, and NK cells, through secreting antibodies to bind to antigens.[21, 22] In addition, plasma cells could also be produced in a T cell independent manner. Only a small amount (10%) of plasma cells eventually turn into long-lived antigen-specific memory B cells, which could quickly and specifically recognize an antigen that has been previously encountered and initiate a corresponding immune response.[23]

T cells, which also originate from bone marrow, are other key players in the adaptive immune system. They induce an immune response by activating antigen-specific cytotoxic T-lymphocytes, phagocytes to secrete many kinds of cytokines in response to specific antigens, which is called cellular immunity.[24] To start a cellular immunity, naive T cells (mature T cells that have not been encountered by their specific antigen in an immune response) first need to meet APCs bearing their antigens. This process is known as T cell priming and is mediated by the recognition of antigenic peptides

loaded on MHC of APCs (macrophages, DCs, and B cells in some circumstances) by the T cell receptor (TCR).[9] Subsequently, T cells undergo proliferation and differentiation to become effector T cells. Cytotoxic T cells (CD8$^+$ T cell) are one of the activated effector T cell that kill infected target cell by apoptosis without using cytokines. Another type of effector T cell is CD4$^+$ Th cell, which can activate macrophages or stimulate B cells to produce antibodies to defend antigen.[9, 25] In the end, memory T cells are generated to induce swift and augmented responses during subsequent infections with the same pathogen.
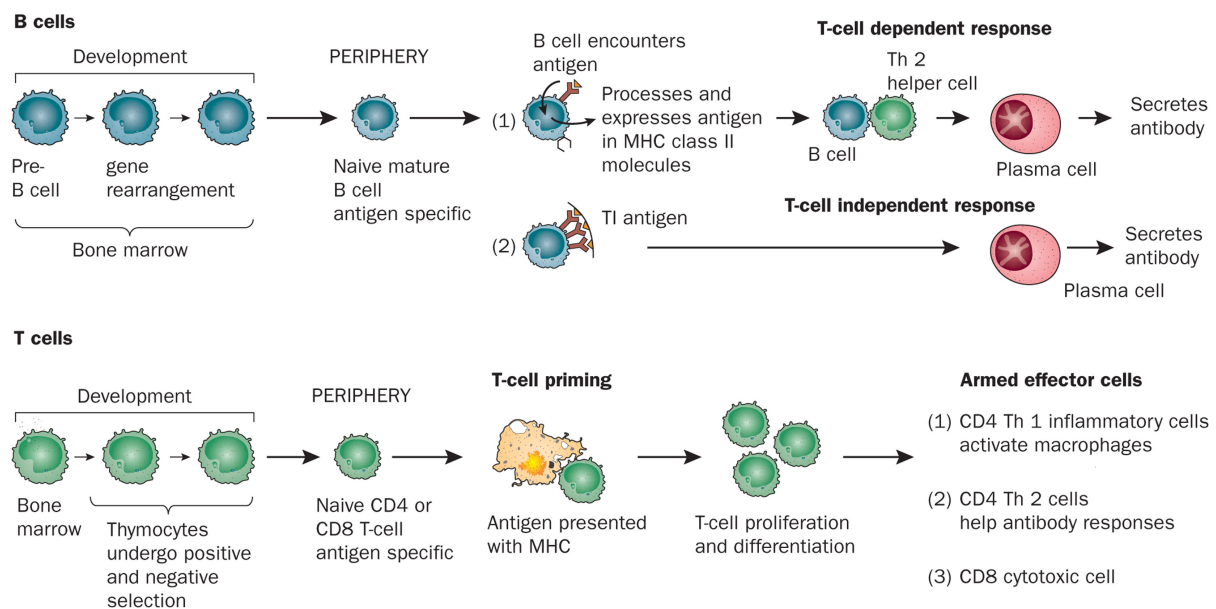
Figure 2. The role difference between B and T cells in adaptive immunity. Copyrights Elsevier.[9]

Compared with humoral immunity, during which B cells recognize antigens in their native condition, cellular immunity needs T cells to recognize their cognate antigens with the help of MHC molecules.[26] Therefore, T cell-mediated activation needs to be tightly regulated to ensure that only a response is elicited by damaging antigens

rather than the self-MHC and peptide since T cells can also interact with their own MHC and peptide. Otherwise, an immune response against the self-tissue results in an autoimmune disease.

1.2   T cell activation

T-cell activation plays a central role in the initiation and regulation of the adaptive immune response. T cells circulate throughout the body until they recognize an antigen presented by the MHC on the surface on an APC. Cell-cell contact by binding TCR to the MHC will trigger an initial activation of T cells. Co-stimulation molecules are normally required to induce a full T cell activation.[27, 28] For instance, helper T cells need to use CD28 to bind to B7.1 (CD80) or B7.2 (CD86) on the APC to initiate T cell proliferation.[29] In fact, there is a cascade of intracellular signaling events taking place during the whole period of T cell activation. Eventually, the resulting effector T cells either moves to the site of the infection or inflammation to deal with the pathogen or kill APC target directly.

1.2.1   T cell subsets

T cells are identified by a surface cluster of differentiation (CD) molecule named CD3 and distinguished from other lymphocytes by the presence of TCRs on the surface. All of T cells stem from hematopoietic stem cells in bone marrow and develop in thymus. The earliest thymocytes are double-negative ($CD4^-CD8^-$) cells and then they further turn into double-positive thymocytes ($CD4^+CD8^+$). In the end, they mature to single-positive ($CD4^+CD8^-$ or $CD4^-CD8^+$) thymocytes through single-positive selection. Therefore, T cell can be classified into three major subsets in human body. The majority of cells are $CD4^+$ and $CD8^+$ populations that express alpha beta (αβ) TCRs. The third T cell subset is $CD4^-CD8^-$, which predominantly consists of the γ/δ T

cell subset that expresses gamma delta (γδ) TCRs.[30-32] The CD4^{+} cells could be further subdivided into at least Th1, Th2, Th9, Th17 and T regulatory (Treg) groups, each with a different profile of cytokine production.[28] The CD8^{+} cytotoxic T cells can also be sorted into Tc1 and Tc2 subpopulations that function in killing target cells.

1.2.2   T cell-APC interaction

A large number of receptor-ligand pairs are involved in the T cells-APCs interactions. These receptors can be classified into three categories attending to their function: TCR, co-stimulatory receptors, and adhesion receptors.

-   TCR is the unique antigen binding receptor expressed on T cells, existing in either α/β or γ/δ forms. In this thesis, the focus is set on the αβ TCRs here because they are largely expressed on CD4^{+} and CD8^{+} cells. In fact, the αβ TCRs exist in a non-covalent complex containing non-polymorphic CD3εγ, CD3εδ and CD3ζζ dimers, know as TCR complex (Figure 3).[33, 34] The binding of TCR α and β chains to peptide antigen presented on MHC complexes (pMHC) of an APC initiates the antigen recognition. In the case of CD4^{+} T cell recognition, peptide antigen is presented by MHC class II whereas MHC class I is responsible for carrying peptides antigen for CD8^{+} T cell. Moreover, co-receptors such as CD4 and CD8 can recognize the invariant part of the MHC molecule to assist TCR-pMHC interaction. In addition, CD3 subunits incorporate immunoreceptor tyrosine-based activation motifs (ITAM) in their cytoplasmic tails, which are responsible for the related signal transduction in T cell activation.[35] It should be emphasized that agonistic antibodies binding to CD3 result in activation of the CD3 signal-transduction complex to transduce essential signals necessary for activation of the T cells.

-   In order to induce a full activation, co-stimulatory receptors are required to

engage in co-stimulation in addition to TCR-mediated antigen specific signal. The co-stimulation is short of specificity and is mediated by the interaction between co-stimulatory molecules expressed on the surfaces of the APC and the T cell. CD28, as one of the best-characterized co-stimulatory molecules on T cells membrane, co-stimulates T cells through the interaction with B7-1 (CD80) or B7-2 (CD86) expressed on APC (Figure 3).[27, 29] Another T-cell co-stimulator is the inducible T-cell co-stimulator (ICOS, CD278), which belongs to the second Ig superfamily co-stimulatory system, and binds to the ligand of ICOS (LICOS, CD275) that is prominently expressed on DCs and B cells. In addition, cytotoxic T-lymphocyte-associated protein 4 (CTLA4, also called CD152) can transduce inhibitory signals by ligation of CD80 or CD86. Since the co-stimulatory system is very complicated, a precisely controlled T cell co-stimulation is required during the interaction between T cell and APC.
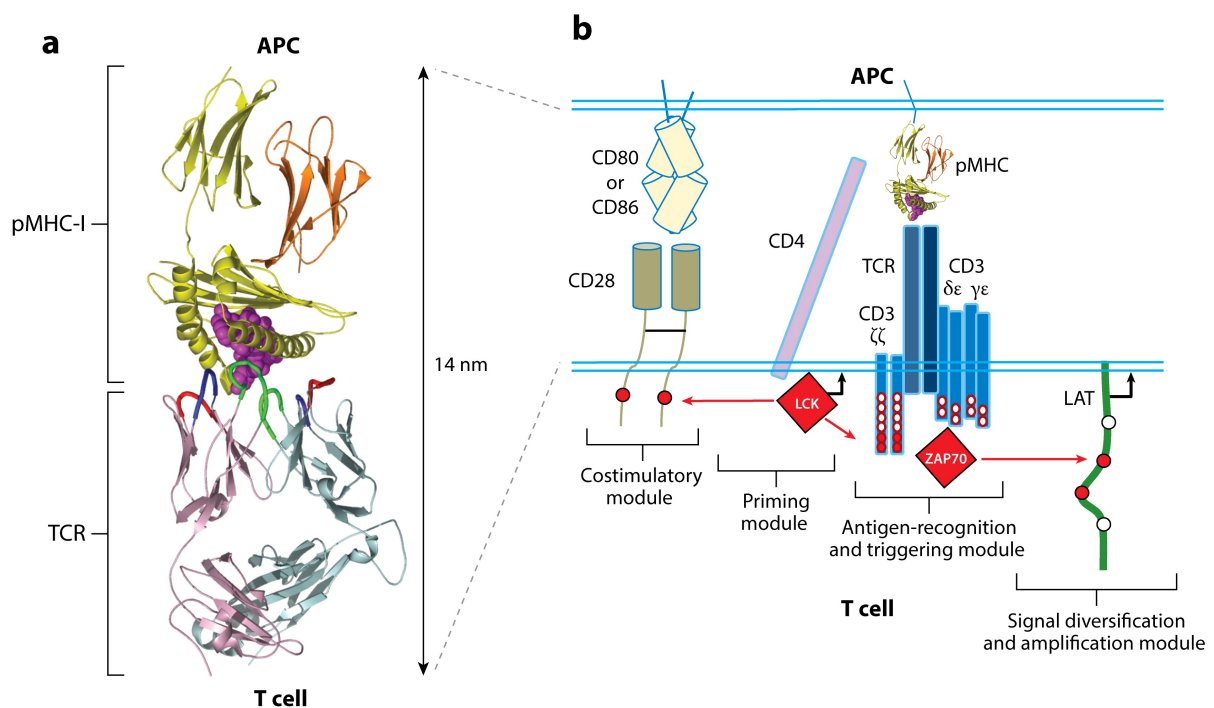
Figure 3. Structure of TCR and pMHC complex (a) and the related molecular interactions between a T cell and APC (b). Copyrights Annual Reviews.[33]

- Adhesion molecules also play critical roles during the interaction between T cell and APC. Lymphocyte function–associated antigen-1 (LFA-1, now known as CD11a/CD18) is a heterodimeric glycoprotein with non-covalently linked subunits (αLβ2) expressed on T cell surface. It belongs to the integrin family and can bind to its ligand, intercellular adhesion molecule-1 (ICAM-1 or now CD54) through αL subunit to increase the adhesion of T cells on APCs.[36, 37] In an inactive state, LFA-1 is bent and has a low affinity for ICAM binding. A conformational change into the fully extended conformation enables LFA-1 to shift from a low binding affinity to a high binding affinity.[38-40] In addition, there are also some other adhesion receptors, such as LFA-2 (CD2) and LFA-3 (CD58), engaged in T cell-APC interaction. LFA-1/ICAM-1 interactions can also provide co-stimulatory signals for T cell activation.

1.2.3　The immunological synapse (IS)

The IS, also taken as the supra-molecular activation cluster (SMAC), refers to the organized cluster of membrane proteins that assemblies at the contact interface between a T cell and an APC.[41] The structure of a mature IS consists of three concentric rings, each containing distinct segregated clusters of proteins. In the center of IS lies the central SMAC (cSMAC), comprising TCRs and associated signaling proteins such as CD4, CD8, CD2, and CD28.[42] Recent studies suggest that the cSMAC is further categorized into two components: the endo-cSMAC in which TCR and CD28 spatially associate for signaling, and the exo-cSMAC which consists of TCR-enriched extracellular vesicles and checkpoint programmed death-1

(PD-1).[43] Around the cSMAC, the peripheral SMAC (pSMAC) region concentrates adhesion molecules like the integrin LFA-1 and the cytoskeletal protein talin. Locating outside of the pSMAC, the distal SMAC (dSMAC) contains a dense ring of filamentous actin (F-actin) and transmembrane tyrosine phosphatase CD45 and CD43, and forms the outer boundary of the IS (Figure 4A, C).[42, 44] At the early stages of IS formation (immature IS), the LFA-1 is located in the center area of the IS and the TCR in a peripheral ring (Figure 4B).[45] This indicates that the T cell signaling events precede the formation of a mature IS, and proves that the molecules within IS reorganize dynamically with time.
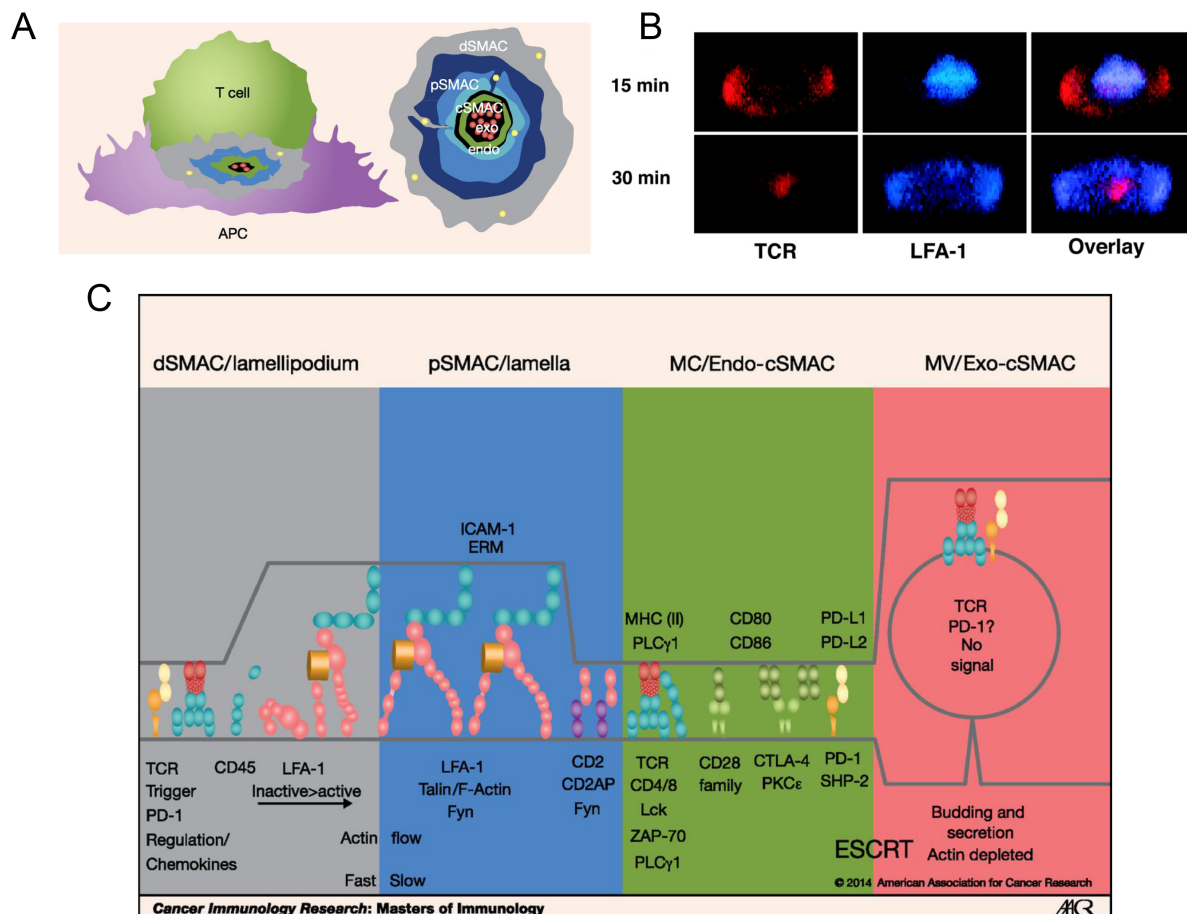
Figure 4. The structure of IS and the molecular interactions within it. (A) Model IS

with elevated (left) and front-on view (right) focusing on T cell-APC interface. (B) Z-stack reconstruction of the T cell-APC interface at 15 and 30 min after conjugate formation. At 15 min, the TCR (red) is localized in a peripheral ring, whereas LFA-1 (blue) is in the center (immature IS). At 30 min, the TCR is now in the center, surrounded by LFA-1 in an outer ring (mature IS). (C) Schematic diagrams of the IS at the junction between a T cell and an APC to show some of the key proteins involved IS formation. Reproduced with permission from American Association for Cancer Research and Science.[44, 45]

The process of IS formation starts by the recognition of pMHC on the APC by TCRs on the T cell during T cell activation, and the initiation of specific signaling pathways through the clustering of receptors at the T cell-APC interface. Actin helps as scaffolding protein for the clustering of the receptors at the membrane. It drives centripetal translocation of microclusters through actin retrograde flow, and spatially organizes them to different domains to form the special structure of IS. It should be noted that actin is always depleted from the central area in a mature IS.[46-48]

The IS has two categories of function including: 1) priming of responses to transmit information to T cell and 2) effector functions in which the secretion of cytokines (CD4$^+$ cell) or lytic granules (CD8$^+$ cell) is achieved. The IS also determines the interaction forces between T cells and APC. It has been demonstrated that these forces develop over time and reach a peak when synapse formation is maximal,[49] suggesting that mechanical cues might be used to regulate the level of T cell activation, which will be discussed in section **1.3** (Biochemical and biophysical models to explore T cell activation).

1.2.4　T cell activation steps and markers

T cell activation initiates with receptor clustering triggering intracellular signaling cascades that ultimately result in cell proliferation, differentiation or death, depending on the intensity of the signals associated to TCR and other receptors at the IS. The T cell activation and response processes involve a sequence of early and late activation steps in which a variety of signaling molecules participate.

1) Early activation

- a. Formation of the proximal signaling complexes

  The complexes formed by TCRs and co-stimulator receptors with the complementary receptors after the initiation of T cell activation are called membrane-proximal signaling complexes (Figure 5B). Specifically, upon recognition of the pMHC by the TCR on the T cell surface, supported by the co-receptors CD4 or CD8, the lymphocyte-specific protein tyrosine kinase (Lck) is activated. Lck further phosphorylates receptor-associated ITAMs in the cytoplasmic tails of CD3, which creates a docking site for a 70-kDa phosphoprotein: the spleen tyrosine kinase (Syk) family member ZAP-70 (TCR zeta (ζ) chain-associated cytoplasmic protein tyrosine kinase (PTK).[50, 51] The tandem Src homology 2 (SH2)-domains of ZAP-70 are engaged with the phosphorylated ITAMs (2 phosphorylation sites) of CD3-zeta to enable the transmembrane protein linker of activated T cells (LAT) to be phosphorylated. Phosphorylated LAT, in turn, provides a docking site for a variety of signaling proteins involving SH2 domain-containing leukocyte protein of 76 kDa (SLP-76), which is also phosphorylated by ZAP-70.[27, 33, 52, 53] The phosphorylated LAT and SLP-76 proteins facilitate many other downstream signaling cascades leading to T-cell activation, proliferation, and differentiation.

- b. Ca^{2+} influx.

  Ca^{2+} influx is an early signaling event that controls a variety of T cell functions.

Formation of the proximal signaling complex activates phosphoinositide-specific phospholipase Cγ1 (PLCγ1), which hydrolyzes the membrane lipid PI(4,5)P2 to produce the second messengers inositol trisphosphate (IP3) and diacylglycerol (DAG). The binding of IP3 to the Ca^{2+}-permeable ion channel receptors (IP3R) on the membrane of endoplasmic reticulum (ER) releases Ca^{2+} into the cytoplasm. Depletion of ER Ca^{2+} induces a continuous Ca^{2+} influx by activating the plasma membrane Ca^{2+} release-activated Ca^{2+} channels (CRAC), the store-operated Ca^{2+} entry (SOCE) (Figure 5C).[27, 54] The intracellular Ca^{2+} concentration largely increases within few seconds after initial APC-T cell contact. The influx of Ca^{2+} serves as a "stop signal" for the T cell by triggering signals to reduce T cell motility and facilitate the formation of an APC-T interface.[55] Ca^{2+} influx occurs in parallel with TCR clustering and regulates rapid cytoskeletal reorganization to support the formation of a stable IS.[56, 57]

- c. Cytoskeletal rearrangements

Although the actin cytoskeleton and TCR signaling complexes have different molecular structures, they intensively cooperate during T cell activation.[58, 59] When T cells are confronted with the adhesion-promoting surface of an APC, a temporary arm-like projection of a cell membrane, a pseudopod, is formed through actin polymerization, followed by myosin generating contractility. This process allows T cells to spread on the APC surface and maximize the cell-cell contact area.[60] As for the T cell signaling, actin functions as a scaffolding meshwork to recruit and stabilize signaling clusters, such as Zap70 and LAT and to regulate T cell signal transduction.[61] The actin retrograde flow helps the TCR microclusters to centripetally translocate to coalesce into cSMACs, and facilitates ligated integrins and associated proteins accumulate at the periphery of IS, finally realizing proteins spatial organization in IS (Figure

5A).[59, 62]

Cytoskeletal reorganization following TCR stimulation consists of actin polymerization and accumulation at the IS area, reorientation of the microtubule-organizing center (MTOC) towards the cell-cell contact interface,[63] and the formation of so-called distal-pole complex with an actin-rich structure on the opposing side of the cell.[48, 64] It has become increasingly clear that actin cytoskeleton generates substantial physical forces and signaling interactions during the regulation of T cell activation at different levels, such as adhesion to APC, cellular polarization, IS formation and maturation, early signaling through the TCR, and release of cytokines or cytolytic granules. Disruption of the cytoskeleton affects the T cell activation process.[61, 65, 66]
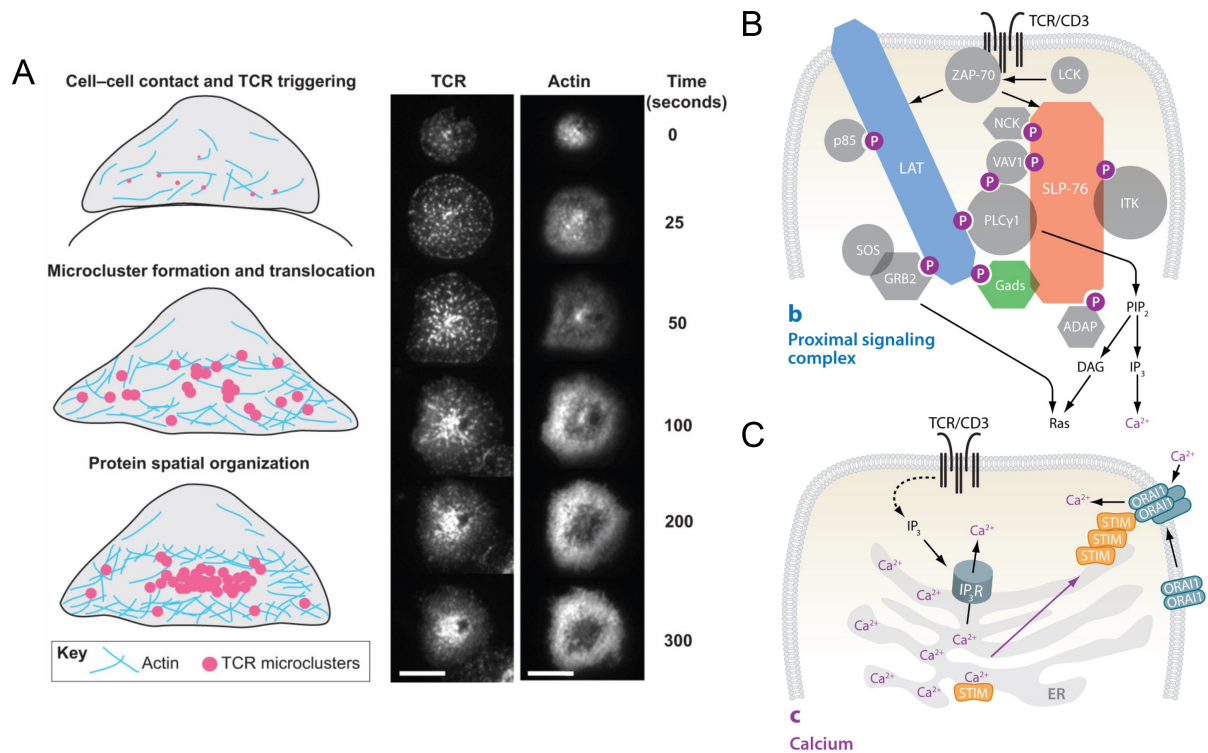
Figure 5. Signaling events during the early T cell activation. (A) A mechanistic

overview of actin reorganization unpon a T cell triggering and TCR microclusters formation and transportation by actin retrograde flow. (B, C) Current knowledge about TCR coupling to downstream pathways (upper, B) and the molecular mechanism of Ca^{2+} influx (lower, C). Reproduced with permission from The Company of Biologists and Annual Reviews.[27, 47]

- d. The early activation markers and gene expression

CD69, as a human transmembrane C-Type lectin protein encoded by the CD69 gene, is regarded as one of the earliest activation markers after the initiation of T cells activation. CD69 is detectable within 1-2 h ligation of the T cell receptor/CD3 complex and peaks around approximately 24 h, revealing how the strength of the activation level changes with time. Once expressed, CD69 performs as a co-stimulatory molecule during T cell activation and proliferation.[67]

CD44 is another activation marker. It is known as a surface adhesion receptor for hyaluronic acid, collagens and matrix metalloproteinases (MMPs), and also engages in cell-cell interactions and migration.[68] CD44 is continually expressed during the activation process, while CD69 expression reduces following the end of TCR stimulation.

Nuclear factor of activated T cells (NFAT) is an important transcription factor used to characterize gene expression changes after TCR stimulation as well as nuclear factor kappa-light-chain-enhancer of activated B cells (NF-kB). Both of them are expressed within a short time (around 0.5 h) following TCR stimulation and regulate the production of cytokines like interleukin-2 (IL-2) and interferon-γ (IFN-γ).[28, 69]

2) Late activation

- Cytokine expression

Cytokines are produced by many immune cells to act as soluble effector and regulatory molecules in a variety of cellular and immunological functions. They are prominently involved in inflammatory responses and defense against foreign invasions. IL-2, initially called T cell growth factor (TCGF), was the first type I cytokine that was produced by Th cells. IL-2 binds to IL-2 receptors, which are expressed by other lymphocytes, to facilitate T cell proliferation and differentiation. Its synthesis is transient, with peak activity occurring 4 hours after T cell activation.[28] The optimal activation of IL-2 expression needs TCR stimulation together with the co-stimulation from co-stimulatory receptors such as CD28, and regulates T cell proliferation, differentiation, and survival.[70] IFN-γ, with the capability to interfere with viral infection, is the only member of type II interferon predominantly produced by CD4^{+} Th1, CD8^{+} CTL, NK and natural killer T cells. It can effectively activate macrophages and thus plays an important role in protection against inflammation and autoimmune disease. It is secreted out about 3-6 h after initial contact of the T cell with the APC. Both IL-2 and IFN-γ are produced intracellularly and then secreted out of T cells.[69] Compared with IFN-γ, IL-2 production needs a prolonged stable contact.[71] The secretion of IL-2 is obviously detected 2-4 h after the formation of a stable IS.[72]

- b. T cell proliferation and differentiation.

T cell proliferation is dependent on repeated encounters with the APC surface. The duration of the stimulation is one of the most important factors that decide the fate of naive T cells. The stimulation includes a phase of sequential encounters between a T cell and APC, and this duration phase is inversely

correlated with the number of pMHC per APC, the APC density, as well as a stable contact phase.[73] Normally, 20 h of sustained contact is necessary for naive T cells to be fully activated and to start proliferating.[74] Each T cell that is effectively stimulated by the antigen expands and progressively differentiates into memory and effector T cells. After activation, CD4$^+$ T cells differentiate into distinct Th cell subtypes that dominate the immune response by secreting specific cytokines, whereas CD8$^+$ T cells become into effector cytotoxic T lymphocytes (CTLs) to kill target cells directly after activation.

- c. Late activation marker

CD25, known as the IL-2 receptor, is a protein product of IL2RA gene. It is normally taken as a late activation marker in T cell activation. CD25 expression is triggered at the beginning time of the brief sequential encounters and peaks between 24 and 48 h after TCR stimulation, finally gets rapidly lost after 72 h stimulation.[75, 76]

The antigen-1 (VLA-1) is another protein complex that defines very late stages of activated T cell differentiation, following either alloantigen or mitogen activation. This protein starts to emerge 2-3 weeks after activation and does not require re-stimulation with antigen. VLA-1 expression was found on nearly all long-term-activated T cell surfaces.[77]

T cell activation outcomes, including cytoplasmic Ca^{2+} flux, pZAP70 expression, microclusters formation and organization, CD44, CD69, and CD25 expression, IL-2 and INF-γ secretion, and T cell proliferation as a function of time course are schematically summarized as below in Figure 6.
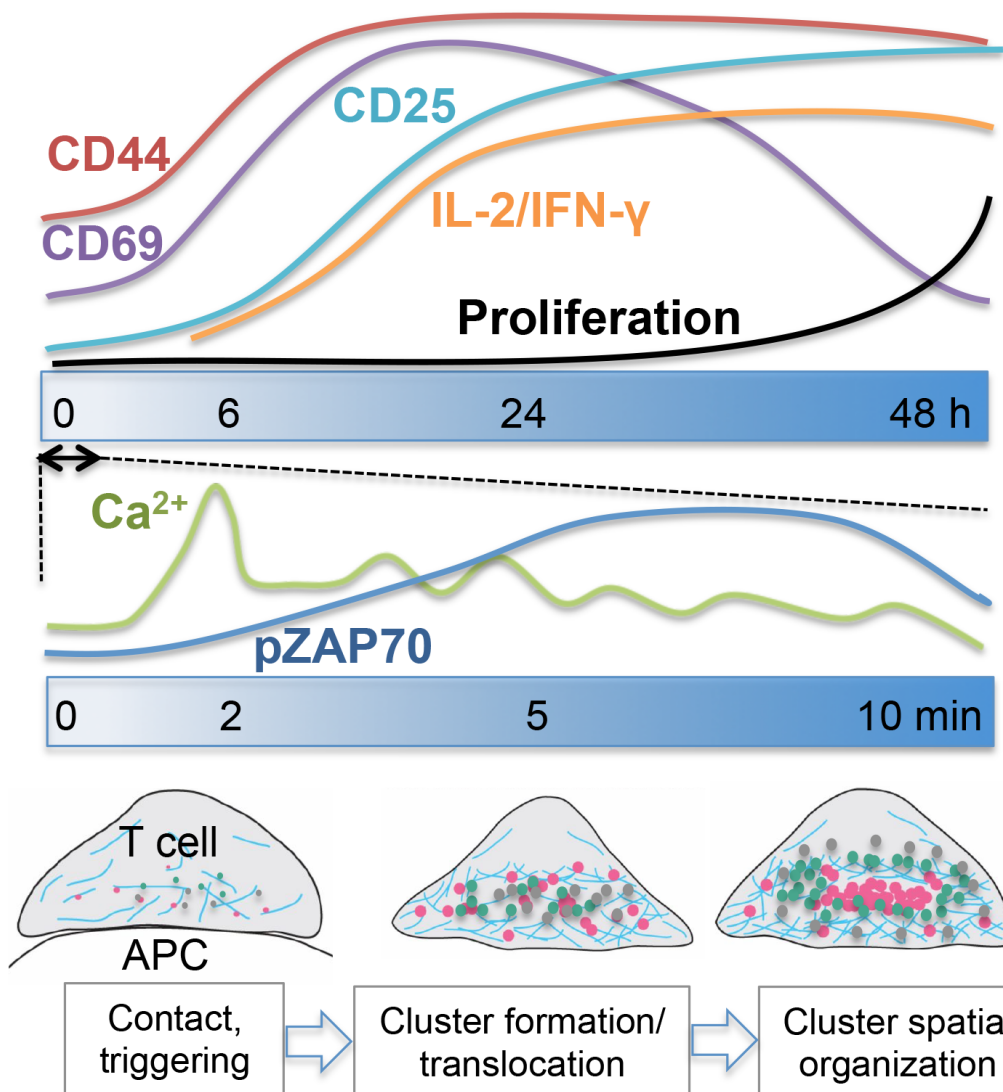
Figure 6. Schematic graph to summarize T cell activation outcomes as a function of time. Cytoplasmic Ca^{2+} concentration increases within seconds after IS formation; pZAP70 expression peaks around 5-10 min after stimulation and then goes down. T cell starts to polarize and IS begins to mature approximately 5-10 min after the IS formation. This process consists of T cell spreading across the surface of APC and the formation of micron-scale clusters of many cell receptors such as TCR, CD3, and CD28. Cell surface activation-markers, i.e., CD25, CD44, and CD69, are gradually upregulated within about 2-4 h, c, followed by enhanced secretion of cytokines, such as IL-2 and INF-γ. Normally, T cells undergo proliferation 24-48 h after TCR

stimulation. Reproduced with permission from American Institute of Physics.[28]

1.2.5 Mechanobiology of T cells

Increasing studies have proved that T cells not only react to the presence of certain receptors at the APC, but can also sense and respond to their mechanical engagement at the APC membrane. Such biophysical signaling processes are called mechanotransduction.[39, 78] The forces involved in mechanotransduction can be induced by membrane undulation/protrusion/retraction and dynamic arrangement of actomyosin cytoskeleton inside the T cell or at the APC, and affect T cell's immune response.

T cell cytoskeleton is demonstrated to be crucial during the formation of TCR- and LFA-1-containing microclusters along the distal edge of T cell-APC interface. These microclusters subsequently reorganize into the cSMAC and pSMAC to define the architecture of IS.[1, 79, 80] Recent experimental evidence also suggests that many of the cell surface molecules involved in T cell activation, such as TCR-CD3 complex and LFA-1, are mechanosensitive proteins. The externally applied force on TCR-CD3 complex has been proved to play a crucial role in TCR triggering.[81-83] LFA-1, which is considered to transmit the cytoskeletal tension to allow mechanical sensing, has also been reported to engage in the mechanosensitivity of T cell spreading and TCR-mediated activation.[7, 40]

Although some achievement has been made in the field of T cell mechanobiology, how the forces T cell experiences and applies contribute to T signaling generation and modulation during T cell activation remains to be further explored. Because the molecules interactions between a real T cell and APC are very complicated, the development of models and tools to measure or apply forces on T cells is crucial to uncover the mechanism by which different receptor pathways interact with each other

to affect the T cell mechanotransduction. The following section is going to discuss more details about model platforms to study the role of mechanics in T cell activation.

1.3 Biochemical and biophysical models to explore T cell activation

Using natural APCs together with their cognate antigen for T cell activation might be the most physiologically close approach to study the receptors and signals involved in T cell activation and response. However, the complexity of the T cell-APC interface, with multiple receptors participating in parallel, and with biochemical, biophysical, and biomechanical signals being involved, makes such studies experimentally difficult. Moreover, isolating APCs to achieve reproducible and quantitative data is a time-consuming and costly process. As a result, many simplified approaches to explore T cell activation have been developed in laboratories.[28] In the following, current approaches to activate T cells without the need of a natural APC are described.

1.3.1 Methods to activate T cells *in vitro*

1) Chemical activation

   Phorbolmyristate acetate (PMA) and ionomycin (Iono), as small organic molecules, can activate protein kinase C (PKC) and then induce an intracellular increase of Ca^{2+} level after diffusing into the cytoplasm. In T cells, the Ca^{2+} jump triggers signaling of the NFAT.[84, 85] As a result, a full T cell activation is achieved, with a continuous production of IL- 2, IL-4, and IFN-γ. This method is nonphysiological and is not antigen specific since it bypasses TCR stimulation and signaling.[86, 87]

2) Activation with soluble APC ligands

   Molecules such as pMHC, anti-CD3, and anti-CD28 have been added to T cell

cultures to stimulate T cells by binding to the TCR/CD3 receptors. TCR and co-receptor-mediated activation events can also be uncovered by using soluble pMHC complexes. People have already suggested that CD8$^+$ (and CD4$^+$) T cells are only activated by soluble pMHC that are at least dimeric and co-engage the co-receptor. Even though, the pMHC dimer and tetramer is only sufficient to initiate signaling (Ca^{2+} signal), further TCR cross-linking is necessary for a sustained full signal.[88, 89] Anti-CD3 and anti-CD28 has different roles in T cell activation. Soluble anti-CD3 can initiate T cell signaling to expand CD8 T cells to generate cell phenotype with higher levels of CD45RA, CD27, and CCR7 expression, but only induce little intracellular IFN-γ or TNF-α.[90] Anti-CD28 alone fails to stimulate T cell activation and it is normally used as together with anti-CD3 to achieve a sustained T cell activation.

3) Activation with surface-bound APC ligands:

Antigen-coated cell culture surfaces mimicking the membrane-bond receptors at the APC surface have also been used to induce T cell activation. This approach allows concentration of the presented ligands at a defined interface, and easy variation of the ligand density, mimicking the spatial clustering features of the IS structure. In fact, antigen presentation in surface-immobilized state seems to be more efficient than incubation with the soluble ligands for T cell stimulation. For example, soluble anti-CD3 induced lower T cell stimulation compared with immobilized anti-CD3 on glass or plastic surfaces, whereas anti-CD28 worked similarly either in solution or on solid surface in the presence of immobilized anti-CD3.[82, 90]

To better understand T cell-APC communication in the immune response, supported lipid bilayers presenting tethered ligands on planar substrate has been used as an important biomolecular tool to surrogate APC. These tools have

provided a spatio-temporal and structural insights into how TCRs integrate and induce signaling during the initial formation of IS upon the recognition of antigens.[91, 92]

The involvement of the cytoskeleton of the T cell and APC in the activation program suggests that the mechanical force applied by the contributing ligands at the IS might also influence T cell stimulation. In agreement with this hypothesis, the mechanical properties of antigen presenting surfaces seem to affect the activation of T cell. APC ligands immobilized on polyacrylamide (PAAm) [81, 93-95] or hyaluronic acid (HA) [96] hydrogels, or on polydimethylsiloxane (PDMS) elastomer [7, 40, 97] surfaces or different mechanical properties have been used as synthetic APC mimics. The mechanics of the surfaces together with the nature (anti-CD3 or pMHC, anti-CD28, ICAM-1) and density of the APC ligands displayed to T cells seem to influence the obtained response (see Section 1.3.4).

4) Force-induced T cell activation

The role of physical forces in TCR triggering has attracted increasing attentions, therefore, many tools has been developed to study T cell activation by externally applied physical forces. For instance, micropipette was used to study T cell signaling by positioning near individual fura-2-AM–labeled (Ca^{2+} indicator) T cells bound to APCs to generate tensive forces on the TCR complex.[98] Optical traps are also used to study force-induced T cell activation by applying force to a streptavidin-coated polystyrene bead that arrayed with specific biotinylated TCR ligand (pMHC).[4] In addition, Atomic force microscopy (AFM) cantilever modified with antigens can also be applied for T cells stimulation and monitoring of mechanical responses of T cell triggering.[83] More details about this field could be seen in the following Section 1.3.3.

1.3.2 Micro- and nanostructured surfaces to mimic the patterned structure of the IS

To study how clustering and organization of receptors at IS influence T cell activation, substrates with patterned ligands have been fabricated as simplified models of the APC surface at the IS. These platforms allow exploring how the physical organization and composition of T cell cognate ligands regulate T cell activation. Basically, three different types of microfabricated platforms have been developed for this purpose: microstructured protein patterns, micropatterned lipid bilayers and nanostructured ligands.

- Micropatterned surfaces presenting key ligands (anti-CD3 and ICAM-1) for T cell activation were fabricated by using a biotinylated photoresist copolymer.[99] Array patterns of surface-tethered anti-CD3 dots or rings were obtained and used for studying T cell activation. T cells stably interacted with the surface immobilized with anti-CD3 dots of 6 μ m diameter or anti-CD3 "quad" patterns dots with 2 μm diameter of each dot). They also proliferated, and secreted cytokines on the anti-CD3 spots. On the contrary, annular geometries of anti-CD3 ligand (an outer diameter of 8 μm and inner diameter of 4 μm) precluded centralized clustering of TCR, and T cells were unable to form stable contacts with T cells and showed aberrant PKC- clustering and significantly alleviated production of IFN- γ (Figure 7A,B). Shen et al.[100] used arrays of dots of anti-CD3, anti-CD28 or ICAM-1 ligands surrounded by a different ligand generated by microcontact printing on a glass surface. Patterns presenting anti-CD28 (smaller, 1 μm diameter spot) around an anti-CD3 dot (larger, 2 μm diameter), induced a higher level of IL-2 secretion than when the two ligands were concentrated in a single spot (2 μm diameter dots with 12 μm pitch)

(Figure 7C,D). These two studies indicate that the ability to arbitrarily and independently manipulate the locations of signaling molecules on surface can offer the opportunity to study T cell activation mechanism from a biophysical perspective.
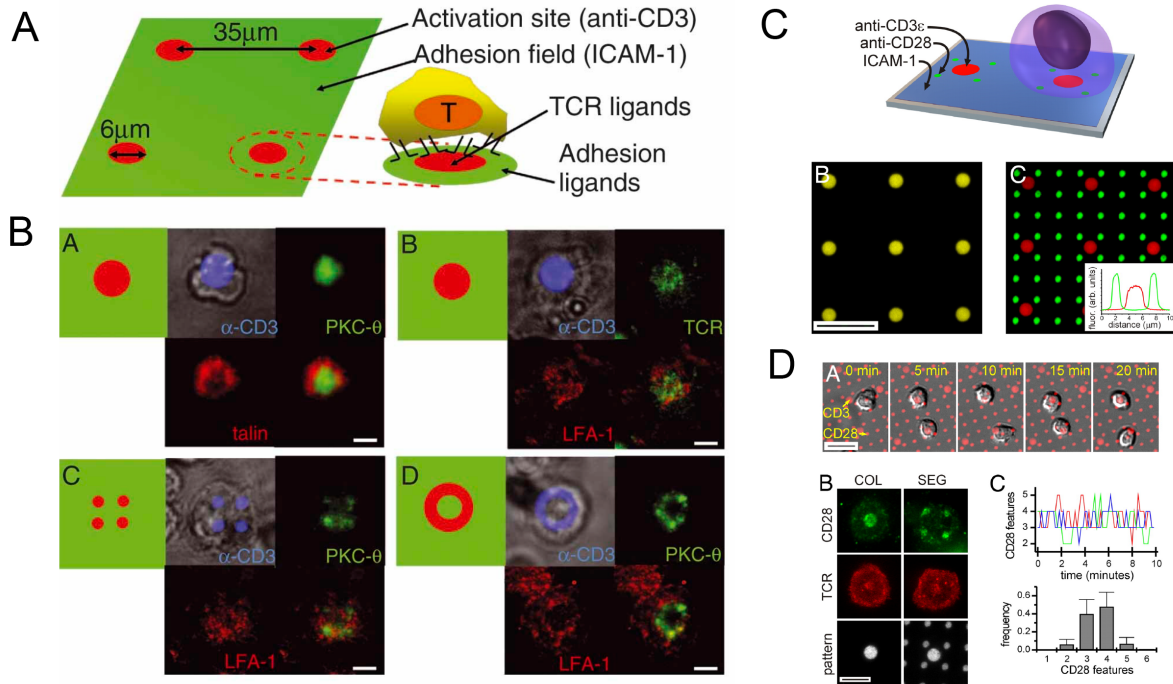
Figure 7. Micropatterned surfaces for the study of TCR triggering. (A) Schematic illustration of IS array. (B) IS formed in T cells on various shapes of anti-CD3 spots. (C) Schematic illustration of micropatterned co-stimulatory ligands. (D) T cell interaction with micropatterned, costimulatory arrays. Reproduced with permission from National Academy of Science U.S.A.[99, 100]

- Micropatterned supported lipid bilayers have been used to study the dynamics of TCR clustering and signaling within the IS. Mossman et al.[101] used supported membranes on a nanostructured substrate to render geometric constraints for IS formation. Specifically, supported membranes have

continuous and fluid lipid bilayer to coat on a silica substrate, were used to fabricate an artificial APC surfaces using different geometrical constraints (unpatterned substrate, 2 μm parallel lines, 5 μm square grid, and concentric hexagonal barriers spaced with 1 μm). Glycosylphosphatidylinositol-linked pMHC and ICAM-1 were co-incorporated into the supported membrane to facilitate the IS formation between a T cell and artificial APC surface. Initial TCR-triggered signaling, as measured by phosphorylated tyrosine level and Ca^{2+} signal were significantly elevated by preventing central clustering of TCRs. Shen et al.[102] constructed bilayers with micropatterned (1.5 μm wide line spaced with 5 μm) ligands by restricting diffusion within SLBs using an appropriately designed physical barrier. Human $CD4^+$ T cell blasts that used to interact with this spatially separated ligands form altered IS configurations on this interdigitating bilayer (Figure 8A). All these studies demonstrated that these micropatterned supported lipid bilayers-based platforms allowed the study complex interplay between lateral mobility and spatial organization of signaling complexes in the context of T cells.

- Nanostructed biointerfaces have also been used for studying how the density number and spatial separation of APC surface ligands influence T cell activation.

Deeg et al.[103] developed surfaces patterned with arrays of hexagonally arranged Au nanoparticles by using block-copolymer micelle nano-lithography, which were further biofunctionalized with pMHC ligands, to study T cell activation (Figure 8B). They found that a minimal density of 90-140 pMHC molecules per μm^2 was required for T cell stimulation and T cell responses were pMHC concentration dependent. In addition, the presented pMHCs number had a larger influence compared with local pMHC density in this context. Dillard et

al.[104] also engineered surfaces with nanodots of anti-CD3 clusters (0.3-1.3 µm diameter spaced by 0.5-4.0 µm) by using nano-sphere lithography (NL). The surface was further treated with metal sputtering and sequential functionalization with biotinylated molecules. Results demonstrated that the local membrane adhesion and topography, the spatial distribution of TCR, and the activity of ZAP70 kinase were all affected by the dot-geometry. On the contrary, the cell spreading area was mainly influenced by the overall average density of the ligands rather than the nanodots characteristics.
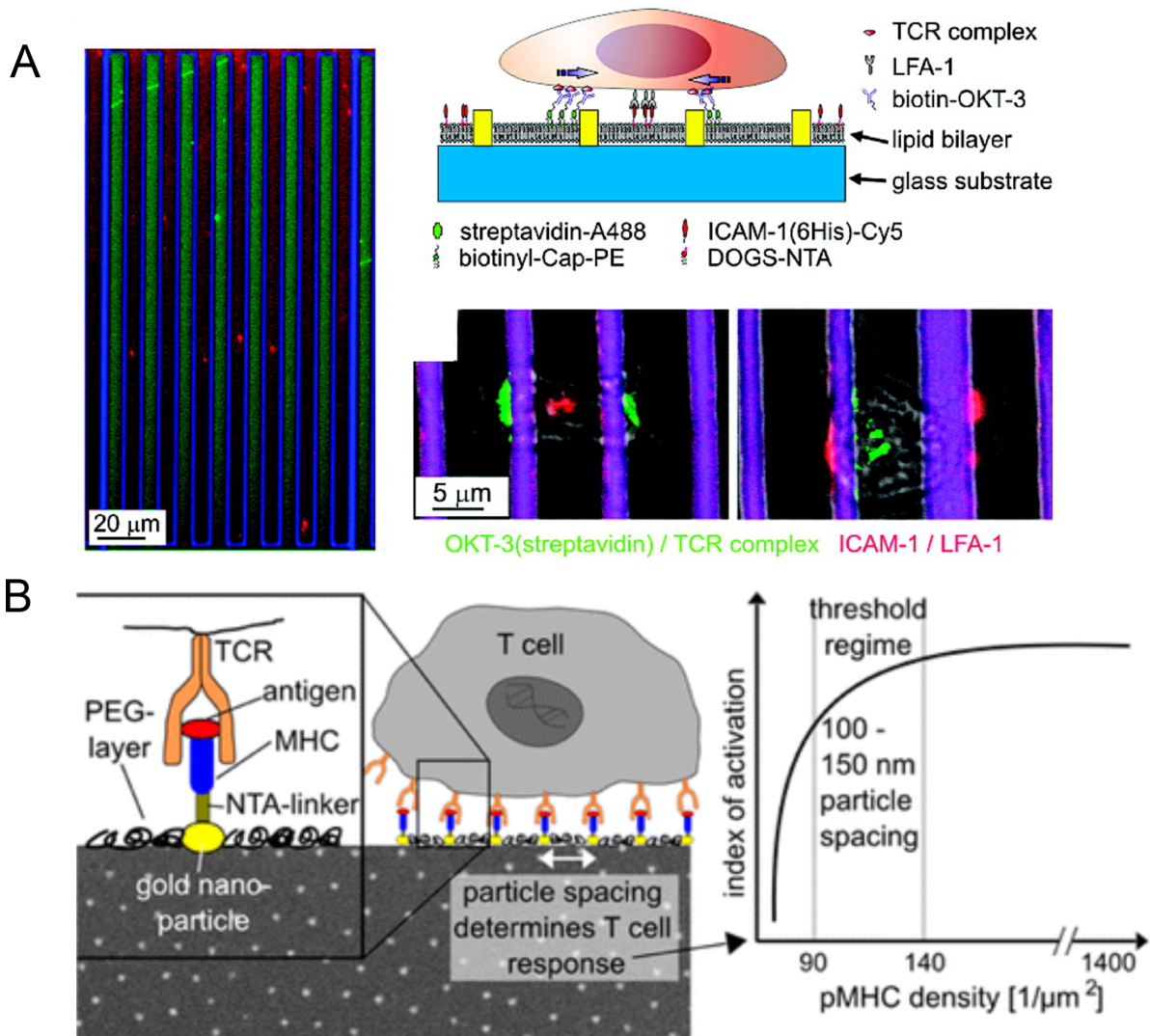
Figure 8. Self-aligning patterns of multiple SLBs and nanofabricated platforms to study TCR triggering. (A) Self-aligned SLBs for patterning the cell-substrate interface. (B) Nanopatterned antigen arrays are used to mimic the APC surface to induce T cell activation. After assessing the activation related signaling, a minimal density of 90-140 stimulating pMHC molecules per μm^2 is required to induce T cell activation and results demonstrated that T cell responses take place on these substrates in a pMHC dose-dependent manner. Also the number of presented pMHCs has a larger effect than local pMHC density. Reproduced with permission from American Chemical Society.[102, 103]

To summarize, artificial APC platforms enable a site-specific and density-controlled immobilization of proteins at molecular level, which provide important insights into the biophysical roles of signaling molecules in T cell triggering and can be employed to apply for further clinical applications, including well-regulated expansion and stimulation of T cells *ex vivo*.

1.3.3 Experimental methods to apply forces to T cells

The role of physical forces in TCR triggering has attracted increasing attentions since the receptor deformation hypothesis was proposed in 2008.[105] This model proposed that TCR triggering is intimately coupled with the motor system of T cells, which generates mechanical forces through the cytoskeleton to deform the membrane at the IS, and thereby push or pull on TCRs to initiate TCR signaling through receptor deformation (Figure 9). Upon the announcement of this model, several researchers inferred that the triggering of TCR signaling comes from mechanical force, which might induce conformational changes of TCR/CD3 complex. Therefore, a series of followed-up studies had emerged by using different methods to

exert physical force on T cells to study the mechanism of TCR triggering. Using optical tweezers to exert a pulling force of 50 pN on pMHC-coated beads attached to the T cell membrane, Kim et al. [1] found that tangential forces, rather than perpendicular ones, could initiate Ca^{2+} influx and suggested TCR/CD3 complex as an anisotropic force sensor.

Other authors reported that TCR complex can initiate T cell signaling in an Src kinase-dependent fashion when mechanical forces are applied on T cells that bound to APCs via TCR.[98] In this study, a micropipette was used to pull and induce shear forces (tangential movement) on T cells that was encountered with fibroblast-based artificial APCs, which expressed anti-CD28 and anti-CD3 ligands (Figure 10A). In contrast to Kim's study, results showed that TCR/CD3 complex did not behave as an anisotropic force sensor. A possible reason for the disagreement is that in Kim's study, tangential movement might be better than vertical movement since it could uncover shielded TCRs, which are largely buried in a thick glycoproteins layer, thus enhancing the chance of a bead binding to the TCR to yield the observed Ca^{2+} influx.
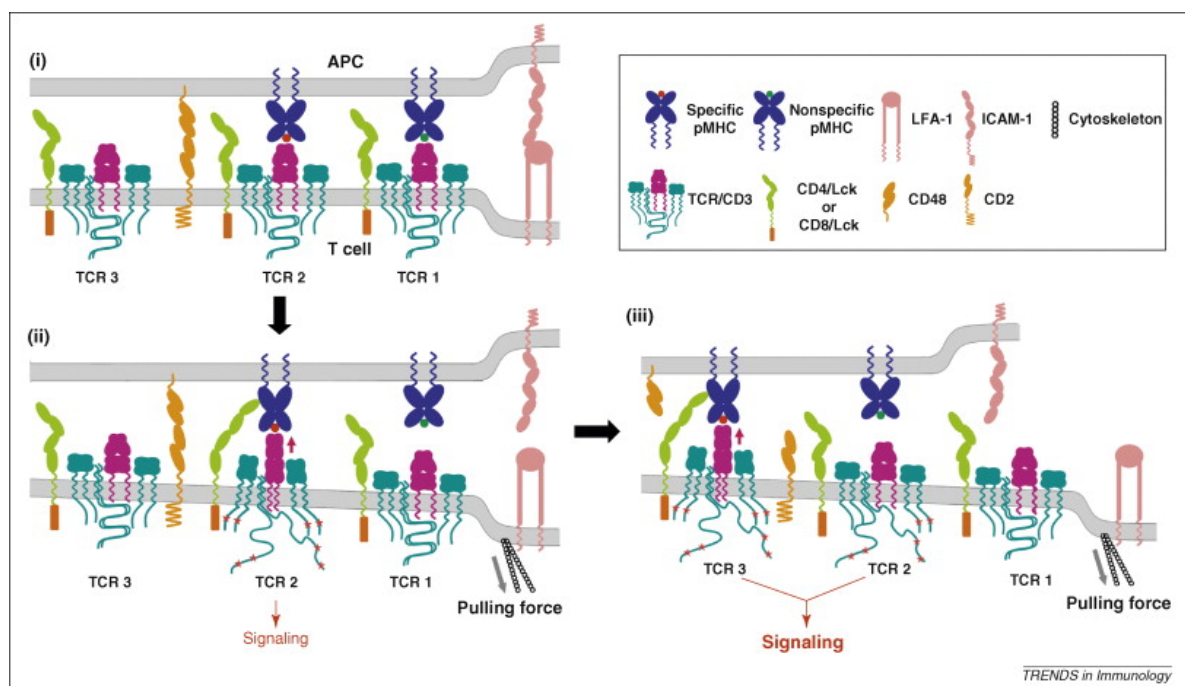
Figure 9. The receptor deformation model of TCR triggering. Copyrights American Society for Biochemistry and Molecular Biology.[105]

Optical tweezers were also used to prove that an extremely high surface concentration of pMHC is required for T cell activation when there is no applied force, whereas an applied force around 10-20 pN (shear direction) is able to trigger Ca^{2+} influx with as few as only two pMHC molecules at the interacting surface.[106]

Liu et al. [4] elaborated on how force regulates the dissociation of TCR-pMHC bond, and examined the magnitude and the duration of the force required for T cell Ca^{2+} triggering. The optimal force-dependent TCR-pMHC kinetic parameter for T cell triggering on the basis of an advanced fluorescence bio-membrane force probe (fBFP) technology and micropipette method was also revealed in their study (Figure 10B).

AFM has also been applied to T cell mechanobiology studies. A mechanical–chemical feedback loop was suggested by Hu et al.,[83] in which forceful contacts are created by TCR-triggered T cells improve access to antigen on APCs surface(Figure 10D). Antigenic stimulation was achieved by using AFM cantilever while imaging was simultaneously peformed with optical microscopy as well as measuring forces on the AFM cantilever. Results demonstrated that Ca^{2+} responses were hardly elicited by using cyclical force alone with control antibodies. Therefore, the mechanical forces must be transduced through TCR engagement to induce specific T cell activation. A pure mechanical stimulation, however, fails to elicit an obvious T cell activation even the force is large enough.

Liu et al. [107] used a nanoscale optomechanical actuator to prove that T cells can rapidly respond to mechanical stimuli by measuring the Ca^{2+} influx in T cell.
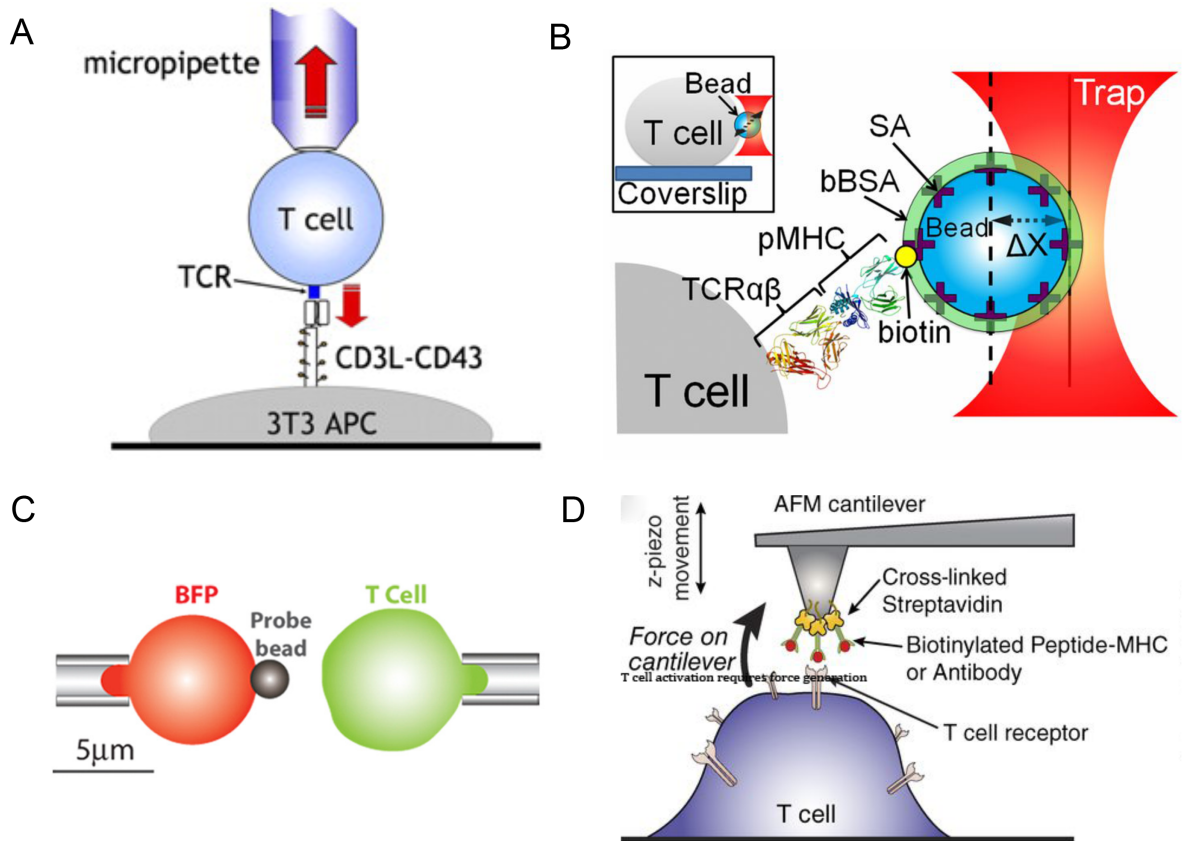
Figure 10. Current tools to study T cell signaling triggered by applied physical force. (A) Tensive forces on the TCR complex are generated via micropipette positioned near individual fura-2-AM–labeled T cells bound to CD3L-CD43 APCs to study T cell signaling. (B) Optical traps are used for application of force to a streptavidin (SA)-coated polystyrene bead arrayed with specific biotinylated TCR ligand (pMHC; in this case VSV8/K^b) and then saturated with bBSA to prevent potential nonspecific streptavidin binding to cells. (C) BFP schematic. A micropipette-aspirated RBC with a probe bead attached to the apex (left) was aligned against a T cell held by an apposing pipette (right). (D) Schematic showing an AFM cantilever for stimulation of T cells and for monitoring mechanical responses. Reproduced with permission from American Institute of Physics. Reproduced with permission from The American Association of Immunologists, National Academy Sciences U.S.A, Cell Press, and

Rockefeller University Press.[4, 83, 98, 106]

All the above-mentioned studies indicate that T cell signaling can be triggered by applied physical force by using micropipette aspiration, fBFP, optical tweezers, and AFM. However, only the early signaling events after short TCR stimulation can be examined by these methods, the late activation signaling, such as cytokine secretion and proliferation, which takes place after long incubation periods, is unable to be explored. In addition, almost all the experimental setups created artificial APCs on stiff substrate such as micro-beads or silicon AFM probes with a stiffness range around the GPa, failing to study T cell triggering in a mechanically physiological condition. Therefore, more and more 2D polymeric substrates have recently been used to study T cell responses to physiological stiffness changes in different activation time scales, which will be summarized in the following section.

1.3.4 Biomaterial-based models to explore T cell mechanotransduction

Hydrogel and elastomeric thin films with mechanical properties covering the stiffness range of cells in the body (Young's Modulus ranging from 50 Pa to 40 kPa),[108] have been modified with APC ligands to mimic the APC surface. These models allow the study of how APC stiffness affects T cell activation and function (Figure 11).[109]

PAAm/HA hydrogel/PDMS substrates (2D)
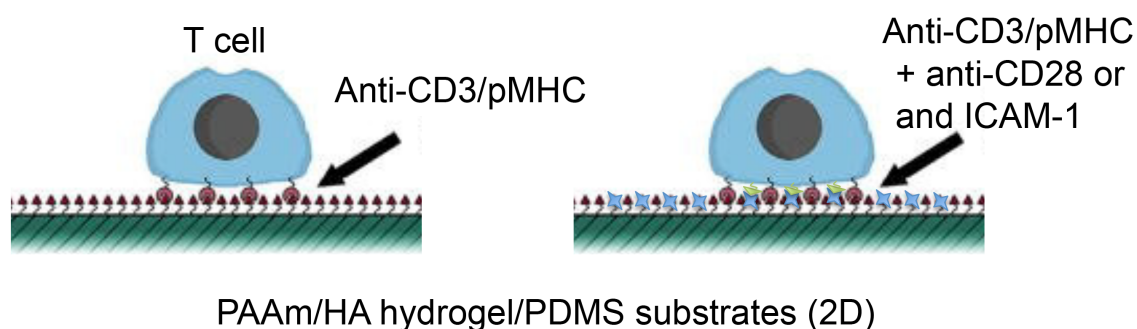
Figure 11. Synthetic polymer substrates with variable stiffness are generally used to explore T cell mechanotransduction. T cells are stimulated by a variety of antibodies (i.e., anti-CD3/pMHC and/or anti-CD28 and/or ICAM-1) that conjugated to the substrate surface. Reproduced with permission from American Institute of Physics.[28]

Judokusumo et al. used anti-CD3 and anti-CD28 coated PAAm hydrogels with Young's Modulus between 2 and 200 kPa) to study the response of mouse naïve $CD4^+$ T lymphocytes to mechanical cues.[93] Both the late T cell activation, as measured by the production of IL-2 (measured at 6 h), and early T cell activation (15-30 min) as measured by Zap70 and Src family kinases phosphorylation, were stronger on stiff (100-200 kPa) than on soft (2-10 kPa) substrates. This study also demonstrated that an intact myosin II activity is required for the mechanotransduction involved in T cell activation.

O'Connor et al. [97] used PDMS substrates with different stiffness (100-2000 kPa) where anti-CD3 (OKT3) and anti-CD28 were physically absorbed to mimic APCs. The soft substrates (~100 kPa) elicited a stronger IL-2 and IFN-γ production (measured at 6 h) and higher T lymphocyte proliferation compared to stiff substrates (>2000 kPa). This result seems inconsistent with the previous study by Judokusumo. [93] However, the different substrate chemistry, cell types, eventually ligand density and stiffness range may account for the contradictory conclusions.

Tabdanov et al. [40] also examined T cell mechanotransduction with the help of PDMS substrates (varying stiffness) presenting anti-CD3 with or without ICAM-1 molecules. T cells on soft substrates (5 kPa) showed less tyrosine phosphorylation (measured at 30 min) than on rigid ones (2000 kPa), and engagement of LFA-1/ICAM-1 potentiated the response to stiff substrates. This was the first that the

role of stiffness in T cell response was studied in the presence of ICAM-1.
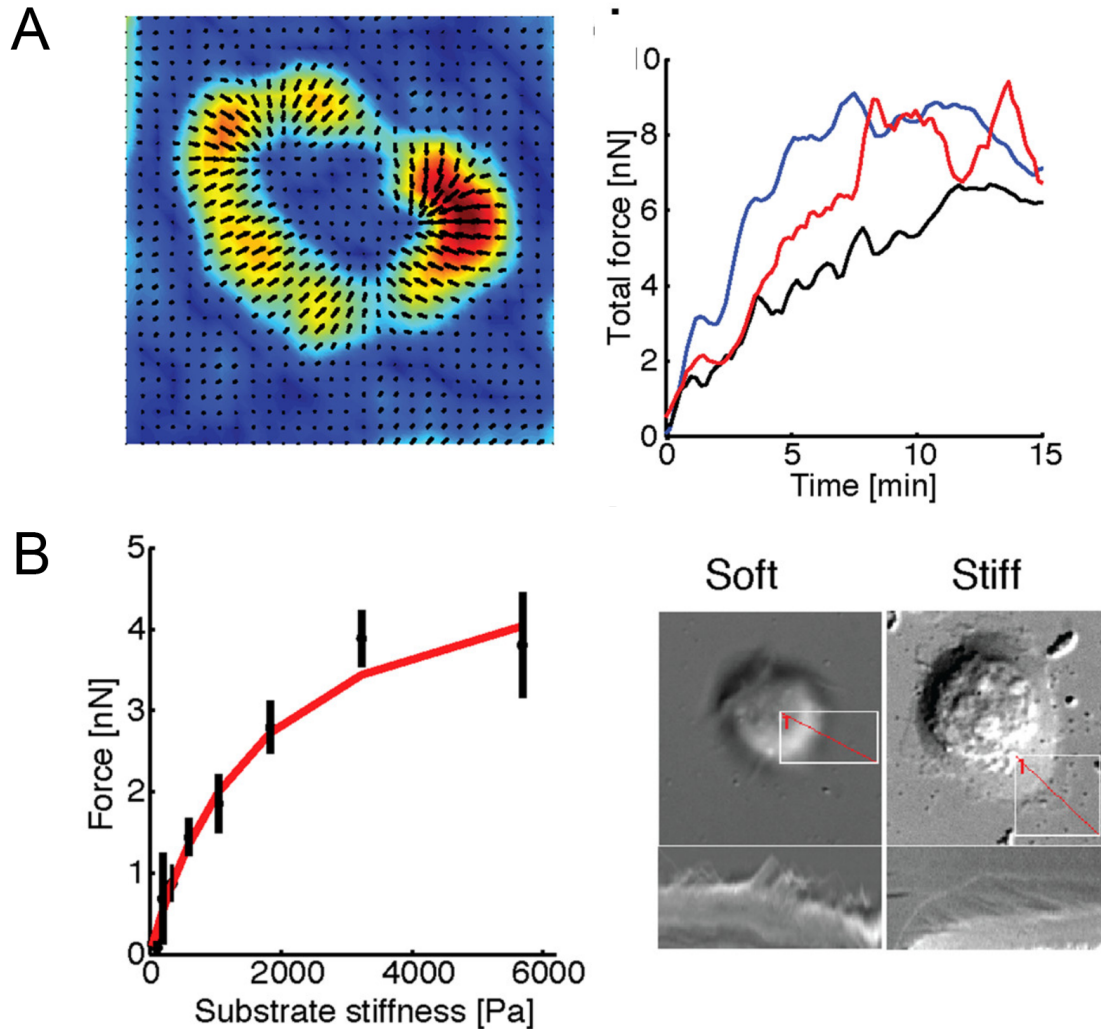
Figure 12. T-cells generate traction force on antigen presenting surface. (A) Traction force on 2D polymeric substrates. Vector map of traction force vectors to show the direction of traction stresses generated by Jurkat T-cells interacting with anti-CD3–coated elastic substrate (stiffness is around 1.2 kPa). Three example cells are shown in tight figure to illustrate the development of total force as a function of time. (B) Substrate stiffness affects traction forces. Average total force exerted by cells increases with substrate stiffness. Right figure shows the two representative cells

spreading behavior on soft (200 Pa) and stiff (10 kPa) substrates. Reproduced with permission from National Academy of Science USA and American Society for Cell Biology.[94]

Saitakis et al. [95] recently explored the response of human primary CD4$^+$ T cells by using PAAm hydrogels (stiffness ranges from 0.5 to 100 kPa) modified with anti-CD3, anti-CD28, or ICAM-1. T cells became more activated on stiffer substrates. Migration, gene expression, cytokine expression and secretion were sensitive to the all substrate stiffness tested here, whereas cell cycle progression (in 24 h) and metabolism were increased by high stiffness (100 kPa) rather than being affected by varying stiffness within the range measured for APCs (from hundreds to thousands Pa). These results suggest that the different TCR-mediated T cell responses can be elevated by substrate stiffness with different sensitivities. This is the first time that the role of matrix stiffness was explored in T cell responses within the context of co-stimulator, anti-CD28 and integrin ligand, ICAM-1.

Hui et al.[94] used anti-CD3 modified PAAm gels to demonstrate that traction force applied by T cell on the substrates increased with substrate stiffness (200 Pa to ~6 kPa) (Figure 12A,B). In addition, the early T cell signaling (measured at 3 min), such as phosphorylation of Zap70, Lat and SLP76, were also enhanced by stiffer substrates (1 and 5 kPa), whereas late T cell signaling (measured at 15 min) decreased with substrate stiffness. This result suggests that T cell mechanosensitivity might have a temporal evolution, and thus the timepoint at which the different responses are measured should be taken into account when it refers to mechanosensitivity.

In a different study, a biphasic mechanosensitivity of TCR-mediated spreading of T cells was observed on PDMS substrates modified with different ligands.[7] When

adhering solely via the TCR complex by using anti-CD3, T cells achieved maximal spreading on substrate stiffness between 3 and 20 kPa. However, in the presence of ICAM-1, a ligand recognizes the integrin LFA-1, cell spreading increased with stiffness (0.5-2440 kPa) up to a saturation value. Authors explain this effect based on that an increased cell spreading lead by increasing effective stiffness of the bonds is overwhelmed with increasing bond breakage, which finally results in a decreased spreading. It was also speculated that the site for mechanosensing is from the link between receptors (TCR or LFA-1) and actin, rather than the ligand/receptor linkage,. This study suggests that mechanosensing during T cell spreading is ligand-specific, and thus the selection of ligands for designing APC models is also an important factor in T cell mechanosensitivity studies.

Basu et al. [81] used fibronectin coated PAAm gel (stiffness ranging from 12 kPa to 50 kPa) to stimulate antigenic peptide ovalbumin (OVA)-loaded APCs overnight, and then the stimulated APCs were further used to physiologically activate T cells. Results demonstrated that $CD8^+$-mediated killing efficiency could be potentiated by APCs that were previously stimulated on stiffer substrates (50 kPa). Thus the T cell mechanotransduction was firstly linked to a physiologically functional readout of T cell activation.

To conclude, the reported studies demonstrate T cell activation can be influenced by the mechanical properties of the substrates onto which the APC ligands are immobilized (Table 1). The fact that the reported results are not fully consistent can be attributed to the differences in the substrate chemistry, the activator types, activator density, or even the types of T cells and outcomes analyzed to characterize T cell functions. This scenario emphasizes the urgent need to design experiments more carefully, control and quantify experimental parameters in a better way, to gain a more convincible conclusion during the studies of T cell mechanobiology.

Table 1. T cell responses to substrate stiffness. Reproduced with permission from American Institute of Physics.[28]

Cell type	Substrate chemistry	Activator	Stiffness range (E)	T cell response measured	Activation outcome	Reference
Mouse naive CD4+	PAA-gels containing streptavidin	Biotinylated anti-CD3, anti-CD28	10–200 kPa	IL-2 production, phosphorylation of SFK and Zap 70	No change in cell response below 10 kPa; Activation increased with stiffness	Judokusumo et al. [93]
Human naive CD4+ and CD8+	PDMS, physical adsorption of proteins	Anti-CD3, anti-CD28	100 kPa–2MPa	IL-2 and IFN-γ production, cell proliferation	Activation decreased with stiffness	O'Connor et al.[97]
Jurkat E6-1	PAA treated with hydrazine hydrate	Only anti-CD3	1, 5 kPa	Phosphorylation of Zap70, Lat, and SLP76	Early signaling increased with stiffness; Late signaling decreased with stiffness	Hui et al. [94]
Human naive CD4+	PDMS, passive adsorption of proteins	Anti-CD3, ICAM-1-Fc	5 kPa–2MPa	Tyrosine phosphorylation	Activation increased with stiffness	Tabdanov et al. [40]
OT1 CTLs and OVA-loaded B16	PAA coated with adsorbed fibronectin	pMHC + APC (B16 melanoma cells)	12, 50 kPa	Target cell killing	CD8+-mediated killing increased with stiffness	Basu et al. [81]
Human primary CD4+	PAA-gels containing streptavidin	Biotinylated ICAM-1, biotinylated anti-CD3 and anti-CD28	0.5, 6.4, 100 kPa	Migration, morphology, metabolism, cell-cycle-related genes, IFN-γ and TFN-a production, CD25 and CD69 surface marker expression	Generally activation increased with stiffness; Some functions had a low stiffness threshold for activation; Some functions were sensitive to higher stiffness regimes	Saitakis et al.[95]
Jurkat E6-1 Human naive CD4+	PDMS and PAA gels coated with BSA-biotin-streptavidin and BSA-NTA (Ni)	Biotinylated anti-CD3 alone or, additionally, with 6His-ICAM-1 or biotinylated anti-CD28	0.5 kPa–40MPa	Cell spreading	T cell spreading response as a function of substrate rigidity, depending on the surface receptors stimulated, the cellular response may be either biphasic or monotonous.	Wahl et al. [7]
B6 murine CD8+, human CD8+	Thiolated HA hydrogel	Anti-CD3 and anti-CD28	0.5, 3kPa	Proliferation, TCR clustering, and differentiation	Proliferation and TCR clustering decreased with stiffness; Ratio of central memory to effector memory CD8+ T cells first increased with stiffness and then decreased with stiffness	Hickey et al. [96]

References

[1] S.T. Kim, K. Takeuchi, Z.Y. Sun, M. Touma, C.E. Castro, A. Fahmy, M.J. Lang, G. Wagner, E.L. Reinherz, The alphabeta T cell receptor is an anisotropic mechanosensor, J. Biol. Chem. 284(45) (2009) 31028-37.

[2] F. Kong, A.J. Garcia, A.P. Mould, M.J. Humphries, C. Zhu, Demonstration of catch bonds between an integrin and its ligand, J. Cell Biol. 185(7) (2009) 1275-84.

[3] D.K. Das, Y. Feng, R.J. Mallis, X. Li, D.B. Keskin, R.E. Hussey, S.K. Brady, J.H. Wang, G. Wagner, E.L. Reinherz, M.J. Lang, Force-dependent transition in the T-cell receptor beta-subunit allosterically regulates peptide discrimination and pMHC bond lifetime, Proc. Natl. Acad. Sci. U. S. A. 112(5) (2015) 1517-22.

[4] B. Liu, W. Chen, B.D. Evavold, C. Zhu, Accumulation of dynamic catch bonds between TCR and agonist peptide-MHC triggers T cell signaling, Cell 157(2) (2014) 357-368.

[5] Y. Sawada, M. Tamada, B.J. Dubin-Thaler, O. Cherniavskaya, R. Sakai, S. Tanaka, M.P. Sheetz, Force sensing by mechanical extension of the Src family kinase substrate p130Cas, Cell 127(5) (2006) 1015-26.

[6] L.A. Chylek, V. Akimov, J. Dengjel, K.T. Rigbolt, B. Hu, W.S. Hlavacek, B. Blagoev, Phosphorylation site dynamics of early T-cell receptor signaling, PLoS One 9(8) (2014) e104240.

[7] A. Wahl, C. Dinet, P. Dillard, A. Nassereddine, P.H. Puech, L. Limozin, K. Sengupta, Biphasic mechanosensitivity of T cell receptor-mediated spreading of lymphocytes, Proc. Natl. Acad. Sci. U. S. A. 116(13) (2019) 5908-5913.

[8] P.J. Delves, I.M. Roitt, The immune system. First of two parts, N. Engl. J. Med. 343(1) (2000) 37-49.

[9] J. Parkin, B. Cohen, An overview of the immune system, Lancet 357(9270) (2001)

1777-89.

[10] K.J. O'Byrne, A.G. Dalgleish, Chronic immune activation and inflammation as the cause of malignancy, Br. J. Cancer 85(4) (2001) 473-83.

[11] A.M. Hammer, N.L. Morris, Z.M. Earley, M.A. Choudhry, The First Line of Defense: The Effects of Alcohol on Post-Burn Intestinal Barrier, Immune Cells, and Microbiome, Alcohol. Res. 37(2) (2015) 209-22.

[12] G. Dranoff, Cytokines in cancer pathogenesis and cancer therapy, Nat. Rev. Cancer 4(1) (2004) 11-22.

[13] V. Brinkmann, U. Reichard, C. Goosmann, B. Fauler, Y. Uhlemann, D.S. Weiss, Y. Weinrauch, A. Zychlinsky, Neutrophil extracellular traps kill bacteria, Science 303(5663) (2004) 1532-5.

[14] H. Rabb, The T cell as a bridge between innate and adaptive immune systems: implications for the kidney, Kidney Int. 61(6) (2002) 1935-46.

[15] N.X. Zheng, Y. Wang, D.D. Hu, L. Yan, Y.Y. Jiang, The role of pattern recognition receptors in the innate recognition of Candida albicans, Virulence 6(4) (2015) 347-61.

[16] A.M. Kerrigan, G.D. Brown, C-type lectins and phagocytosis, Immunobiology 214(7) (2009) 562-75.

[17] C. Rosales, E. Uribe-Querol, Phagocytosis: A Fundamental Process in Immunity, Biomed Res. Int. 2017 (2017) 9042851.

[18] T. Ito, J.M. Connett, S.L. Kunkel, A. Matsukawa, The linkage of innate and adaptive immune response during granulomatous development, Front. Immunol. 4 (2013) 10.

[19] M.D. Cooper, The early history of B cells, Nat. Rev. Immunol. 15(3) (2015) 191-7.

[20] M.I. Yuseff, P. Pierobon, A. Reversat, A.M. Lennon-Dumenil, How B cells capture, process and present antigens: a crucial role for cell polarity, Nat. Rev. Immunol. 13(7) (2013) 475-86.

[21] S. Crotty, A brief history of T cell help to B cells, Nat. Rev. Immunol. 15(3) (2015) 185-9.

[22] J.S. Blum, P.A. Wearsch, P. Cresswell, Pathways of antigen processing, Annu. Rev. Immunol. 31 (2013) 443-73.

[23] M. McHeyzer-Williams, S. Okitsu, N. Wang, L. McHeyzer-Williams, Molecular programming of B cell memory, Nat. Rev. Immunol. 12(1) (2011) 24-34.

[24] A.M. Kruisbeek, Introduction: regulation of T cell development by the thymic microenvironment, Semin. Immunol. 11(1) (1999) 1-2.

[25] S.L. Swain, L.M. Bradley, M. Croft, S. Tonkonogy, G. Atkins, A.D. Weinberg, D.D. Duncan, S.M. Hedrick, R.W. Dutton, G. Huston, Helper T-cell subsets: phenotype, function and the role of lymphokines in regulating their development, Immunol. Rev. 123 (1991) 115-44.

[26] F.A. Bonilla, H.C. Oettgen, Adaptive immunity, J. Allergy Clin. Immunol. 125(2 Suppl 2) (2010) S33-40.

[27] J.E. Smith-Garvin, G.A. Koretzky, M.S. Jordan, T cell activation, Annu. Rev. Immunol. 27 (2009) 591-619.

[28] A. de la Zerda, M.J. Kratochvil, N.A. Suhar, S.C. Heilshorn, Review: Bioengineering strategies to probe T cell mechanobiology, APL Bioeng. 2(2) (2018) 021501.

[29] O. Acuto, F. Michel, CD28-mediated co-stimulation: a quantitative support for TCR signalling, Nat. Rev. Immunol. 3(12) (2003) 939-51.

[30] P.E. Love, A. Bhandoola, Signal integration and crosstalk during thymocyte migration and emigration, Nat. Rev. Immunol. 11(7) (2011) 469-77.

[31] U. Koch, F. Radtke, Mechanisms of T cell development and transformation, Annu Rev. Cell Dev. Biol. 27 (2011) 539-62.

[32] H.T. Petrie, J.C. Zuniga-Pflucker, Zoned out: functional mapping of stromal

signaling microenvironments in the thymus, Annu. Rev. Immunol. 25 (2007) 649-79.

[33] B. Malissen, P. Bongrand, Early T cell activation: integrating biochemical, structural, and biophysical cues, Annu. Rev. Immunol. 33 (2015) 539-61.

[34] M.E. Call, J. Pyrdol, M. Wiedmann, K.W. Wucherpfennig, The organizing principle in the formation of the T cell receptor-CD3 complex, Cell 111(7) (2002) 967-79.

[35] C. Xu, E. Gagnon, M.E. Call, J.R. Schnell, C.D. Schwieters, C.V. Carman, J.J. Chou, K.W. Wucherpfennig, Regulation of T cell receptor activation by dynamic membrane binding of the CD3epsilon cytoplasmic tyrosine-based motif, Cell 135(4) (2008) 702-13.

[36] E.O. Long, ICAM-1: getting a grip on leukocyte adhesion, J. Immunol. 186(9) (2011) 5021-3.

[37] D.E. Staunton, M.L. Dustin, T.A. Springer, Functional cloning of ICAM-2, a cell adhesion ligand for LFA-1 homologous to ICAM-1, Nature 339(6219) (1989) 61-4.

[38] W.A. Comrie, A. Babich, J.K. Burkhardt, F-actin flow drives affinity maturation and spatial organization of LFA-1 at the immunological synapse, J. Cell Biol. 208(4) (2015) 475-91.

[39] V. Vogel, M.P. Sheetz, Cell fate regulation by coupling mechanical cycles to biochemical signaling pathways, Curr. Opin. Cell Biol. 21(1) (2009) 38-46.

[40] E. Tabdanov, S. Gondarenko, S. Kumari, A. Liapis, M.L. Dustin, M.P. Sheetz, L.C. Kam, T. Iskratsch, Micropatterning of TCR and LFA-1 ligands reveals complementary effects on cytoskeleton mechanics in T cells, Integr. Biol. 7(10) (2015) 1272-84.

[41] A. Grakoui, S.K. Bromley, C. Sumen, M.M. Davis, A.S. Shaw, P.M. Allen, M.L. Dustin, The immunological synapse: a molecular machine controlling T cell activation, Science 285(5425) (1999) 221-7.

[42] C.R.F. Monks, B.A. Freiberg, H. Kupfer, N. Sciaky, A. Kupfer, Three-dimensional segregation of supramolecular activation clusters in T cells, Nature 395(6697) (1998) 82-86.

[43] M.L. Dustin, A.K. Chakraborty, A.S. Shaw, Understanding the structure and function of the immunological synapse, Cold Spring Harb Perspect. Biol. 2(10) (2010) a002311.

[44] M.L. Dustin, The immunological synapse, Cancer Immunol. Res. 2(11) (2014) 1023-33.

[45] K.H. Lee, A.D. Holdorf, M.L. Dustin, A.C. Chan, P.M. Allen, A.S. Shaw, T cell receptor signaling precedes immunological synapse formation, Science 295(5559) (2002) 1539-42.

[46] M. Huse, Mechanical forces in the immune system, Nat. Rev. Immunol. 17(11) (2017) 679-690.

[47] Y. Yu, A.A. Smoligovets, J.T. Groves, Modulation of T cell signaling by the actin cytoskeleton, J. Cell Sci. 126(Pt 5) (2013) 1049-58.

[48] P. Beemiller, M.F. Krummel, Mediation of T-cell activation by actin meshworks, Cold Spring Harb Perspect. Biol. 2(9) (2010) a002444.

[49] B.H. Hosseini, I. Louban, D. Djandji, G.H. Wabnitz, J. Deeg, N. Bulbuc, Y. Samstag, M. Gunzer, J.P. Spatz, G.J. Hammerling, Immune synapse formation determines interaction forces between T cells and antigen-presenting cells measured by atomic force microscopy, Proc. Natl. Acad. Sci. U. S. A. 106(42) (2009) 17852-7.

[50] A.C. Chan, M. Iwashima, C.W. Turck, A. Weiss, ZAP-70: a 70 kd protein-tyrosine kinase that associates with the TCR zeta chain, Cell 71(4) (1992) 649-62.

[51] M. Iwashima, B.A. Irving, N.S. van Oers, A.C. Chan, A. Weiss, Sequential interactions of the TCR with two distinct cytoplasmic tyrosine kinases, Science 263(5150) (1994) 1136-9.

[52] H. Wang, T.A. Kadlecek, B.B. Au-Yeung, H.E. Goodfellow, L.Y. Hsu, T.S. Freedman, A. Weiss, ZAP-70: an essential kinase in T-cell signaling, Cold Spring Harb Perspect. Biol. 2(5) (2010) a002279.

[53] J. Bubeck Wardenburg, C. Fu, J.K. Jackman, H. Flotow, S.E. Wilkinson, D.H. Williams, R. Johnson, G. Kong, A.C. Chan, P.R. Findell, Phosphorylation of SLP-76 by the ZAP-70 protein-tyrosine kinase is required for T-cell receptor function, J. Biol. Chem. 271(33) (1996) 19641-4.

[54] M. Oh-hora, A. Rao, Calcium signaling in lymphocytes, Curr. Opin. Immunol. 20(3) (2008) 250-8.

[55] J. Delon, N. Bercovici, G. Raposo, R. Liblau, A. Trautmann, Antigen-dependent and -independent Ca^{2+} responses triggered in T cells by dendritic cells compared with B cells, J. Exp. Med. 188(8) (1998) 1473-84.

[56] N. Joseph, B. Reicher, M. Barda-Saad, The calcium feedback loop and T cell activation: how cytoskeleton networks control intracellular calcium flux, Biochim. Biophys. Acta 1838(2) (2014) 557-68.

[57] S. Feske, Calcium signalling in lymphocyte activation and disease, Nat. Rev. Immunol. 7(9) (2007) 690-702.

[58] S. Kumari, S. Curado, V. Mayya, M.L. Dustin, T cell antigen receptor activation and actin cytoskeleton remodeling, Biochim. Biophys. Acta 1838(2) (2014) 546-56.

[59] J.K. Burkhardt, E. Carrizosa, M.H. Shaffer, The actin cytoskeleton in T cell activation, Annu. Rev. Immunol. 26 (2008) 233-59.

[60] J. Jacobelli, F.C. Bennett, P. Pandurangi, A.J. Tooley, M.F. Krummel, Myosin-IIA and ICAM-1 regulate the interchange between two distinct modes of T cell migration, J. Immunol. 182(4) (2009) 2041-50.

[61] I. Tskvitaria-Fuller, A.L. Rozelle, H.L. Yin, C. Wulfing, Regulation of sustained actin dynamics by the TCR and costimulation as a mechanism of receptor localization,

J. Immunol. 171(5) (2003) 2287-95.

[62] M.L. Dustin, J.A. Cooper, The immunological synapse and the actin cytoskeleton: molecular hardware for T cell signaling, Nat. Immunol. 1(1) (2000) 23-9.

[63] A. Kupfer, G. Dennert, Reorientation of the microtubule-organizing center and the Golgi apparatus in cloned cytotoxic lymphocytes triggered by binding to lysable target cells, J. Immunol. 133(5) (1984) 2762-6.

[64] P. Cullinan, A.I. Sperling, J.K. Burkhardt, The distal pole complex: a novel membrane domain distal to the immunological synapse, Immunol. Rev. 189 (2002) 111-22.

[65] K. Badour, J. Zhang, K.A. Siminovitch, The Wiskott-Aldrich syndrome protein: forging the link between actin and cell activation, Immunol. Rev. 192 (2003) 98-112.

[66] M. Vicente-Manzanares, F. Sanchez-Madrid, Role of the cytoskeleton during leukocyte responses, Nat. Rev. Immunol. 4(2) (2004) 110-22.

[67] D. Cibrian, F. Sanchez-Madrid, CD69: from activation marker to metabolic gatekeeper, Eur. J. Immunol. 47(6) (2017) 946-953.

[68] R. González-Amaro, J.R. Cortés, F. Sánchez-Madrid, P. Martín, Is CD69 an effective brake to control inflammatory diseases, Trends Mol. Med. 19(10) (2013) 625-32.

[69] N. Blanchard, M. Decraene, K. Yang, F. Miro-Mur, S. Amigorena, C. Hivroz, Strong and durable TCR clustering at the T/dendritic cell immune synapse is not required for NFAT activation and IFN-gamma production in human CD4^{+} T cells, J. Immunol. 173(5) (2004) 3062-72.

[70] W. Liao, J.X. Lin, W.J. Leonard, IL-2 family cytokines: new insights into the complex roles of IL-2 as a broad regulator of T helper cell differentiation, Curr. Opin. Immunol. 23(5) (2011) 598-604.

[71] V. Hurez, A. Saparov, A. Tousson, M.J. Fuller, T. Kubo, J. Oliver, B.T. Weaver,

C.T. Weaver, Restricted clonal expression of IL-2 by naive T cells reflects differential dynamic interactions with dendritic cells, J. Exp. Med. 198(1) (2003) 123-32.

[72] A. Weiss, R. Shields, M. Newton, B. Manger, J. Imboden, Ligand-receptor interactions required for commitment to the activation of the interleukin2 geneLigand-receptor interactions required for commitment to the activation of the interleukin2 gene, J. Immunol. 138(7) (1987) 2169-76.

[73] G. Iezzi, K. Karjalainen, A. Lanzavecchia, The duration of antigenic stimulation determines the fate of naive and effector T cells, Immunity 8(1) (1998) 89-95.

[74] Q. Ma, Y. Wang, A.S. Lo, E.M. Gomes, R.P. Junghans, Cell density plays a critical role in ex vivo expansion of T cells for adoptive immunotherapy, J. Biomed. Biotechnol. 2010 (2010) 386545.

[75] B. Fazekas de St Groth, A.L. Smith, C.A. Higgins, T cell activation: in vivo veritas, Immunol. Cell. Biol. 82(3) (2004) 260-8.

[76] T. Lischke, A. Hegemann, S. Gurka, D. Vu Van, Y. Burmeister, K.P. Lam, O. Kershaw, H.J. Mollenkopf, H.W. Mages, A. Hutloff, R.A. Kroczek, Comprehensive analysis of CD4+ T cells in the decision between tolerance and immunity in vivo reveals a pivotal role for ICOS, J. Immunol. 189(1) (2012) 234-44.

[77] M.E. Hemler, J.G. Jacobson, M.B. Brenner, D. Mann, J.L. Strominger, VLA-1: a T cell surface antigen which defines a novel late stage of human T cellactivation, Eur. J. Immunol. 15(5) (1985) 502-8.

[78] J.K. Kim, Y.J. Shin, L.J. Ha, D.H. Kim, D.H. Kim, Unraveling the Mechanobiology of the Immune System, Adv. Healthcare Mater. 8(4) (2019) e1801332.

[79] S. Ghassemi, N. Biais, K. Maniura, S.J. Wind, M.P. Sheetz, J. Hone, Fabrication of elastomer Pillar Arrays with Modulated Stiffness for Cellular Force Measurements, J. Vac. Sci. Technol., B: Microelectron. Nanometer Struct. –Process., Meas., Phenom. 26(6) (2008) 2549-2553.

[80] Y. Klieger, O. Almogi-Hazan, E. Ish-Shalom, A. Pato, M.H. Pauker, M. Barda-Saad, L. Wang, M. Baniyash, Unique zeta-chain motifs mediate a direct TCR-actin linkage critical for immunological synapse formation and T-cell activation, Eur. J. Immunol. 44(1) (2014) 58-68.

[81] R. Basu, B.M. Whitlock, J. Husson, A. Le Floc'h, W. Jin, A. Oyler-Yaniv, F. Dotiwala, G. Giannone, C. Hivroz, N. Biais, J. Lieberman, L.C. Kam, M. Huse, Cytotoxic T Cells Use Mechanical Force to Potentiate Target Cell Killing, Cell 165(1) (2016) 100-110.

[82] K.T. Bashour, A. Gondarenko, H. Chen, K. Shen, X. Liu, M. Huse, J.C. Hone, L.C. Kam, CD28 and CD3 have complementary roles in T-cell traction forces, Proc. Natl. Acad. Sci. U. S. A. 111(6) (2014) 2241-6.

[83] K.H. Hu, M.J. Butte, T cell activation requires force generation, J. Cell Biol. 213(5) (2016) 535-42.

[84] T. Chatila, L. Silverman, R. Miller, G. R., Mechanisms of T cell activation by the calcium ionophore ionomycin, J. Immunol. 143(4) (1989) 1283-9.

[85] Q. Han, N. Bagheri, E.M. Bradshaw, D.A. Haflerd, D.E. Lauffenburger, J.C. Love, Polyfunctional responses by human T cells result from sequential release of cytokines, Proc. Natl. Acad. Sci. U. S. A. 109(5) (2012) 1607-12.

[86] I. Olsen, L.M. Sollid, Pitfalls in determining the cytokine profile of human T cells, J. Immunol. Methods. 390(1-2) (2013) 106-12.

[87] T. Yahata, N. Abe, C. Yahata, Y. Ohmi, A. Ohta, K. Iwakabe, S. Habu, H. Yagita, H. Kitamura, N. Matsuki, M. Nakui, M. Sato, T. Nishimura, The essential role of phorbol ester-sensitive protein kinase C isoforms in activation-induced cell death of Th1 cells, Eur. J. Immunol. 29(3) (1999) 727-32.

[88] J.J. Boniface, J.D. Rabinowitz, C. Wülfing, J. Hampl, Z. Reich, J.D. Altman, R.M. Kantor, C. Beeson, H.M. McConnell, M.M. Davis, Initiation of signal transduction

through the T cell receptor requires the multivalent engagement of peptide/MHC ligands, Immunity 9(4) (1998) 459-66.

[89] M.A. Doucey, D.F. Legler, N. Boucheron, J.C. Cerottini, C. Bron, I.F. Luescher, CTL activation is induced by cross-linking of TCR/MHC-peptide-CD8/P56 lck adducts in rafts., Eur. J. Immunol. 31(5) (2001) 1561-70.

[90] Y. Li, R.J. Kurlander, Comparison of anti-CD3 and anti-CD28-coated beads with soluble anti-CD3 for expanding human T cells: differing impact on CD8 T cell phenotype and responsiveness to restimulation, J. Transl. Med. 8 (2010) 104.

[91] K. Mossman, J. Groves, Micropatterned supported membranes as tools for quantitative studies of the immunological synapse, Chem. Soc. Rev. 36(1) (2007) 46-54.

[92] A.J. Torres, R.L. Contento, S. Gordo, K.W. Wucherpfennig, J.C. Love, Functional single-cell analysis of T-cell activation by supported lipid bilayer-tethered ligands on arrays of nanowells, Lab Chip 13(1) (2013) 90-9.

[93] E. Judokusumo, E. Tabdanov, S. Kumari, M.L. Dustin, L.C. Kam, Mechanosensing in T lymphocyte activation, Biophys. J. 102(2) (2012) L5-7.

[94] K.L. Hui, Balagopalan, L.L.E. Samelson, A. Upadhyaya, Cytoskeletal forces during signaling activation in Jurkat T-cells, Mol. Biol. Cell 26(4) (2015) 685-95.

[95] M. Saitakis, S. Dogniaux, C. Goudot, N. Bufi, S. Asnacios, M. Maurin, C. Randriamampita, A. Asnacios, C. Hivroz, Different TCR-induced T lymphocyte responses are potentiated by stiffness with variable sensitivity, eLife 6 (2017).

[96] J.W. Hickey, Y. Dong, J.W. Chung, S.F. Salathe, H.C. Pruitt, X. Li, C. Chang, A.K. Fraser, C.A. Bessell, A.J. Ewald, S. Gerecht, H.Q. Mao, J.P. Schneck, Engineering an Artificial T-Cell Stimulating Matrix for Immunotherapy, Adv. Mater. 31(23) (2019) e1807359.

[97] R.S. O'Connor, X. Hao, K. Shen, K. Bashour, T. Akimova, W.W. Hancock, L.C.

Kam, M.C. Milone, Substrate rigidity regulates human T cell activation and proliferation, J. Immunol. 189(3) (2012) 1330-9.

[98] Y.C. Li, B.M. Chen, P.C. Wu, T.L. Cheng, L.S. Kao, M.H. Tao, A. Lieber, S.R. Roffler, Cutting Edge: mechanical forces acting on T cells immobilized via the TCR complex can trigger TCR signaling, J. Immunol. 184(11) (2010) 5959-63.

[99] J. Doh, D.J. Irvine, Immunological synapse arrays: patterned protein surfaces that modulate immunological synapse structure formation in T cells, Proc. Natl. Acad. Sci. U. S. A. 103(15) (2006) 5700-5.

[100] K. Shen, V.K. Thomas, M.L. Dustin, L.C. Kam, Micropatterning of costimulatory ligands enhances CD4+ T cell function, Proc. Natl. Acad. Sci. U. S. A. 105(22) (2008) 7791-6.

[101] K.D. Mossman, G. Campi, J.T. Groves, M.L. Dustin, Altered TCR signaling from geometrically repatterned immunological synapses, Science 310(5751) (2005) 1191-3.

[102] K. Shen, J. Tsai, P. Shi, L.C. Kam, Self-aligned supported lipid bilayers for patterning the cell-substrate interface, J. Am. Chem. Soc. 131(37) (2009) 13204-5.

[103] J. Deeg, M. Axmann, J. Matic, A. Liapis, D. Depoil, J. Afrose, S. Curado, M.L. Dustin, J.P. Spatz, T cell activation is determined by the number of presented antigens, Nano Lett. 13(11) (2013) 5619-26.

[104] P. Dillard, F. Pi, A.C. Lellouch, L. Limozin, K. Sengupta, Nano-clustering of ligands on surrogate antigen presenting cells modulates T cell membrane adhesion and organization, Integr. Biol. 8(3) (2016) 287-301.

[105] Z. Ma, T.H. Finkel, T cell receptor triggering by force, Trends Immunol. 31(1) (2010) 1-6.

[106] Y. Feng, K.N. Brazin, E. Kobayashi, R.J. Mallis, E.L. Reinherz, M.J. Lang, Mechanosensing drives acuity of alphabeta T-cell recognition, Proc. Natl. Acad. Sci.

U. S. A. 114(39) (2017) E8204-E8213.

[107] Z. Liu, Y. Liu, Y. Chang, H.R. Seyf, A. Henry, A.L. Mattheyses, K. Yehl, Y. Zhang, Z. Huang, K. Salaita, Nanoscale optomechanical actuators for controlling mechanotransduction in living cells, Nat. Methods 13(2) (2016) 143-6.

[108] P.A. Janmey, C.A. McCulloch, Cell mechanics: integrating cell responses to mechanical stimuli, Annu. Rev. Biomed. Eng. 9 (2007) 1-34.

[109] C. Hivroz, M. Saitakis, Biophysical Aspects of T Lymphocyte Activation at the Immune Synapse, Front. Immunol. 7 (2016) 46.

Chapter 2

2 Development of an automated microcontact printing method to obtain micropatterns on soft hydrogels

2.1 Introduction

In order to study how geometrical, mechanical and compositional parameters affect cellular states, a number of biomaterial-based platforms have been developed as model microenvironments with adjustable properties to be used for the study of cell responses. In most of these models, hydrogels with defined mechanical properties and decorated with ligands that can interact with membrane receptors and participate in mechanosensory cascades are used. These platforms have mainly been used to study the response of cells to the compositional and mechanical properties of the extracellular matrix (ECM).[1-6] In the last years, some of these methods have been employed to explore cell-cell interactions, especially during the IS formation in the context of T cells-APCs interaction.

In order to localize the geometry and composition of the interaction site on the biomaterial surface, protein patterning methods are used.[7-10] In the following some of these techniques are shortly described. Examples preferentially related to work with 2D cultures of cells (including immune cells) are described:

- Photolithography, also called optical lithography or UV lithography, transfers a geometrical pattern from a photomask to a photosensitive material, in most cases a polymeric photoresist using light exposure.[8, 11-14] After a developing process, the different surface chemistry between exposed and

non exposed regions generates a chemical pattern that can be exploited to immobilize different biomolecules. Using this technique Doh et al. even used a biotinylated photoresist to obtain bicompoment protein patterns of T cell receptor (TCR) ligands (anti-CD3) surrounded by a backfilled intercellular adhesion molecule-1 (ICAM-1) background to study T cell–APC interactions.[6]

- Colloidal lithography uses a colloidal monolayer on a surface as a template to obtain patterns, especially in nanoscale.[15, 16] The free surface areas are back-filled with a targeted molecule, and the protein pattern is formed after removing the nanospheres with a solvent.[17]

- Nanoimprinting lithography uses a rigid inorganic stamp to imprint topography into polymeric surface that is heated beyond the glass transition temperature. The imprinted pattern represents a physical relief which can be functionalized with a specific protein in a subsequent step.[8, 18]

- Electron beam lithography is a mask-less patterning technique that uses electron beam to scan over the surface to write a patterns at nanoscale resolution (5-10 nm). Christman et al. successfully prepared growth factors patterns on Poly(sodium 4-styrenesulfonate-co-poly(ethylene glycol) methacrylate) (pPEGMA) films with this method.[19]

- Photopatterning of molecular layers of photoactivatable molecules. This methodology makes use of photoinduced reactions, such as bond cleavage,[20, 21] thiol-ene addition,[22, 23] Michael-addition [24] and cycloaddition,[25] or photodegradation reactions [26] and photogenerated surface charge changes [27] to selectively immobilize proteins or peptides on substrates. For instance, photo-activatable cell adhesive peptides (cRGD, laminin peptidomimetic IKVAV, etc.) have been used to create patterns with

selective cell adhesion by UV light exposure. Using a photoregulated charge change or a photogenerated aldehyde, a protein pattern that mediated selective cell adhesion to a hydrogel has also been realized.[26, 27]
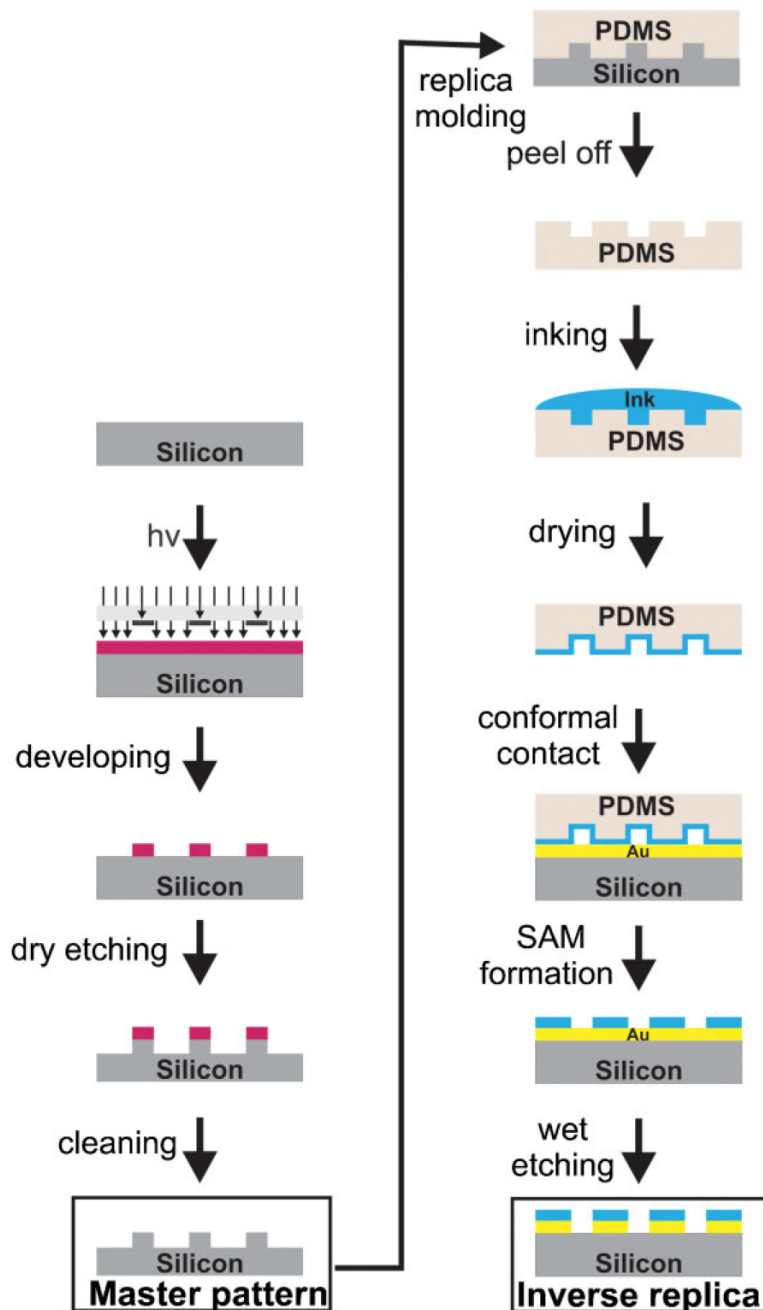
Scheme 1. Schematic comparison of photolithography versus microcontact printing. The crucial step in both techniques consists of the accurate transfer of the patterned etch-resist layer. Copyrights Wiley-VCH Verlag GmbH & Co. KGaA.[7]

- The microcontact printing method uses a poly(dimethylsiloxane) (PDMS) elastomeric stamp to transfer a protein pattern from the stamp to different substrates (Scheme 1).[7, 28] The microcontact printing method involves 3 steps: First, PDMS stamps are prepared by replicating the patterns from a rigid template, normally generated by photolithography. Second, the stamp is immersed into the protein solution (ink) and is brought in contact with the surface to be patterned for a certain time and at controlled pressure. Finally, the stamp is removed from the substrate, and the inked molecules remain anchored to the substrate surface reproducing the geometry of the stamp. Many studies have used this method to prepare patterned surface to regulate a variety of cell behaviors such as cell adhesion,[29] differentiation,[30] and division.[31]

Microcontact printing, as a facile, efficient, and inexpensive technique, has become widely used for functional patterned surfaces fabrication on a range of substrates from rigid glass and polystyrene to soft materials such as PDMS and hydrogels. Patterns with submicron dimensions can be obtained. The quality of the microcontact printed patterns depends on several parameters:

- The rigidity of the PDMS stamp plays a role for pattern resolution. Stamp deformation, which can happen during contact or stamp removal from the template, determines the resolution limits of this technique.[32-34] The height of the stamp divided by their lateral dimensions is taken as the aspect ratio of a pattern. A high aspect ratio always leads to a buckling and lateral collapse of

the stamp features, whereas roof collapse takes place when at low aspect ratios.[33, 35] In addition to the careful design of the stamp features, the contact pressure applied on PDMS stamp should also be precisely controlled to avoid the excessive deformation of the stamp.

- The solvents used for the preparation of inked molecules solutions can also influence the microcontact printing process since many organic solvents can make the PDMS stamp swell more ore less, changing the dimensions of the stamp feature.[36] Ethanol is preferably used as the inks solvent because it has a minimal swelling effect on the PDMS.[37]

- PDMS has a low surface energy and water-soluble inks do not wet the PDMS surface. The PDMS surface oxidation (with oxygen plasma, for example) allows the printing of such polar inks owing to the polar and hydrophilic thin silica-like surface layer generated from oxidation.[38] Nevertheless, this silica-like layer can create cracks on the surface because it has different mechanical properties from PDMS itself. These cracks can lead to unexpected topography on printed surface and the recovery of the hydrophobicity of their surface,[38, 39] which largely limits the applicability and reuse of PDMS stamp.[40, 41]

- The viscosity of the inks also plays a role, as inks can spread from the edge of the contact area to the other areas,[42, 43] especially when sub-micrometer features are prepared.

- The printing time, the ink concentration on PDMS stamp, as well as the vapor pressure, temperature, and surrounding humidity also affect the patterning results.[7, 44, 45]

When the surface to be patterned is very soft and deformable, like in the case of hydrogels, the microcontact printing is more challenging. In that case, chemical and

technical issues need to be considered. From the chemical point of view, the hydrogel surface requires to be modified so that the microcontact printed molecules can stably bind to it. To this end, Tay et al. [30] used the photoactivatable reagent sulfo-SANPAH to mediate cross-linking of microcontact printed fibronectin onto polyacrylamide (PAAm) hydrogel surfaces. Lee et al. [46] and Mao et al. [47] converted amide groups into reactive hydrazide groups in PAAm by using hydrazine hydrate in order to react with microcontact printed glycoproteins. N-hydroxyethylacrylamide monomer was copolymerized with PAAm to enhance hydrophilicity of the PAAm network and obtain improved protein patterns on the hydrogel surface.[2, 29] On the technical side, achieving a conformal contact between soft substrates and stamps is a major issue when microcontact printing is performed manually. In most cases the air-dried hydrogel surface is brought in contact with stamp by placing a weight onto the PDMS stamp.[48] Alternatively, inked PDMS stamps can be dried first and then gently applied on hydrogel surface directly.[29] Microcontact printing on freeze-dried hydrogels has also been reported.[49] Manual operation, however, requires a skillful operator able to adjust the stamping force adequately.[50] Otherwise, the backing of the over-deformed stamp can contact the substrate surface, or the insufficient-deformed stamp fails to contact well with substrate surface, resulting in an unsuccessful printing.[51] This limits the reproducibility of the microcontact printing process. Automated systems overcome this limitation [52] and lead to more uniform and homogenous patterns.

In this chapter, the optimization of an automated method to microcontact print protein patterns on biotinylated polyacrylamide-co-polyacrylic acid (PAAm-co-AA) hydrogels (stiffness of 2, 12, and 50 kPa) is described. A pneumatically-controlled and commercial available microcontact printer was used for the printing process. Patterns of streptavidin and other biotinylated proteins (anti-CD3) were successfully obtained

on our substrates. Multistep printing process was optimized to achieve multiprotein patterns (anti-CD3/ICAM-1) on the same substrate surface as mimetic IS arrays. The biofunctionalities of anti-CD3 and anti-CD3/ICAM-1 patterns on hydrogels were tested with Jurkat T-cells and results demonstrated our platforms could be used for T cell mechanotransduction studies.

2.2   Results and discussion

2.2.1 Preparation of PAAm hydrogels of different stiffness and biotinylation

As mechanically defined substrates for interacting with the cells, PAAm-co-AA hydrogels discs were prepared by copolymerization of AAm monomer with bis-AAm crosslinker and AA (Figure 1) between two coverslips following reported protocols.[53] A constant AA/AAm ratio 10% was used for all hydrogel monomer mixture (Table 1) to keep a comparable AA density in all hydrogels. By tuning the bis-AAm/AAm ratio from 0.25% to 4.17%, hydrogels with different Young's Modulus (stiffness) between 2 and 50 kPa were obtained (Figure 2A,B).
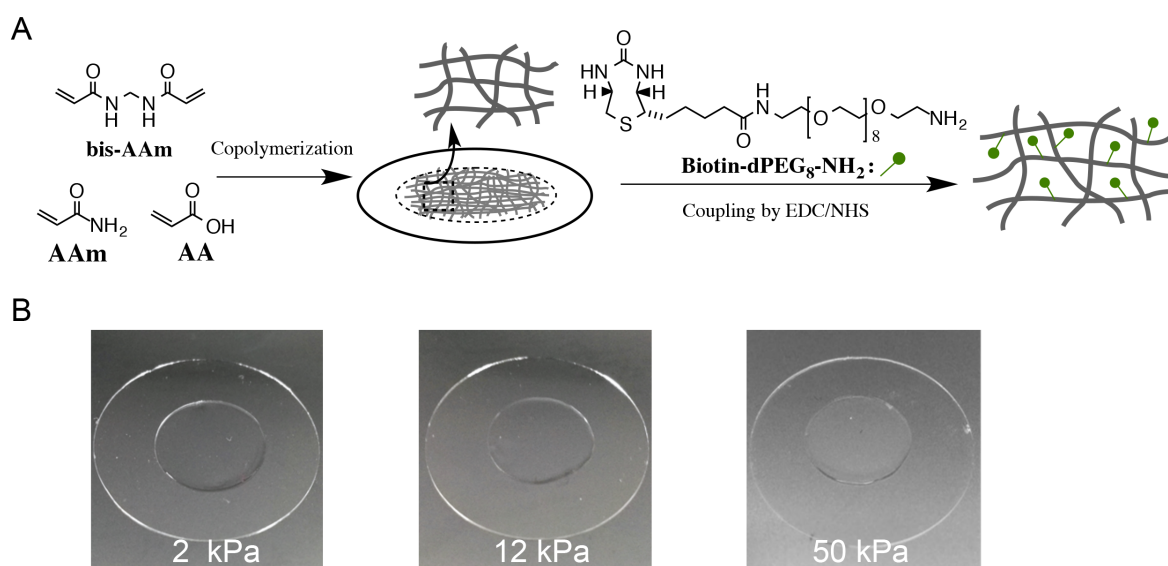
Figure 1. (A) Schematic diagram to show the preparation and biofunctionalization of PAAm-co-AA hydrogel with different stiffness. (B) Images to show hydrogels formed between 3-APS-silanized coverslips (25 mm) and Sigmacote-coated slides (13 mm).

Table 1. Composition of PAAm-co-AA hydrogels (in total volume of 5 mL PBS) and corresponding Young's Modulus values as measured by AFM indentation.

AAm (mg)	bis-AAm (mg)	AA (μL)	bis-AAm/AAm ratio (%)	AA/AAm ratio (%)	Young's Modulus E (kPa)
600	1.5	30	0.25	5	2.0
600	2.5	30	0.42	5	5.2
600	5.5	30	0.92	5	11.6
600	10	30	1.67	5	18.9
600	17.5	30	2.92	5	31.4
600	21	30	3.50	5	38.0
600	25	30	4.17	5	50.0
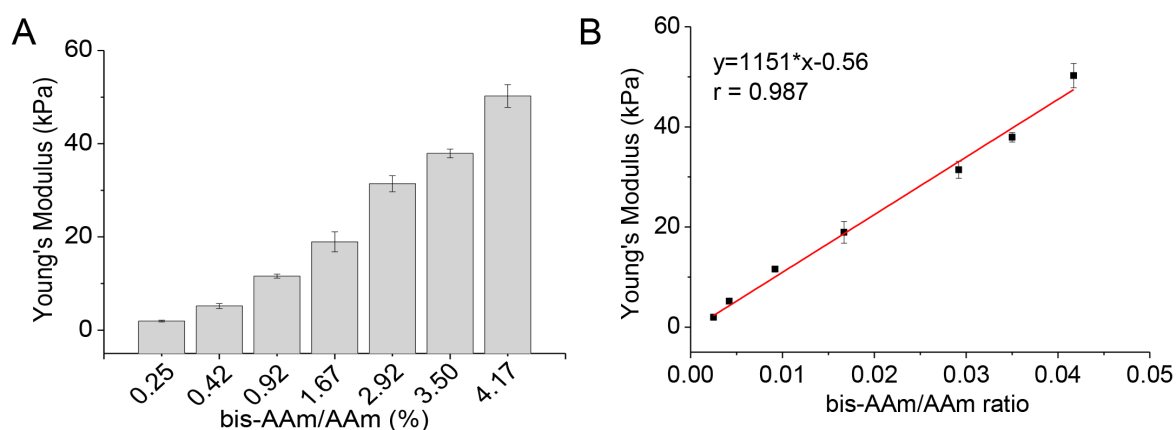
Figure 2. (A) Young's Modulus of PAAm-co-AA hydrogels as a function of

bis-AAm/AAm ratios. (B) The Young's Modulus of hydrogels is linearly correlated with bis-AAm/AAm ratio.

The Young's Modulus of the gels was measured by atomic force microscope (AFM) by recording force vs. indentation depth data. Hydrogels with Young's Modulus of 2, 12, and 50 kPa were used for further studies. Anti-CD3 functionalized hydrogels, which will be used in the following T cell experiments, showed no significant changes compared with hydrogels before functionalization in stiffness (Figure 3A). The swelling ratio of the hydrogels was determined by using a gravimetric method. Swelling ratios of 14.2, 13.1 and 9.8 were obtained for hydrogels with stiffness of 2, 12, and 50 kPa, respectively (Figure A1). The thickness of the hydrogels was measured by confocal microscope after functionalization with the dye pararosaniline base (Figure 3B,C). The z-axis scan imaging across the hydrogel thickness showed a homogeneous fluorescence distribution (Figure 3B), indicating that AA was uniformly copolymerized through the film. Hydrogel films with thickness between 70 and 80 μm (swollen state, Figure 3C) were targeted by adjusting the volume of the monomer mixture (Table A1). This hydrogel thickness here guarantees that the cells do not feel the mechanical properties of the underlying glass surface [54, 55].

PAAm-co-AA hydrogels were further biotinylated for the binding of streptavidin and then other biotinylated proteins on the surface. The PAAm-co-AA film was activated by EDC/NHS (39/12 mg/mL), followed by modification with biotin-PEG$_8$-NH$_2$ (1 mg/mL) solution for 2 h at room temperature. The biotinylated hydrogels can be directly used for the binding of streptavidin with or without micropattering.
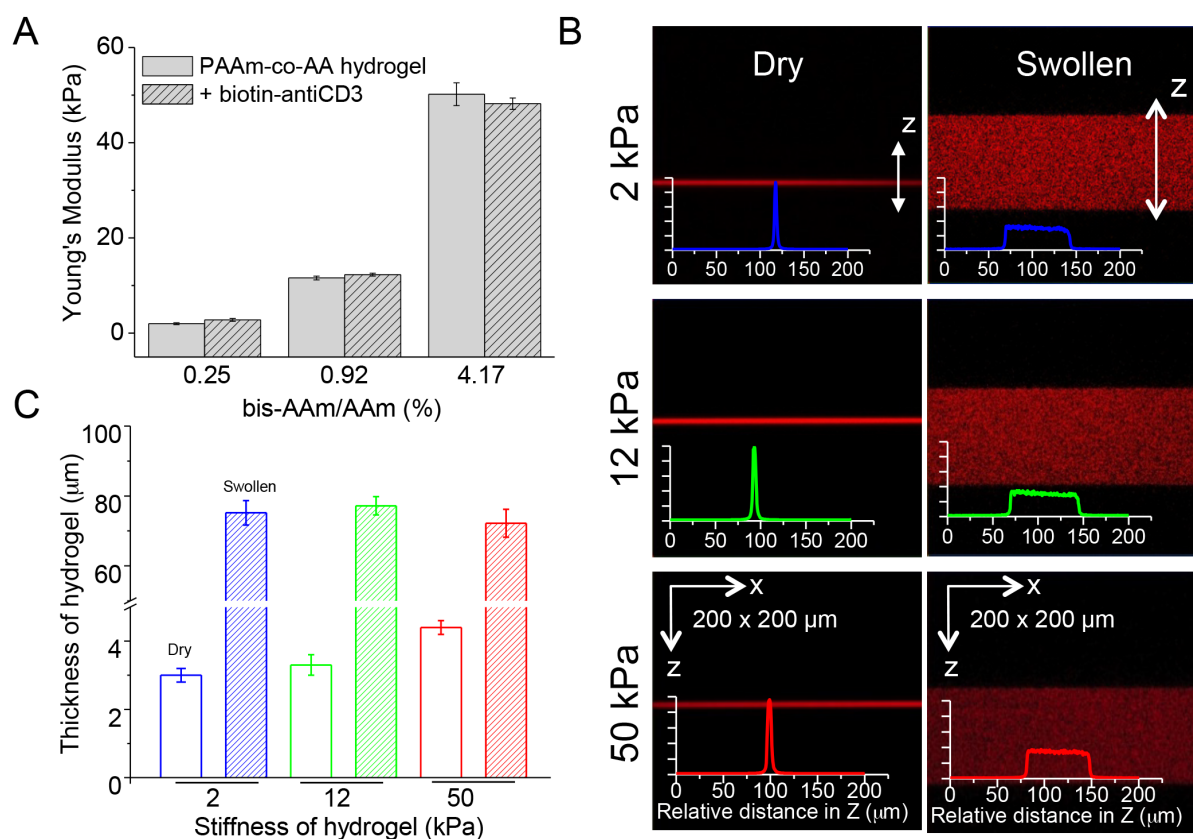
Figure 3. Young's Modulus and thickness measurement of hydrogels with different stiffness (2, 12, and 50 kPa). (A) Young's Modulus (taken as stiffness here) of hydrogels before and after functionalization with biotin-antiCD3. n=128. (B) Fluorescence images and intensity profiles of pararosaniline-modified hydrogels after z-axis scan imaging by confocal microscope. Both the dry (left) and swollen hydrogel (right) were measured. (C) Quantification of the thickness of hydrogels in both dry (empty boxes) and swollen (stripe boxes) states. n=10. Three independent experiments were used for statistical analysis. Data are presented as mean ± SD.

2.2.2 Optimization of the automatized microcontact printing process for obtaining streptavidin patterns on hydrogels of different stiffness

In order to obtain homogeneous and reproducible micropatterned protein arrays on

the soft biotinylated PAAm hydrogels (2-50 kPa), an experimental protocol for automated microcontact printing was established. To this end, a commercial microcontact printer (μCP 4.1, GeSiM mbH) was used here and self-made PDMS stamps were prepared. PDMS stamps were obtained by double soft molding from a lithographic master with the help of cast station system (Figure A2, 4A), which makes it possible to perform the subsequent automated microcontact printing by our system. The stamp has a 10 x 10 mm^2 patterned field with 5 μm square patterns separated by 5 μm or 5 x 5 mm^2 patterned field with dots of 5, 6, and 8 μm diameter separated by 5, 30, and 35 μm, respectively. In the following text, the critical steps of the microcontact printing will be described.

The typical steps and key components of the microcontact printing are represented in Figure 4B,C. The biotinylated hydrogel supported by glass slides were dried before the printing process in order to improve their mechanical stability for withstanding the printing procedure and to avoid sticking, slip, or breaking of hydrogel. PDMS stamps were treated with oxygen plasma (0.3 Mbar, 2 min) and then inked with streptavidin solution (100 μg/mL, 20 μL for 10 $\times$ 10 mm^2 and 10 μL for 5 $\times$ 5 mm^2 PDMS stamp) immediately for 0.5 h at RT followed by drying with clean N$_2$. The relative position of the PDMS stamp to the dried hydrogel surface were calibrated by the height sensor installed in the printing head of microcontact printer, and then the PDMS stamp could be precisely brought to contact with hydrogel film. A defined printing pressure was applied to the PDMS stamp for a certain time to transfer the protein to the hydrogel surface. Finally, the micropatterned surface could be used directly or further functionalized with another ligand followed by biotin-PEG blocking.
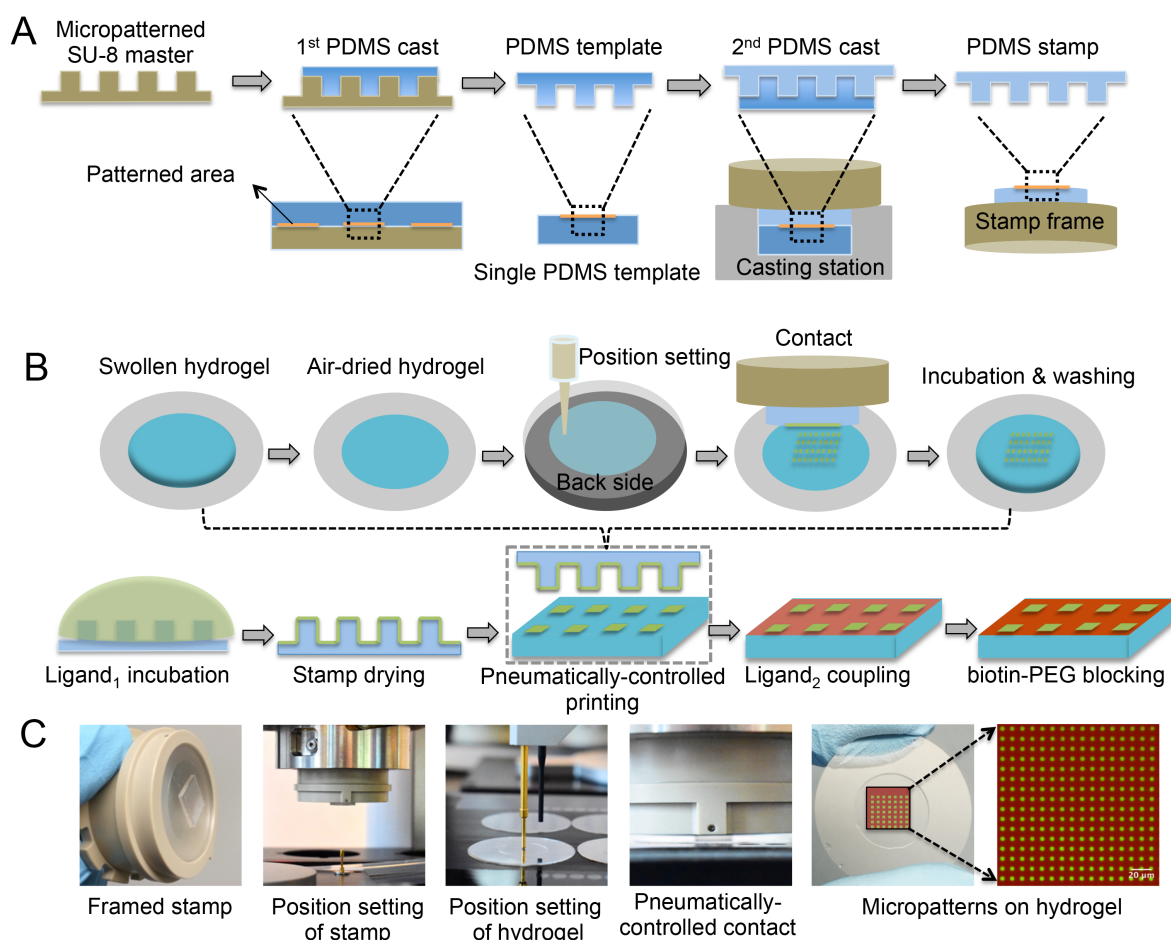
Figure 4. Surface micropatterning of hydrogels by a pneumatically-controlled microcontact printer. (A) Process flow to show the preparation of PDMS stamp molded in a stamp frame for microcontact printing. A conventionally fabricated SU-8 master is replicated by pouring liquid PDMS prepolymer onto the master followed with curing. The formed PDMS film (negative) is released and then cut into right size to serve as a template to generate a new PDMS stamp (positive) in a stamp frame after a second PDMS casting. (B) Schematic diagram to show the micropatterning process on hydrogel surface. After hydrogel polymerization and biotinylation, hydrogels were air-dried to enable the application of the microcontact printing technique, then the relative heights of dry hydrogel and PDMS stamp were set by specific sensors. PDMS stamp was inked in ligand solution (streptavidin or antibody) for 1 h and then semi-dried for the ligand (streptavidin) transfer. Afterwards, stamp was brought to

contact with hydrogel in a pneumatic way with specific printing pressure and dwell time. Another ligand (biotinylated molecule) could be further modified on the remaining unpatterned area. Finally, the hydrogel was blocked with biotin-PEG and used for cell culture. (C) Bench-scale examples of key microcontact printing steps, illustrating bench-level implementation.

In order to optimize the printing parameters, the system was first tested using a PDMS stamp containing 5 μm square pillars (height of 5 μm) with a gap of 5 μm. A concentration of 100 μg/mL streptavidin-594 solution was used as ink for the straightforward micropatterning of protein on hydrogels. As shown in Figure 5, fluorescent images of micropatterned streptavidin were clearly obtained on biotinylated hydrogels of different stiffness (2, 12, and 50 kPa). Under optimized conditions, homogenous arrays of 5 μm squares were observed on biotinylated hydrogels, indicating an effective transfer of streptavidin from PDMS stamp to the hydrogel with our method. It should be noted that the micropatterned streptavidin was inhomogenous on hydrogel without biotinylation (Figure A3). Moreover, the fluorescence intensity profile of micropatterned streptavidin in the x-y plane was similar on all hydrogels, independently of the mechanical properties of hydrogels (Figure 5A,B). The dimensions of the micropatterned fields and the protein density were maintained after reconstitution of the hydrogels in PBS buffer. Note that the edges of the patterned features were sharply defined, even on the soft (2 kPa) hydrogel across the whole field. Z stack imaging across the swollen hydrogel film revealed that the fluorescent signal from the streptavidin was restricted within the top 4-5 μm layer of the hydrogels (Figure 5C), indicating that streptavidin are stably and selectively immobilized at the printed surface.
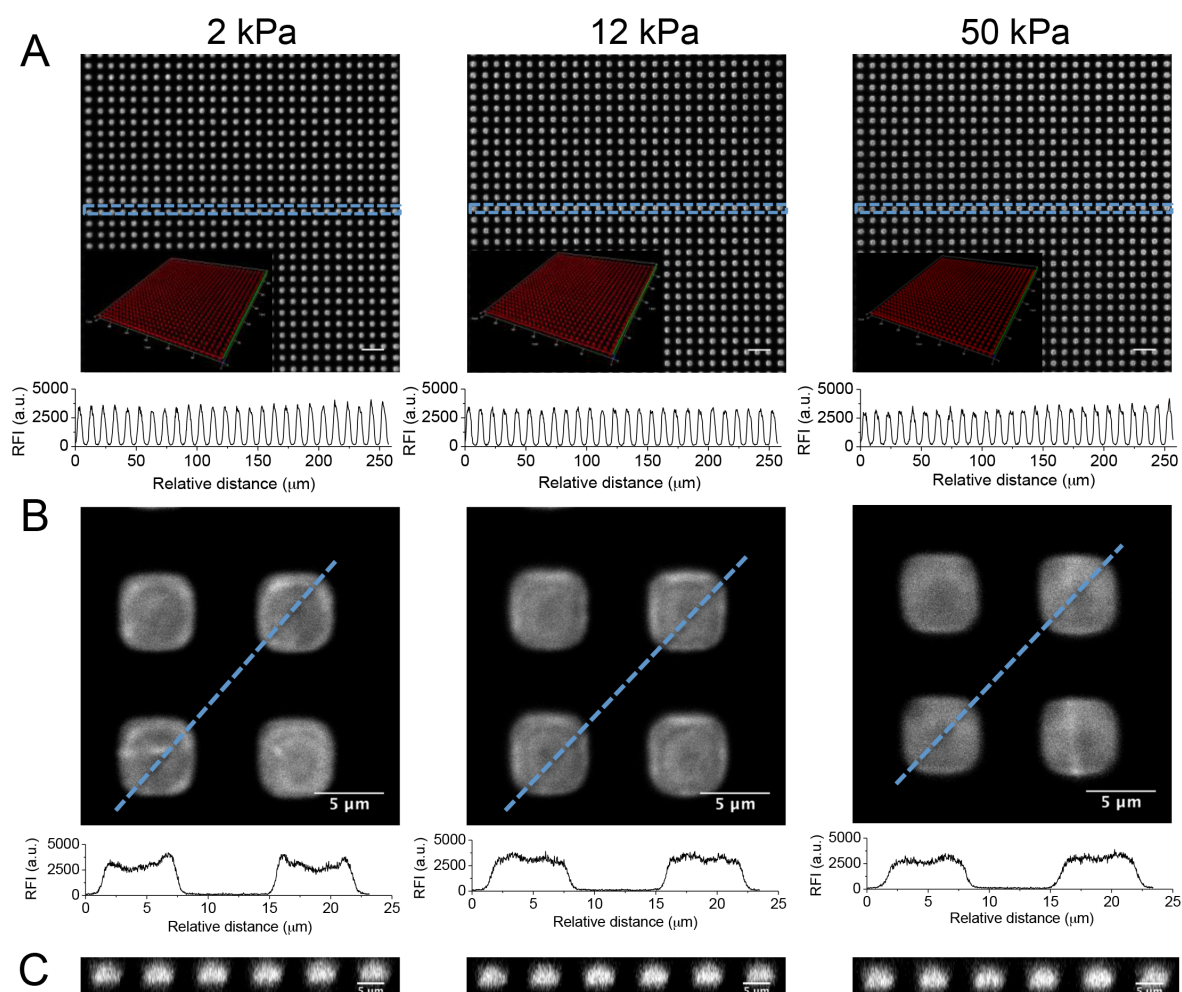
Figure 5. Fluorescence images to show micropatterned streptavidin-594 on hydrogels of 2, 12, and 50 kPa. (A) Homogeneous streptavidin-594 patterns with 5 μm squares on gels of different stiffness. Scale bar 20 μm. Lower panel shows the fluorescence intensity profiles. (B) Zoom-out from images in (A) showing the fluorescence images and intensity profiles at higher magnification. (C) Reconstructed Z stack images of micropatterned hydrogels revealing the streptavidin distribution in the hydrogel (confined to the top 4-5 μm).

Different experimental parameters were tried during the optimization of microcontact printing process on the hydrogels. In the following, the influence of the printing

pressure, the contact time, and the drying of hydrogel and inked stamp on the micropatterning will be shortly described. Increasing printing pressure from 8 to 12 kPa (contact time was kept for 5 min) enhanced the transfer efficiency of the streptavidin, as indicated by the higher fluorescence intensity on the hydrogel with increasing printing pressure (Figure 6A). A higher printing pressure (15 kPa) however did not lead to a higher fluorescence intensity, indicating that 12 kPa printing pressure is already sufficient for the efficient transfer of streptavidin from PDMS stamp to hydrogel surface within 5 min (Figure 6A).
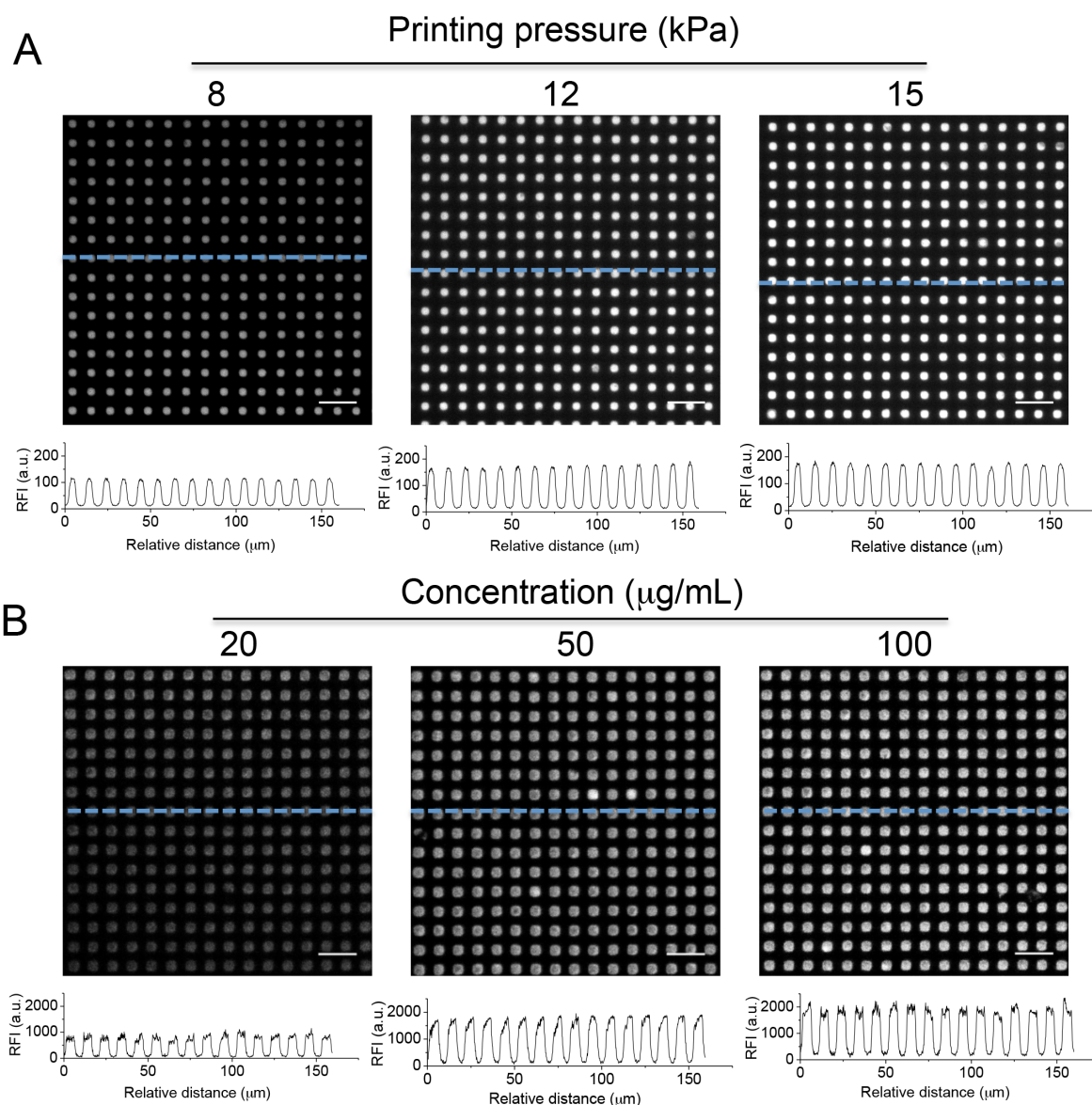
Figure 6. (A) Fluorescence images of micropatterned streptavidin-594 generated under varying printing pressure (8, 12 and 15 kPa) and corresponding fluorescence intensity profiles on hydrogel (50 kPa). Scale bar, 20 μm. (B) Fluorescence microscopy images to show micropatterned streptavidin-488 generated with increasing concentrations (20, 50, and 100 μg/mL) of inking solutions. The Corresponding fluorescence intensity profiles on hydrogel are shown in the lower panel. Scale bar, 20 μm.

We further tested whether this method allows a controlled variation of the protein density on the hydrogel surface. Micropatterned streptavidin on 50 kPa hydrogel were prepared by using PDMS stamp inked with different concentrations (20, 50, and 100 μg/mL) of streptavidin-594. Homogenous micropatterned streptavidin were obtained in all three conditions. A higher fluorescence intensity of micropatterned streptavidin was observed on substrate using more concentrated inking solution, indicating that the streptavidin density on hydrogel surface can be tuned by adjusting the inking concentration of streptavidin (Figure 6B). Micropatterned arrays generated with 50 and 100 μg/mL inking solutions lead to a similar fluorescence density, indicating that it might reach a saturation level of streptavidin transfer with our method here.

The transfer efficiency of streptavidin was also increased by increasing the contact time from 0.5 to 5 min, as revealed by the stronger fluorescence of micropatterned streptavidin on hydrogel (Figure 7). Longer contact times (10 min) did not lead to higher fluorescence intensity (Figure 7, right).

Printing time (min)

| 0.5 | 1 | 5 | 10 |
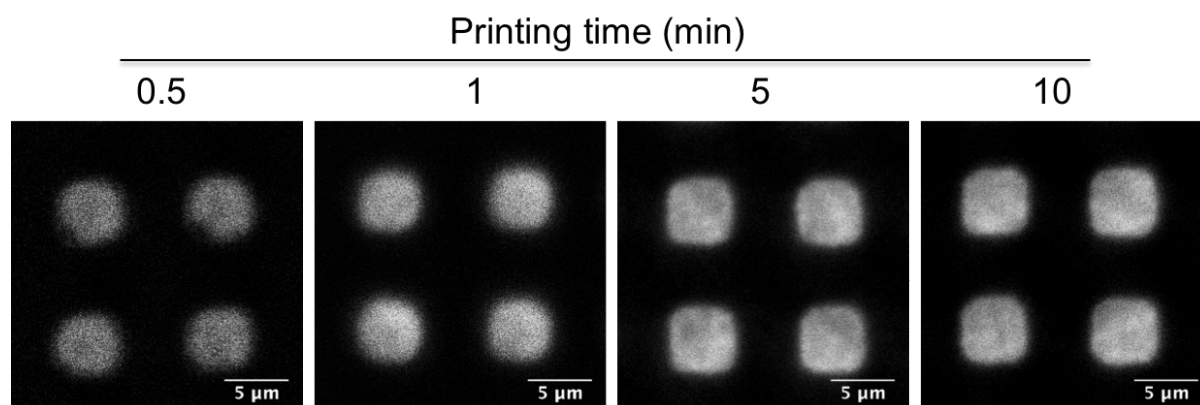
Figure 7. Fluorescence images of micropatterned streptavidin-594 and corresponding fluorescence intensity profiles on hydrogel (50 kPa) generated under different printing time.

The drying step of the ink on the stamp could also affect the quality of the micropatterned surface. The best micropatterns were obtained when the stamp was dried horizontally using a gentle N_2 flow (ca. 5 bar). If the stamp was dried vertically with a strong N_2 flow ($\geq$ 10 bar), defects in the micropatterns would be obviously observed (Figure 8). The dryness of inked stamp also has a significant effect on the performance of micropatterned protein. Both insufficient-drying and over-drying of the inked stamp could result into patterns with defects (Figure A4). Drying the hydrogel film before microcontact printing (15-20 min in fume hood) is also required to obtain micropatterned surface with a good quality.
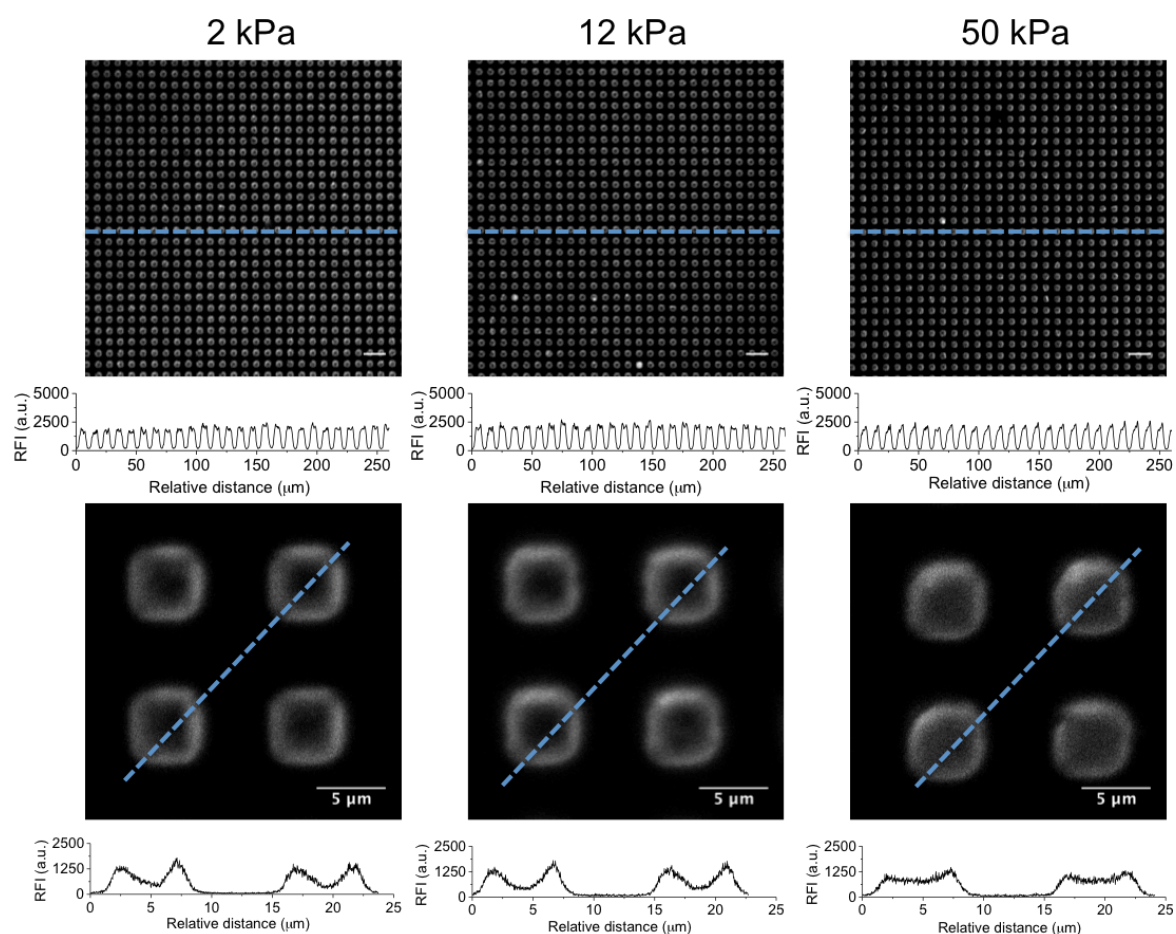
Figure 8. Fluorescence images of micropatterned streptavidin-594 generated by drying stamp vertically with N_2 flow and corresponding fluorescence intensity profiles on hydrogel (50 kPa).

We also tested the possibility to obtain multicomponent protein patterns on the hydrogel. In a first attempt, micropatterned streptavidin-488 surface were back-filled with streptavidin-647. Uniform micropatterned streptavidin-488 (5 x 5 μm^2 squares) and streptavidin-647 background was obtained in a 200 x 200 μm^2 area on all hydrogel surfaces (Figure 9A). The fluorescence intensity of back-filled streptavidin-647 was also shown to be independent of the Young's Modulus of hydrogel (Figure 9B). This indicates that the functionalization of the hydrogel with streptavidin (both printed and backfilled) might be determined by the biotin in

hydrogel, which could be similar in all hydrogels since the concentration of AA that used for biotin coupling is kept the same, rather than by the mechanical properties of hydrogels. Both the micropatterned and backfilled streptavidin distributed within the top 4-5 μm layer of the hydrogels, as indicated by the reconstructed z-stack images of hydrogels (Figure 9B). In addition, micropatterned streptavidin-488 (dots with 5 μm diameter) and streptavidin-647 (5 μm squares) were also successfully prepared on the hydrogels by sequential microcontact printing steps. It showed that both the micropatterned dots and squares were well defined and uniform across the surfaces of all hydrogels tested here (Figure 9C). In conclusion, these experiments demonstrate the possibility to create complex and uniform protein micropatterns on hydrogels by our method.
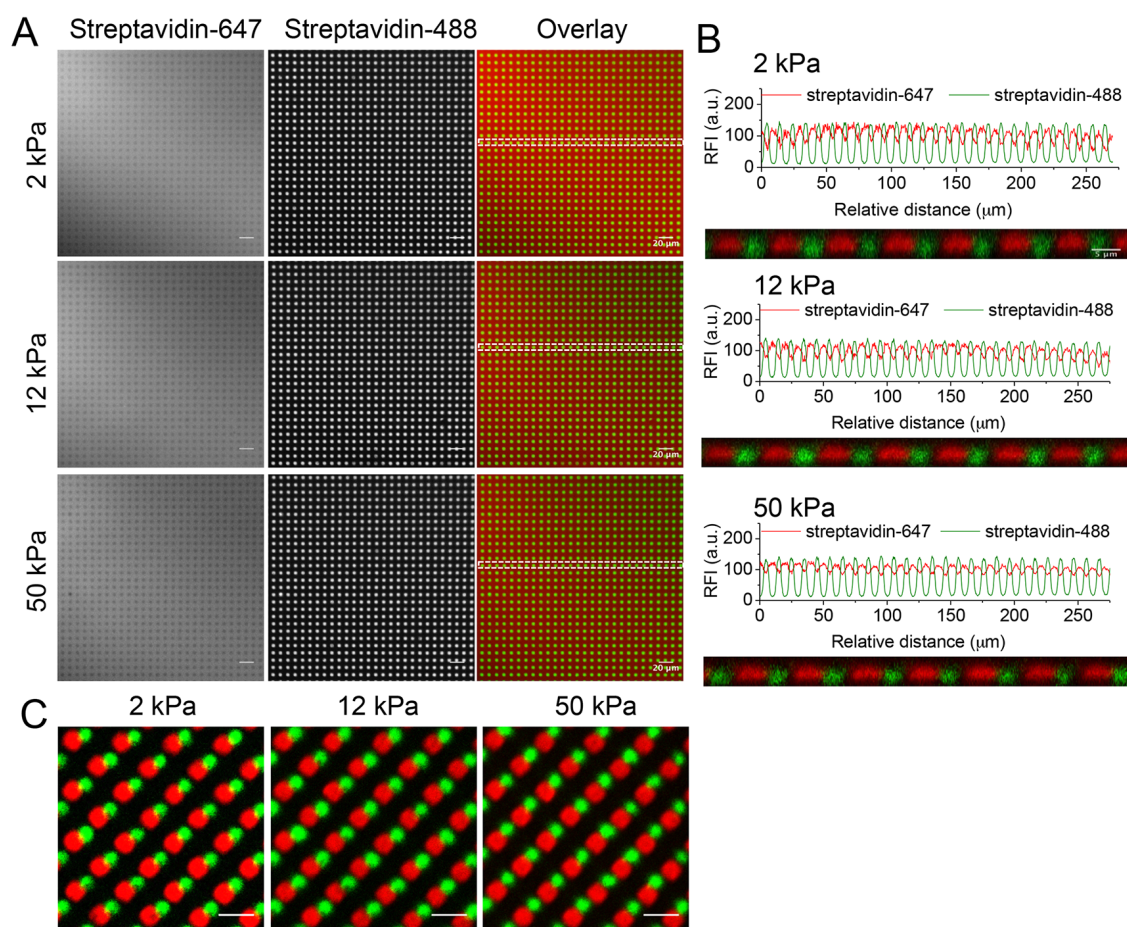
Figure 9. Preparation of multicomponent protein (streptavidin) patterns on the hydrogel of different stiffness. (A) Fluorescence microscopy images of micropatterned streptavidin-488 (5 µm squares) on hydrogels backfilled with streptavidin-647. (B) The fluorescence intensity profiles across the array showing the uniform and comparable surface density of protein in the patterned sites across the surfaces of the hydrogels with different stiffness. The Z stack image across the reconstructed hydrogels shows the penetration depth of the protein inside the gel. (C) Fluorescence images to show sequential micropatterned streptavidin-488 (5 µm dots) and streptavidin-647 (5 µm squares) on hydrogel of different stiffness. Before printing, the biotinylated hydrogels were functionalized with streptavidin. Scale bar, 10 µm.

2.2.3 Anti-CD3 micropatterns by conjugation to microcontact printed streptavidin

We further used the micropatterned streptavidin to mediate the site-specific immobilization of biotinylated proteins. For this purpose, micropatterned streptavidin (dots with 8 µm diameter) was incubated with biotinylated anti-CD3 (100 µg/mL, 100 µL), which can recognize CD3 co-receptor in TCR/CD3 complex to initiate T cell activation. After that, PE-anti-IgG was further incubated to label anti-CD3 for the visualization of anti-CD3 pattern. Uniform fluorescence was obtained across the micropatterned areas (Figure 10A). Moreover, a similar fluorescence signal, as measured by the mean fluorescence intensity of micropatterned area, was observed on all hydrogels independent of the Young's Modulus (Figure 10B). These results indicate that the micropatterned streptavidin can be used for the specific binding of biotinylated anti-CD3 at concentration dependent on the streptavidin ink, and independently of the Young's Modulus of the hydrogel.

We also tested the biological activity of the immobilized anti-CD3 by incubating a

pattern of biotinylated anti-CD3 with Jurkat cells. Micropatterned streptavidin (dots with 8 μm diameter) was functionalized with biotinylated anti-CD3 (labeled with Alexa Fluor 555) as mentioned above. Attachment of Jukart cells to the anti-CD3 areas was observed on all hydrogels 30 min after seeding (Figure 10C), indicating that the immobilized anti-CD3 on micropatterned streptavidin can be recognized by CD3 co-receptor on T cell surface. This assay confirms the bioactivity of the immobilized anti-CD3 ligand on the surface of streptavidin-patterned hydrogels. Similarly, this platform can be further used for T cell studies, especially T cell mechanotransduction studies, which will be presented in the following chapters.
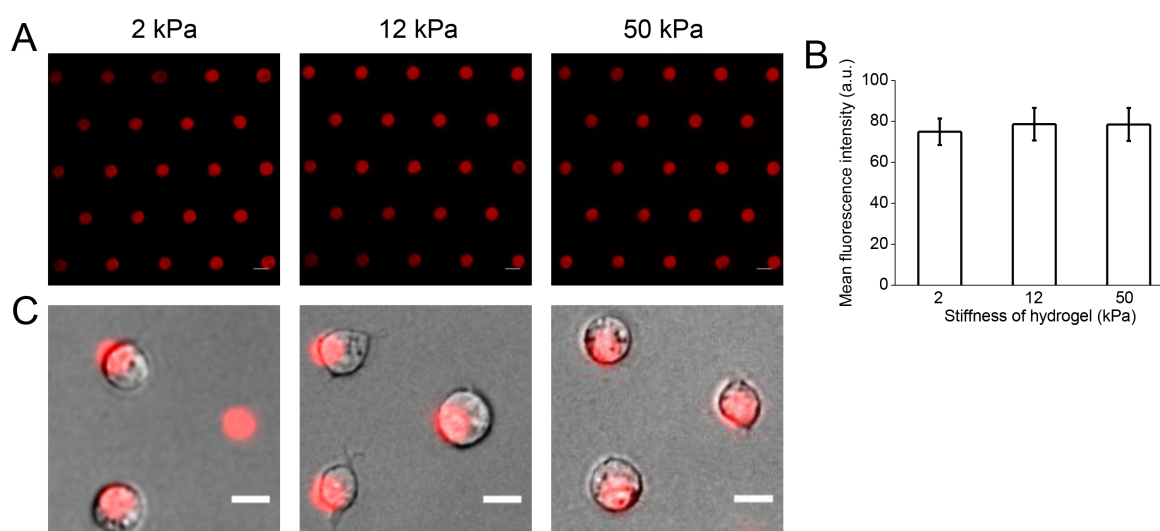
Figure 10. Anti-CD3 micropatterns by conjugation to microcontact printed streptavidin and its bioactivity test with Jurkat T-cell. (A) Micropatterned anti-CD3 (dots with 8 μm diameter) on hydrogel surface as revealed by labeling using PE-anti-IgG. (B) Mean fluorescence intensity of PE-anti-IgG on hydrogels of different stiffness. (C) Recognition of micropatterned anti-CD3 (labeled with Alexa Fluor 555) by Jurkat T-cell 30 min after cell seeding. Scale bar, 10 μm.

2.2.4 Bifunctional anti-CD3/ICAM-1 patterns on hydrogels

An alternative method was used to prepare bicomponent protein patterns on hydrogels. Specifically, biotinylated hydrogels were firstly incubated with streptavidin and then microcontact printed with biotinylated anti-CD3. Uniform micropatterned anti-CD3 dots (labeled with Alexa Fluor 555) with 6 μm diameter were successfully prepared on the hydrogels (Figure 11A). Quantification analysis further demonstrated that the density of micropatterned anti-CD3 was similar on all hydrogels, as measured by the mean fluorescence intensity (Figure 11B).

In order to introduce ICAM-1 ligand, a ligand recognized by LFA-1 to mediate the adhesion between T cells and antigen presenting cells, around anti-CD3 pattern, as it appears in the natural IS, the micropatterned anti-CD3 surface (dots with 6 μm diameter) was further back-filled with ICAM-1. For this purpose the anti-CD3 patterned hydrogel was first incubated with biotin-anti-Fc to backfill the streptavidin background of a 50 kPa hydrogel pre-patterned with anti-CD3 and then incubated with ICAM-1-Fc labeled with Alexa Fluor 488. Homogeneous ICAM-1-Fc fluorescence signal was visible on the background of micropatterned anti-CD3 surface (Figure 11C), indicating the selective immobilization of the two proteins on the hydrogel. To further verify the biological function of the mimetic IS surface, Jurkat cells were seeded on the bifunctional patterns. Cells attached to the mimetic IS surface centered on micopatterned anti-CD3 (dots with 6 μm diameter), validating the bioactivity of the mimetic IS surface to support T cell adhesion (Figure 11D). Furthermore, Immunostaining of pTyr and pZap70, which was used as early marker of T cell activation, indicated that Jukart T-cells can be activated by this mimetic IS surface (Figure 11D).

In the future, this platform could be further developed as more advanced mimics of APCs to study how T cell activation is regulated by spatially organized anti-CD3 and

ICAM-1 on hydrogel of different stiffness.
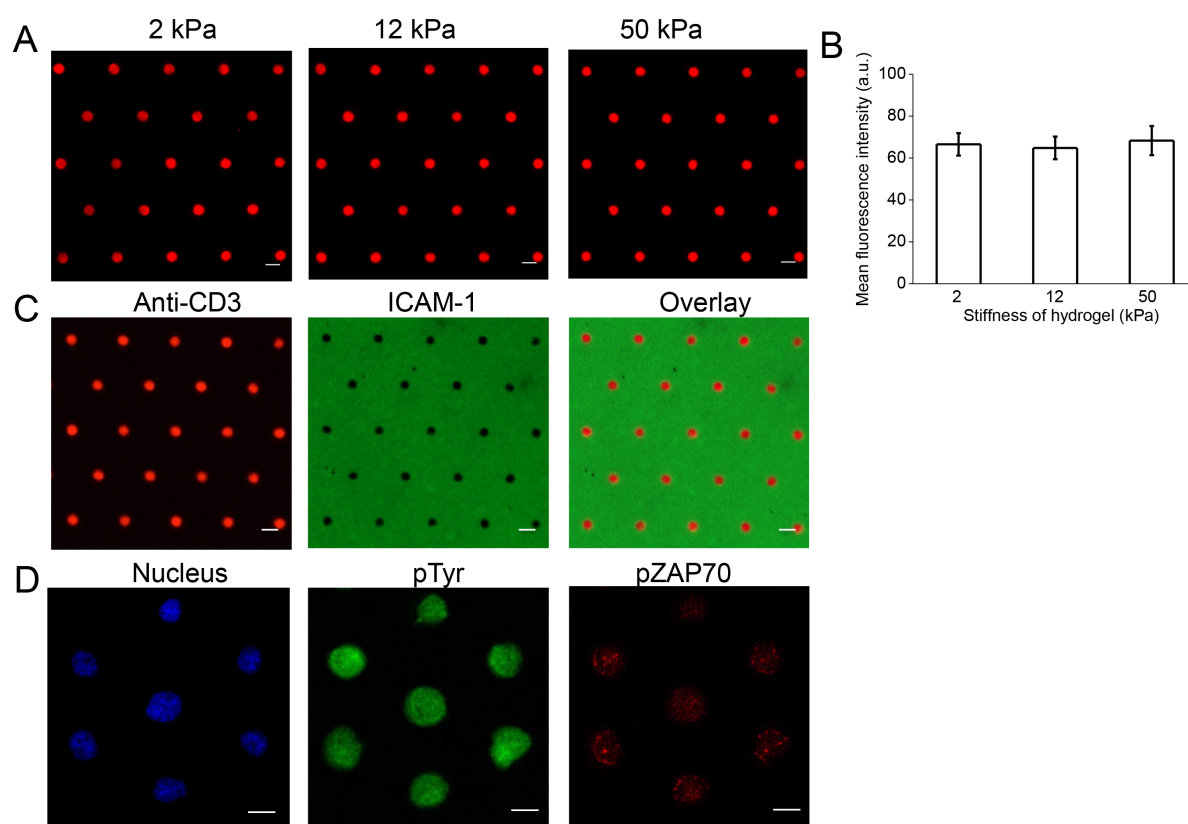
Figure 11. Micropatterned anti-CD3/ICAM-1 on hydrogel surfaces as mimics of the ligand arrangement at the IS. (A) Fluorescence images of microcontact printed dot arrays (6 μm diameter) of anti-CD3 on hydrogels of different stiffness. (B) Mean fluorescence intensity of micropatterned anti-CD3 dots on hydrogels of different stiffness. (C) Micropatterned anti-CD3 dot pattern with and ICAM-1 background on 50 kPa hydrogel (D) Attachment of Jurkat cells to anti-CD3/ICAM-1 micropatterns and immunostaining images of pTyr and pZAP70 signals 15 min after cell seeding. Scale bar represents 10 μm.

2.3   Conclusion

A method to pattern proteins on soft biotinylated PAAm hydrogels of Young's Modulus 2, 12 and 50 kPa using an automated microcontact printing system was successfully established. The geometry, and protein density in the patterns was tuned by the geometry of the stamp and the concentration of the protein ink and other printing parameters (printing pressure, printing time, and drying condition for substrates and stamp). Homogenous anti-CD3 and anti-CD3/ICAM-1 patterns with similar protein density were obtained on hydrogels of different stiffness. T cell assay confirms anti-CD3 and anti-CD3/ICAM-1 patterns on hydrogel can be used for T cell studies.

2.4   Materials and methods

Reagents and materials

Chemicals and solvents with p.a. purity were used as purchased unless specified. Acrylamide (AAm), acrylic acid (AA), N,N'-methylene-bis-acrylamide (bis-AAm), ammonium persulfate (APS, 10% w/v in PBS), tetramethylethylnediamine (TEMED), 3-acryloxypropyl-trimethoxysilane (3-APS), Sigmacote®, NaOH (5 M), NaCl (0.5 M) PBS buffer (1 X, pH 7.0-7.4), 2-(N-morpho)-ethanesulfonic acid solution (MES buffer, 0.1 M, pH = 4.5), ethanol (97%), pararosaniline base, biotin-PEG$_8$-NH$_2$, N-hydroxysuccinimide (NHS), dimethylaminopropyl-3-ethylcarbodiimide hydrochloride (EDC), were purchased from Sigma-Aldrich Chemie GmbH. Biotin-PEG-OH (5 kDa) was from Nanocs. Inc. Streptavidin, Alexa Fluor 488 streptavidin (streptavidin-488), Alexa Fluor 594 streptavidin (streptavidin-594), Alexa Fluor 647 streptavidin (streptavidin-647), Alexa Fluor 488 NHS ester, Alexa Fluor 555 NHS ester and Fluo-4-AM calcium indicator were from Thermo Fisher Scientific. The following antibodies were purchased from Biolegend GmbH: biotinylated mouse anti human CD3 (OKT3), recombinant mouse ICAM-1-Fc chimera (without carrier), biotin

anti-human IgG Fc, Alexa Fluor 647 anti-Zap70 (Y319)/Syk (Y352) antibody, Alexa Fluor 488 anti-Phosphotyrosine antibody, and PE goat anti-mouse IgG antibody.

Stamp fabrication

Photolithographic masters for stamp fabrication were prepared by optical lithography using SU-8 photoresist according to established methods.[56, 57] Masters with 5 x 5 and 10 x 10 mm^2 patterned fields containing square (5 x 5 μm^2) and round (diameter is 6 and 8 μm) pillars of 5 μm height were used here.

Before the fabrication of PDMS stamps, it is necessary to create a rigid master first. A chromium photomask (Compugraphics Jena Gmbh, Germany) with micropatterns of different shapes (squares, circles, lines, etc.) was generated to transfer micropatterns to a SU-8 master by photolithography in a research cleanroom (Science park 2, Saarbrücken, Germany). The SU-8 master fabrication process can be illustrated in the following 8 steps:

- 1) Clean silicon wafers (P-type, approximately 75 mm in diameter, 380 mm in thickness, Si-Mat Germany) by sonication in acetone for 5 min, then dry with compressed N$_2$, finally heat it at 120 °C for 10 min.

- 2) Spin coating of the negative SU-8 3005 photoresist (MicroChem Corp, USA) onto wafer. Here we set a program to generate a layer thickness of around 5 μm according to the spin coating protocol for SU-8 3005 photoresist (the rotation speed, acceleration and the SU-8 photoresist viscosity will together define the thickness of the SU-8 photoresist layer on wafer).

- 3) Heat the spin-coated photoresist to evaporate the solvent to make the SU-8 photoresist more solid following a temperature ramp (3 min at 65 °C, 5 min at 95 °C, then slowly cool down to RT over 30 min, the so-called soft baking process).

- 4) Remove the edge bead (this step is optional).

- 5) Expose spin-coated photoresist to UV light (wavelength 365 nm) to initiate the cross linkage by the activation of PhotoActiv Component (PAC). This activation will change the local properties of the resin, which finally becomes insoluble in solvent after baking. The area exposed to the UV light will become hard and the other part will dissolve during the development step. The exposure time used here is 20 s (with a PL-360-LP filter), the power of the lamp is 15 mW/cm^2 and the contact mode is a hard contact.

- 6) Heat the exposed photoresist following the same temperature ramp as indicated in the soft baking step (the so-called post-baking process).

- 7) Develop the substrate with SU-8 developer (Mainly composed of propylene glycol monomethyl ether acetate, MicroChem Corp, USA).

- 8) Bake the final substrate at 150°C for 30 mins to suppress internal strength to avoid cracks on the surface or even delamination of the layer (the hard baking process). SU-8 master with different micropatterns is thus created to be for stamp fabrication.

The micropatterned PDMS stamps were fabricated by double soft molding from the SU-8 photolithographic master. A special stamp frame was employed here to adapt the stamp to be held by the printing head of GeSiM microcontact printer. The PDMS prepolymer mixture (polymer/curing agent ratio was 10:1 by weight) was cast on the SU-8 master and cured at 90 °C for 2 h. A 10 × 10 mm^2 size area was cut from the patterned field (5 x 5 or 10 × 10 mm^2) and then treated with ultrasound in ethanol solution, dried under a compressed filtered N$_2$ flow, and subsequently mounted in the casting station to prepare the PDMS stamp (Figure A2). The PDMS prepolymer mixture was injected into the chamber of stamp frame fixed in the casting station and then cured at 90 °C for 2h, finally the PDMS stamp with 5 x 5 or 10 × 10 mm^2 size

were obtained. Before the soft molding steps, both the SU-8 master and PDMS stamp (negative) were passivated by direct exposure to 1H,1H,2H,2H-Perfluorodecyltrichlorosilane in the gas phase using an evacuated container for 30 min. This so-called fluorosilanization step is necessary to reduce sticking of the PDMS cast to the master and facilitate the separation of the soft molded PDMS stamp.

Preparation of poly PAAm-co-AA hydrogel thin films

Hydrogel discs of ca. 13 mm diameter were prepared between two coverslips. One coverslip (diameter 25 mm, VWR) was functionalized with 3-APS to support covalent binding to the PAAm-co-AA hydrogel. The other coverslip (diameter 13 mm, VWR) was coated with Sigmacote reagent to get a hydrophobic surface and avoid sticking of hydrogel. Glass coverslips were cleaned first by immersing them in ethanol and treated in an ultrasound bath for 5 min, washed twice with MilliQ water and dried with N_2. A second cleaning step by plasma etching was performed in a Pico Low-pressure (air, 0.3 Mbar, 5 min) Plasma System (Diener, Ebhausen) for 2 min. The 25 mm glass slides were immersed in 1% 3-APS solution (95% ethanol/4% water mixture) overnight and washed with MilliQ water. After drying with N_2, coverslips were baked for 1 h at 80°C in vacuum and kept in N_2 for use. The 13 mm glass coverslips were immersed in Sigmacote solution with continuous shaking for 60 min and washed twice with MilliQ water.

PAAm-co-AA hydrogels with different stiffness were prepared by mixing AAm monomer with bis-AAm crosslinker in different ratios while keeping a constant ratio of AA for biofunctionalization (Table 1).[53, 58] Hydrogel thin films were prepared between two circular glass coverslips. AAm and bis-AAm were dissolved in PBS (5 mL) at different ratios. The AA (30 μL, 0.6% by weight) was added and the pH of

solution was adjusted to 7.5-8.0 by using NaOH (5 M). A volume of 200 μL monomer solution was degassed for 1 min, followed by mixing with 2 μL APS (10% in water) and 0.2 μL TEMED in seconds. A volume of 8-12 μL (8, 10, and 12 μL was for 2, 12, and 50 kPa, respectively) mixed solution was quickly placed on 3-APS-functionalized coverslips and covered with Sigmacote coated coverslips. After 10 min the sandwich-like substrate was immersed in PBS overnight and the Sigmacote coverslips were easily removed. The hydrogel discs supported on the glass coverslips were kept in cold PBS until further use. Hydrogels remained attached to coverslip and stably fixed to it during all experiments.

Characterization of the stiffness of hydrogels by AFM

The stiffness of glass supported hydrogel discs were characterized with an AFM (Nanowizard I, JPK instruments, Berlin, Germany) before and after biofunctionalization. Force-indentation profiles of hydrogels were recorded using a micromanipulator-controlled stage and a silicon nitride cantilever (a spring constant of 0.4713 N/m, Nanoworld, Neuchatel, Switzerland) functionalized with a polystyrene bead (Diameter 6.1 μm, SQUBE). Force maps of 16 force curves within an area of 100 x 100 μm^2 were recorded on at least four different positions of hydrogel. Piezo approach/retraction speed was 5 μm/s and a relative setpoint of 5 nN was chosen. All hydrogels were measured in PBS at room temperature. Young's Modulus was calculated by fitting force vs. indentation depth data to a linearized Hertz model derived for a spherical indenter by using JPK image processing software (a poisson ratio of 0.5 was used here). Three samples (each stiffness) were used for data analysis.

Measurement of hydrogels thickness by confocal fluorescence microscopy

The hydrogel was functionalized with pararosaniline base dye as described above. After washing with PBS twice, the fluorescence intensity across the film thickness was imaged using a confocal microscope (ZEISS LSM 880 with Airyscan, Germany). A scan in z-axis (200 nm interval, 40 ×/W objective) across the hydrogel from the bottom glass to the top was performed until no fluorescence was observed. The dry thickness of hydrogel was measured in the same way after overnight drying of the hydrogel at room temperature (RT). Thickness values between 3 and 5 μm were obtained (Figure 3C)

Measurement of swelling ratio

The swelling ratio of the hydrogel discs was measured by gravimetric method. The gels supported on glass were swollen for 24 hours in PBS at room temperature. Samples were weighted and the swollen weight value (Wet_w) was obtained. After drying at 45 °C for 24 h under vacuum, samples were weighed to get dry weights (Dry_w). The swelling ratios of samples prepared in eppendorf tubes were also measured. 200 μL of monomer mixture were left in a 1.5 mL-eppendorf tube for polymerization, and the dry and wet weights were obtained in analogous way to the films. At least 3 replicas were done for each stiffness sample. The swelling ratio (%) was calculated as *(Wet_w-Dry_w)/Dry_w x 100.* Swelling ratios of 14.2, 13.1 and 9.8 were obtained for hydrogels with Young's Modulus 2, 12 and 50 kPa, respectively (Figure A1).

Functionalization of PAAm-co-AA hydrogels with biotin-PEG$_8$-NH$_2$ and streptavidin

The PAAm-co-AA film was covered with 100 μL EDC/NHS solution (39 mg/12 mg in 0.1 M MES buffer) for 15 min, washed thoroughly with PBS and directly incubated

with pararosaniline base dye (100 μL, 0.5 mg/mL) or biotin-PEG$_8$-NH$_2$ (100 μL, 1 mg/mL) solution in a petri dish for 2 h at room temperature. The biotinylated hydrogels were washed by PBS for 3 times and kept in PBS at 4°C until use.

For streptavidin-functionalized hydrogels, 100 μL streptavidin solution (100 μg/mL) was incubated with 2 kPa hydrogel for 1-1.5 h and 12 and 50 kPa for 2.5-3 h, which resulted in comparable fluorescence distribution profiles and peak fluorescence intensities of streptavidin in hydrogels (detailed in Chapter 3)

Micropatterning of streptavidin on hydrogels of different stiffness

Biotinylated PAAm hydrogels with different stiffness were washed twice with MilliQ water and slowly dried in a fume hood over 15-20 min. PDMS stamps were treated with sonication in acetone and ethanol for 5 min, respectively, washed twice with MilliQ water and then dried with compressed N$_2$ flow. The stamps were treated with oxygen plasma (0.3 Mbar, 2 min) in a plasma cleaner (Diener plasma GmbH), and then a fixed volume of the streptavidin solution (100 μg/mL, 20 μL for 10 $\times$ 10 mm^2 and 10 μL for 5 $\times$ 5 mm^2 PDMS stamp) was immediately dropped on the stamp and kept for 0.5 h at RT (kept in a humid container to avoid solution dry). The extra solution was removed by a pipette and the stamp surface was dried by using a gentle N$_2$ flow (5 bar, 10 s). After keeping the stamp in a humid container (95-98% humidity) for 5 mins, microcontact printing was performed with a commercial μContact Printer (μCP 4.1, GeSiM, Germany) using a pneumatic control system in a clean bench at RT. The optimized printing pressure was 12 kPa and the contact time was 5 min. Before the printing process, the relative z-positions of PDMS stamps and dried hydrogels were measured by the printer sensor installed in the printing head of μContact Printer. Multiple protein micropatterns could also be fabricated on the same hydrogel film by further backfilling the background surface with streptavidin again.

After microcontact printing, hydrogels were left in ambient humidity at 4°C for 1 h to allow a better streptavidin binding. Finally, the micropatterned hydrogels were washed with PBS twice. For the cell experiments, the micropatterned hydrogels were further blocked with biotin-PEG (1mg/mL, 100 μL).

Double microcontact printing on hydrogel

A PDMS stamp (5 μm square patterns) was inked with streptavidin-647 solution (100 μg/mL, 20 μL) for 0.5 h. Another stamp (5 μm dots) was inked with streptavidin-488 solution (100 μg/mL, 10 μL) for 0.5 h. These two streptavidin stamps were sequentially brought to contact with biotinylated hydrogel at optimized printing conditions. The hydrogel was kept at the same position during the whole process while the relative position of the second PDMS stamp to hydrogel surface was precisely adjusted by the microcontact printer. The obtained micropatterns were left in ambient humidity at 4°C for 1 h followed by washing with PBS and then used for imaging with confocal microscopy (Zeiss LSM 880 AiryScan, Germany).

Micropatterned anti-CD3 on hydrogels of different stiffness

Two different protocols were applied to prepare micropatterned anti-CD3 on the hydrogels.

Method 1: biotinylated anti-CD3 (100 μg/mL, 100 μL) was incubated on hydrogel films previously microcontact printed with streptavidin overnight at 4 °C. After washing with sterile PBS for 3 times, PE goat anti-mouse IgG was employed to label the anti-CD3 coupled to micropatterned streptavidin.

Method 2: Fluorescently labeled biotinylated anti-CD3 (555-biotin-anti-CD3, 100 μg/mL) was directly printed on streptavidin-modified hydrogels using the same printing conditions as for streptavidin micropatterning. After the printing, the

micropatterned hydrogels were left in ambient humidity at 4°C for 1 h to allow the sufficient binding of biotin-anti-CD3 to streptavidin. After washing twice with PBS, The hydrogels were finally incubated with biotin-PEG (100 μg/mL, 100 μL) for 1 h at 4°C to block the streptavidin background functionalities.

In order to get a micropatterned anti-CD3/ICAM-1 surface (mimetic IS surface), the micropatterned anti-CD3 hydrogel (created with method 2 on hydrogel of 50 kPa) was firstly incubated with biotinylated anti-human IgG Fc overnight (4°C), and then incubated with ICAM-1-Fc chimera for another 1 h at RT. The hydrogel were finally washed with PBS twice and further incubated with biotin-PEG for 1 h. ICAM-1-Fc was labeled with Alexa Fluor 488 for visualization.

Fluorescence intensity characterization

Fluorescence images were acquired using a confocal microscope. Initially, Z-stack images with 250 nm intervals were acquired for each substrate. Then the fluorescent Z-stack images (20 Z-stack images were acquired for micropatterned streptavidin and 555-biotin-anti-CD3 within the top 5 μm layer of hydrogel and 8 Z-stack images were acquired for PE-anti-IgG that bound to micropatterned anti-CD3 within the top 2 μm layer of hydrogel) were summed up into one image for image analysis after the backgrounds were subtracted from the total gray level intensity of the images. Finally, plot profile across micropatternd areas was analyzed by ImageJ software (INM) and the mean fluorescence intensities of micropatterned 555-biotin-anti-CD3 and PE-anti-IgG antibody were normalized to the total patterned area.

For the PE-anti-IgG immunochemistry, hydrogels with micropatterned streptavidin were firstly incubated with biotinylated anti-CD3 solution (100 μg/mL) for 1 h at RT, then washed three times with PBS and further incubated with PE-anti-IgG antibody (0.2 mg/mL) overnight at 4 °C. All the substrates were washed three times in PBS

and mounted in Slow Fade Gold Antifade (Molecular Probes, Invitrogen, Cergy Pontoise, France) before fluorescence imaging with a 20 ×/W objective by confocal microscope (Zeiss LSM 880 AiryScan, Germany).

Cell culture

Jurkat T-cells, clone E6-1 (ATCC® TIB-152™) were cultured in RPMI-1640 Medium (Gibco) supplemented with 10% fetal bovine serum (Gibco), 100 units/mL penicillin, and 100 μg/mL streptomyocin at 37°C, 5% CO_2.

Interaction of Jurkat cell with micropatterned hydrogel

Jurkat cells were seeded at a concentration of 50000 cells per hydrogel to interact with micropatterned hydrogel surfaces for 0.5 h before fixation with 4% PFA. As for micropatterned anti-CD3 surface, the fluorescent images of micropatterned streptavidin and bright field images of Jurkat cell were acquired by Zeiss Axio Observer microscope (Germany). As for mimetic IS surface, cell were stained with Alexa Fluor 488 anti-Phosphotyrosine and Alexa Fluor 647 anti-Zap70 (Y319)/Syk (Y352) antibody to label pTyr and pZAP70, respectively, and then mounted (mouting medium with DAPI was used to label cell nuclei) for imaging with confocal microscope (ZEISS LSM 880 with Airyscan, Germany).

Appendix Chapter 2

Table A1. Swelling ratios of PAAm-co-AA hydrogels with different stiffness

Young's modulus E (kPa)	2	12	50
Volume of monomers solution (μL)	8.0	10.0	12.0
Bis-AAm/AAm	0.25 %	0.92 %	4.17 %
Swelling ratio (PAAm-co-AA)	14.2 ± 2.0	13.1 ± 1.6	9.8 ± 1.1
Swelling ratio (PAAm-co-AA/biotin-streptavidin)	15.8 ± 1.7	13.8 ± 1.2	10.4 ± 1.3
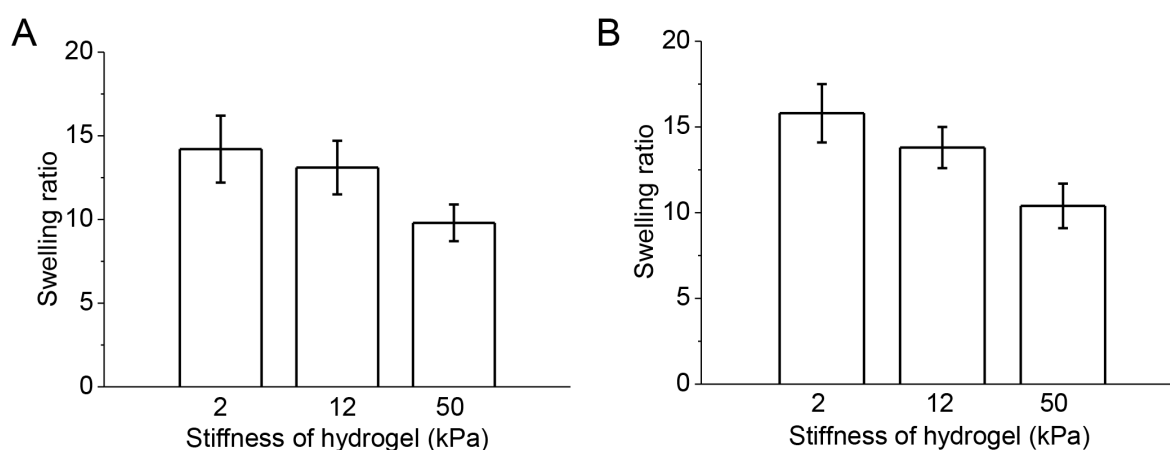
Figure A1. Swelling ratios of PAAm-co-AA hydrogels (2 kPa, 12 kPa, and 50 kPa) before (A) and after (B) functionalization with biotin-streptavidin, n=5. Swelling ratios were calculated with the following equation: *Swelling ratio (%) = (Wet weight – Dry weight)/Dry weight x 100.*

| Pit platform (15x15x1.3mm) | Mounting with silicon master | Mounting with PDMS Template |
| Covered with mould to shape PDMS stamp | Injection of prepolymer of PDMS | Prepared PDMS stamp after curing (90 ℃, 2 h) |
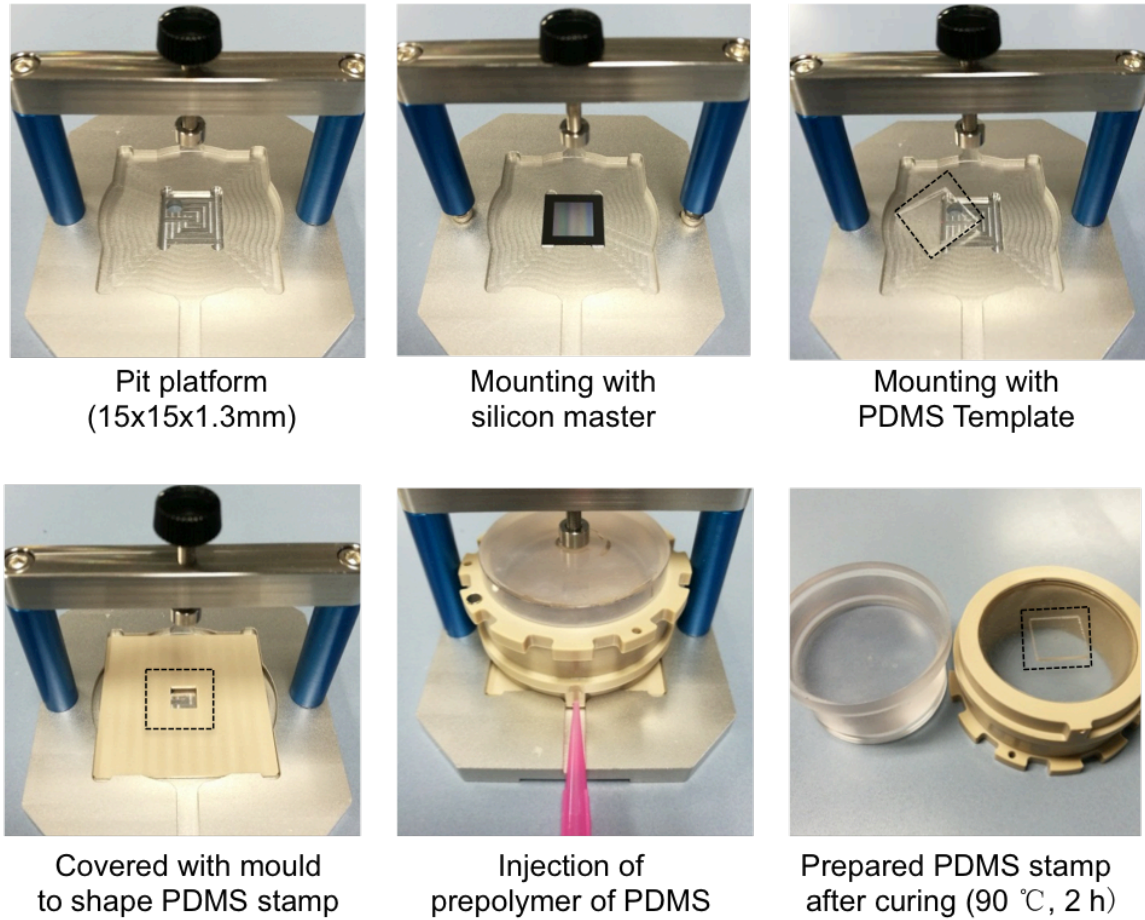
Figure A2. Bench-scale examples to show key steps of PDMS stamp fabrication in a stamp frame, illustrating bench-level implementation.

| Without biotinylation | Biotinylation |
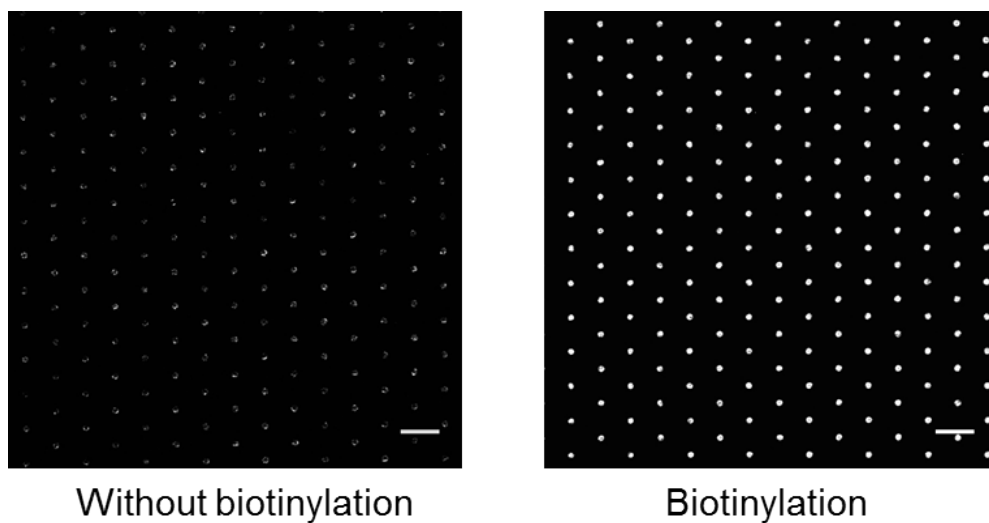
Figure A3. Fluorescence images to show micropatterned streptavidin-594 dots on hydrogels with or without biotinylation. Scale bar, 20 μm.

A   wet   B   super dry   C   semi-dry
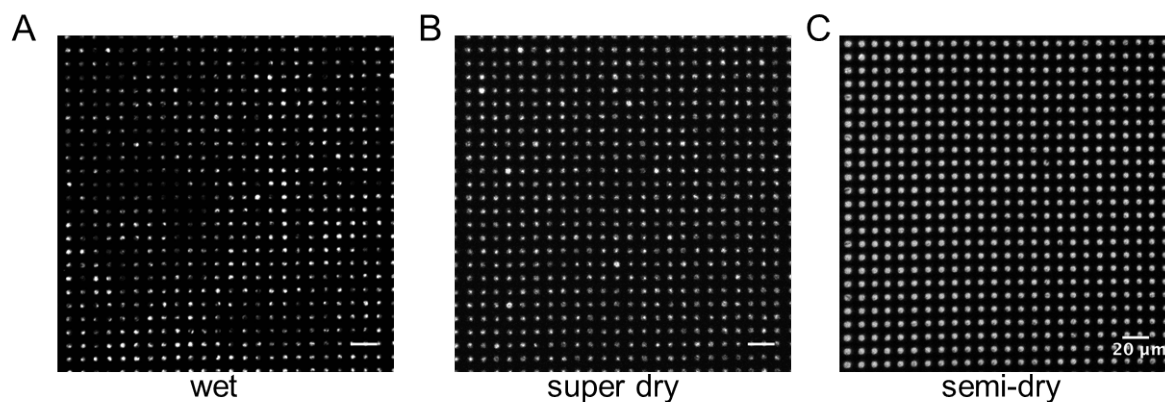
Figure A4. Fluorescence images of micropatterned streptavidin-594 generated in wet (A), super dry (B) and semi-dry (C) conditions. Wet condition means micropatterning on swollen hydrogel, super dry means both the stamp and hydrogel were completely dry and semi-dry means humid stamp printing on dry hydrogel. Scale bar, 20 μm.

References

[1] D.E. Discher, P. Janmey, Y.L. Wang, Tissue cells feel and respond to the stiffness of their substrate, Science 310(5751) (2005) 1139-43.

[2] T. Grevesse, M. Versaevel, G. Circelli, S. Desprez, S. Gabriele, A simple route to functionalize polyacrylamide hydrogels for the independent tuning of mechanotransduction cues, Lab Chip 13(5) (2013) 777-80.

[3] M. Thery, Micropatterning as a tool to decipher cell morphogenesis and functions, J. Cell Sci. 123(Pt 24) (2010) 4201-13.

[4] T. Vignaud, L. Blanchoin, M. Thery, Directed cytoskeleton self-organization, Trends Cell Biol. 22(12) (2012) 671-82.

[5] A. Mitra, S. Venkatachalapathy, P. Ratna, Y. Wang, D.S. Jokhun, G.V. Shivashankar, Cell geometry dictates TNFalpha-induced genome response, Proc. Natl. Acad. Sci. U. S. A. 114(20) (2017) E3882-E3891.

[6] J. Doh, D.J. Irvine, Immunological synapse arrays: patterned protein surfaces that modulate immunological synapse structure formation in T cells, Proc. Natl. Acad. Sci. U. S. A. 103(15) (2006) 5700-5.

[7] A. Perl, D.N. Reinhoudt, J. Huskens, Microcontact Printing: Limitations and Achievements, Adv. Mater. 21(22) (2009) 2257-2268.

[8] W.-D. Liu, B. Yang, Patterned surfaces for biological applications: A new platform using two dimensional structures as biomaterials, Chin. Chem. Lett. 28(4) (2017) 675-690.

[9] Z. Nie, E. Kumacheva, Patterning surfaces with functional polymers, Nat. Mater. 7(4) (2008) 277-90.

[10] W. Liu, Y. Li, B. Yang, Fabrication and applications of the protein patterns, Sci. China: Chem. 56(8) (2013) 1087-1100.

[11] P. Pavli, P.S. Petrou, A.M. Douvas, D. Dimotikali, S.E. Kakabakos, P. Argitis, Protein-resistant cross-linked poly(vinyl alcohol) micropatterns via photolithography using removable polyoxometalate photocatalyst, ACS Appl. Mater. Interfaces 6(20) (2014) 17463-73.

[12] Z. Chen, S. He, H.J. Butt, S. Wu, Photon upconversion lithography: patterning of biomaterials using near-infrared light, Adv. Mater. 27(13) (2015) 2203-6.

[13] A. Waldbaur, B. Waterkotte, K. Schmitz, B.E. Rapp, Maskless projection lithography for the fast and flexible generation of grayscale protein patterns, Small 8(10) (2012) 1570-8.

[14] C. Reuther, R. Tucker, L. Ionov, S. Diez, Programmable patterning of protein bioactivity by visible light, Nano Lett 14(7) (2014) 4050-7.

[15] J. Zhang, B. Yang, Patterning Colloidal Crystals and Nanostructure Arrays by Soft Lithography, Adv. Funct. Mater. 20(20) (2010) 3411-3424.

[16] J. Zhang, Y. Li, X. Zhang, B. Yang, Colloidal self-assembly meets nanofabrication: from two-dimensional colloidal crystals to nanostructure arrays, Adv. Mater. 22(38) (2010) 4249-69.

[17] G. Singh, H.J. Griesser, K. Bremmell, P. Kingshott, Highly Ordered Nanometer-Scale Chemical and Protein Patterns by Binary Colloidal Crystal Lithography Combined with Plasma Polymerization, Adv. Funct. Mater. 21(3) (2011) 540-546.

[18] L.J. Guo, X. Cheng, C.F. Chou, Fabrication of size-controllable nanofluidic channels by nanoimprinting and its application for DNA stretching, Nano Lett. 4(1) (Chia-Fu Chou) 69-73.

[19] K.L. Christman, E. Schopf, R.M. Broyer, R.C. Li, Y. Chen, H.D. Maynard, Positioning multiple proteins at the nanoscale with electron beam cross-linked functional polymers, J. Am. Chem. Soc. 131(2) (2009) 521-7.

[20] C.A. DeForest, D.A. Tirrell, A photoreversible protein-patterning approach for guiding stem cell fate in three-dimensional gels, Nat. Mater. 14(5) (2015) 523-31.

[21] T.T. Lee, J.R. Garcia, J.I. Paez, A. Singh, E.A. Phelps, S. Weis, Z. Shafiq, A. Shekaran, A. Del Campo, A.J. Garcia, Light-triggered in vivo activation of adhesive peptides regulates cell adhesion, inflammation and vascularization of biomaterials, Nat. Mater. 14(3) (2015) 352-60.

[22] R.J. Wade, E.J. Bassin, W.M. Gramlich, J.A. Burdick, Nanofibrous hydrogels with spatially patterned biochemical signals to control cell behavior, Adv. Mater. 27(8) (2015) 1356-62.

[23] C.A. DeForest, K.S. Anseth, Cytocompatible click-based hydrogels with dynamically tunable properties through orthogonal photoconjugation and photocleavage reactions, Nat. Chem. 3(12) (2011) 925-31.

[24] R.G. Wylie, S. Ahsan, Y. Aizawa, K.L. Maxwell, C.M. Morshead, M.S. Shoichet, Spatially controlled simultaneous patterning of multiple growth factors in three-dimensional hydrogels, Nat. Mater. 10(10) (2011) 799-806.

[25] G. Delaittre, N.K. Guimard, C. Barner-Kowollik, Cycloadditions in modern polymer chemistry, Acc. Chem. Res. 48(5) (2015) 1296-307.

[26] Z. Ming, J. Fan, C. Bao, Y. Xue, Q. Lin, L. Zhu, Photogenerated Aldehydes for Protein Patterns on Hydrogels and Guidance of Cell Behavior, Adv. Funct. Mater. 28(14) (2018) 1706918.

[27] Z. Ming, X. Ruan, C. Bao, Q. Lin, Y. Yang, L. Zhu, Micropatterned Protein for Cell Adhesion through Phototriggered Charge Change in a Polyvinylpyrrolidone Hydrogel, Adv. Funct. Mater. 27(25) (2017) 1606258.

[28] J.P. Renault, A. Bernard, A. Bietsch, B. Michel, H.R. Bosshard, E. Delamarche, M. Kreiter, B. Hecht, U.P. Wild, Fabricating Arrays of Single Protein Molecules on Glass Using Microcontact Printing, J. Phys. Chem. 107(3) (2003) 703-711.

[29] J. Lantoine, T. Grevesse, A. Villers, G. Delhaye, C. Mestdagh, M. Versaevel, D. Mohammed, C. Bruyere, L. Alaimo, S.P. Lacour, L. Ris, S. Gabriele, Matrix stiffness modulates formation and activity of neuronal networks of controlled architectures, Biomaterials 89 (2016) 14-24.

[30] C.Y. Tay, Y.-L. Wu, P. Cai, N.S. Tan, S.S. Venkatraman, X. Chen, L.P. Tan, Bio-inspired micropatterned hydrogel to direct and deconstruct hierarchical processing of geometry-force signals by human mesenchymal stem cells during smooth muscle cell differentiation, NPG Asia Mater. 7(7) (2015) e199-e199.

[31] H.R. Jung, K.H. Song, J.T. Chang, J. Doh, Geometrically controlled asymmetric division of CD4+ T cells studied by immunological synapse arrays, PLoS One 9(3) (2014) e91926.

[32] C.Y. Hui, A. Jagota, Y.Y. Lin, E.J. Kramer, Constraints on Microcontact Printing Imposed by Stamp Deformation, Langmuir 18(4) (2002) 1394-1407.

[33] K.G. Sharp, G.S. Blackman, N.J. Glassmaker, A. Jagota, C.Y. Hui, Effect of stamp deformation on the quality of microcontact printing: theory and experiment, Langmuir 20(15) (2004) 6430-8.

[34] E. Delamarche, H. Schmid, B. Michel, H. Biebuvck, Stability of molded polydimethylsiloxane microstructures, Adv. Mater. 9(9) (1997) 741-746.

[35] P. Roca-Cusachs, F. Rico, E. Martínez, J. Toset, R. Farré, D. Navajas, Stability of microfabricated high aspect ratio structures in poly(dimethylsiloxane), Langmuir 21 (2005) 5542-8.

[36] E. Favre, Swelling of crosslinked polydimethylsiloxane networks by pure solvents: Influence of temperature, Eur. Polym. J. 32(10) (1996) 1183-1188.

[37] J. Lee, C. Park, G.M. Whitesides, Solvent Compatibility of Poly(dimethylsiloxane)-Based Microfluidic Devices, Anal. Chem. 75(23) (2003) 6544-6554.

[38] M.J. Owen, P.J. Smith, Plasma treatment of polydimethylsiloxane, J. Adhes. Sci. Tech. 8(10) (1994) 1063-1075.

[39] B. Olander, A. Wirsen, A.-C. Albertsson, Oxygen microwave plasma treatment of silicone elastomer: Kinetic behavior and surface composition, J. Appl. Polym. Sci. 91(6) (2004) 4098 - 4104

[40] H. Hillborg, M. Sandelin, U.W. Gedde, Hydrophobic recovery of polydimethylsiloxane after exposure to partial discharges as a function of crosslink density, Polymer 42(17) (2001) 7349-7362.

[41] H. Hillborg, N. Tomczak, A. Olàh, H. Schönherr, G.J. Vancso, Nanoscale hydrophobic recovery: A chemical force microscopy study of UV/ozone-treated cross-linked poly(dimethylsiloxane), Langmuir 20(3) (2004) 785-94.

[42] Y. Xia, G.M. Whitesides, Use of controlled reactive spreading of liquid alkanethiol on the surface of gold to modify the size of features produced by microcontact Printing, J. Am. Chem. Soc. 117(11) (1995) 3274-3275.

[43] R.B. Sharpe, D. Burdinski, J. Huskens, H.J. Zandvliet, D.N. Reinhoudt, B. Poelsema, Spreading of 16-Mercaptohexadecanoic Acid in Microcontact Printing, Langmuir 20(20) (2004) 8646-8651.

[44] E. Delamarche, H. Schmid, A. Bietsch, N.B. Larsen, H. Rothuizen, B. Michel, H. Biebuyck, Transport Mechanisms of Alkanethiols during Microcontact Printing on Gold, J. Phys. Chem. B 102(18) (1998) 3324-3334.

[45] R.K. Workman, S. Manne, Molecular transfer and transport in noncovalent microcontact printing, Langmuir 20(3) (2004) 805-15.

[46] J. Lee, A.A. Abdeen, D. Zhang, K.A. Kilian, Directing stem cell fate on hydrogel substrates by controlling cell geometry, matrix mechanics and adhesion ligand composition, Biomaterials 34(33) (2013) 8140-8.

[47] A.S. Mao, J.W. Shin, D.J. Mooney, Effects of substrate stiffness and cell-cell

contact on mesenchymal stem cell differentiation, Biomaterials 98 (2016) 184-91.

[48] B. Sarker, C. Walter, A. Pathak, Direct Micropatterning of Extracellular Matrix Proteins on Functionalized Polyacrylamide Hydrogels Shows Geometric Regulation of Cell–Cell Junctions, ACS Biomater. Sci. Eng. 4(7) (2018) 2340-2349.

[49] A.G. Castaño, V. Hortigüela, A. Lagunas, C. Cortina, N. Montserrat, J. Samitier, E. Martínez, Protein patterning on hydrogels by direct microcontact printing: application to cardiac differentiation, RSC Adv. 4(55) (2014) 29120.

[50] I. Elloumi-Hannachi, M. Maeda, M. Yamato, T. Okano, Portable microcontact printing device for cell culture, Biomaterials 31(34) (2010) 8974-9.

[51] D. Qin, Y. Xia, G.M. Whitesides, Soft lithography for micro- and nanoscale patterning, Nat. Protoc. 5(3) (2010) 491-502.

[52] N. Tanaka, H. Ota, K. Fukumori, J. Miyake, M. Yamato, T. Okano, Micro-patterned cell-sheets fabricated with stamping-force-controlled micro-contact printing, Biomaterials 35(37) (2014) 9802-9810.

[53] A. Farrukh, J.I. Paez, M. Salierno, A. del Campo, Bioconjugating Thiols to Poly(acrylamide) Gels for Cell Culture Using Methylsulfonyl Co-monomers, Angew. Chem., Int. Ed. Engl. 55(6) (2016) 2092-6.

[54] A. Buxboim, K. Rajagopal, A.E. Brown, D.E. Discher, How deeply cells feel: methods for thin gels, J. Phys.: Condens. Matter 22(19) (2010) 194116.

[55] S. Sen, A.J. Engler, D.E. Discher, Matrix strains induced by cells: Computing how far cells can feel, Cell. Mol. Bioeng. 2(1) (2009) 39-48.

[56] L.F. Boesel, C. Greiner, E. Arzt, A. del Campo, Gecko-inspired surfaces: a path to strong and reversible dry adhesives, Adv. Mater. 22(19) (2010) 2125-37.

[57] C. Greiner, E. Arzt, A. del Campo, Hierarchical Gecko-Like Adhesives, Adv. Mater. 21(4) (2009) 479-482.

[58] A. Farrukh, J.I. Paez, M. Salierno, W. Fan, B. Berninger, A. Del Campo,

Bifunctional Poly(acrylamide) Hydrogels through Orthogonal Coupling Chemistries, Biomacromolecules 18(3) (2017) 906-913.

Chapter 3

3 Study of T cell activation (ZAP70 phosphorylation) on anti-CD3 micropatterned hydrogels to validate them as APC mimics

3.1 Introduction

T cells probe the mechanical properties of antigen presenting cells (APCs) as they explore for targets.[1-4] The binding and clustering of complementary receptors at the cell-cell interface, and their engagement to the cytoskeletal components (actin, microtubules) allow for dynamic force application and sensing, and constitute the basis for mechanosignaling at the immunological synapse (IS). Considerable experimental evidence (discussed in recent reviews [5, 6]) demonstrates that different mechanosensing elements might be involved in the sequential steps of the immune response, from the early recognition and receptor assembly process to IS formation, T cell activation [7] and final cytotoxic events.[8] By means of tuning forces and time scales, T cells might exploit mechanical signaling to transport information in parallel channels, or for differentiation between coexisting signals.[7, 9, 10] Unraveling how molecular and mechanical signals regulate and eventually trigger T cell activation at different levels of the immune response is fundamental for understanding the human immune system, and can also lead to new scenarios for diagnostic strategies and immuno-therapeutics.[11, 12]

Bioengineered platforms established in mechanobiology studies for studying cell-matrix interactions over the last two decades [13, 14] have been incorporated into the T cell community in the last years to study T cell mechanoresponses.[10] The

most extended approach relies in the use of soft hydrogels (i.e. poly(acrylamide) (PAAm) [7-9, 15] or hyaluronic acid [11]) or elastomeric (PDMS) films [16-18] modified with T cell ligands to mimic the APC surface and to bind to targeted T cell receptors (TCR) and/or co-stimulatory molecules. By using soft matrices with different mechanical properties representing a range of expected physiological relevance (typically with Young's Modulus between 0.5 and 100 kPa), the mechanical engagement of APC ligands at the IS during the different phases of the immune response has been modeled. The easy and flexible control over molecular/mechanical properties, with the possibility to measure activation markers and T cell forces at short and long time scales, make these experimental approaches very useful to study mechanotransduction events at cell-cell-like interfaces. Different activation responses have been found depending on the type of ligand [2, 19] or ligand combinations,[17, 20, 21] their density [22] and spatial organization,[21, 23] and the Young's Modulus of the various soft matrixes to which they are attached (mainly summarized in two review articles [5, 10]). Early activation markers (i.e. tyrosine phosphorylation,[9, 15, 17] TCR clustering,[11] and CD69 surface marker expression [7]) and late activation markers (i.e. CD25 surface marker expression,[7] IL-2 and IFN-γ production,[7, 15, 16] cell proliferation and differentiation [11, 16] and target cell killing efficiency [8]) on different T cell subtypes (Jurkat T-cell,[9, 18] naïve CD4$^+$ [7, 15-17] and CD8$^+$ [8, 11, 16]) have been tested. These platforms can be even further developed for measuring the forces applied by T cells when combined with fluorescent beads in traction force microscopy [9] or post arrays.[20] Reported results from such biomimetic IS have shown striking, though partially contradictory features about T cell response.[10] A recent report [18] provides news insights to conciliate contradictory outcomes in part, and highlights the need of better control and definition of the properties of the APC mimetic surface for conclusive, quantitative and

comparable results about the obtained T cell responses.

Major reasons for the inconsistent results are attributed to the various cell types, substrate chemistry, antibody immobilization strategy and stiffness range of the hydrogels used for the experiments, in addition to the insufficient characterization of their physical and biochemical properties of the artificial bio-interface. The immobilization chemistry affects the bioactivity of the surface in terms of surface-presented ligand density and functional state. Moreover, ligand density is not necessarily constant when varying the stiffness of the substrate, and is rarely quantified in the reported literature. A general observation from some of those studies [7, 15, 18] is that the spreading area or protrusion size of the T cell on the APC biomimetic surfaces increases with increasing stiffness. The spreading area influences the number of receptors that can be clustered at the IS and this can, by itself, amplify T cell responses.[23] None of the reported studies has considered how possible variations in ligand density or spreading area would affect the conclusions made in terms of hydrogel stiffness.

This chapter describes how biomimetic APC surfaces with controlled ligand density, IS dimensions (i.e. spreading area) and stiffness can be used to unequivocally assessing T response to varying stiffness of APC mimics. Homogeneous APC ligand patterns of specific geometries and equal ligand density prepared by automated microcontact printing will be used to study the response of T cells to the mechanical engagement of anti-CD3 antibody by quantifying pZAP70 expression.

The methodology presented in this work (as shown in Figure 1) can provide valuable methodological guidance to the immunobiology community to make advanced use of synthetic bio-interfaces for the study of cell-cell interfaces and related mechanobiology.
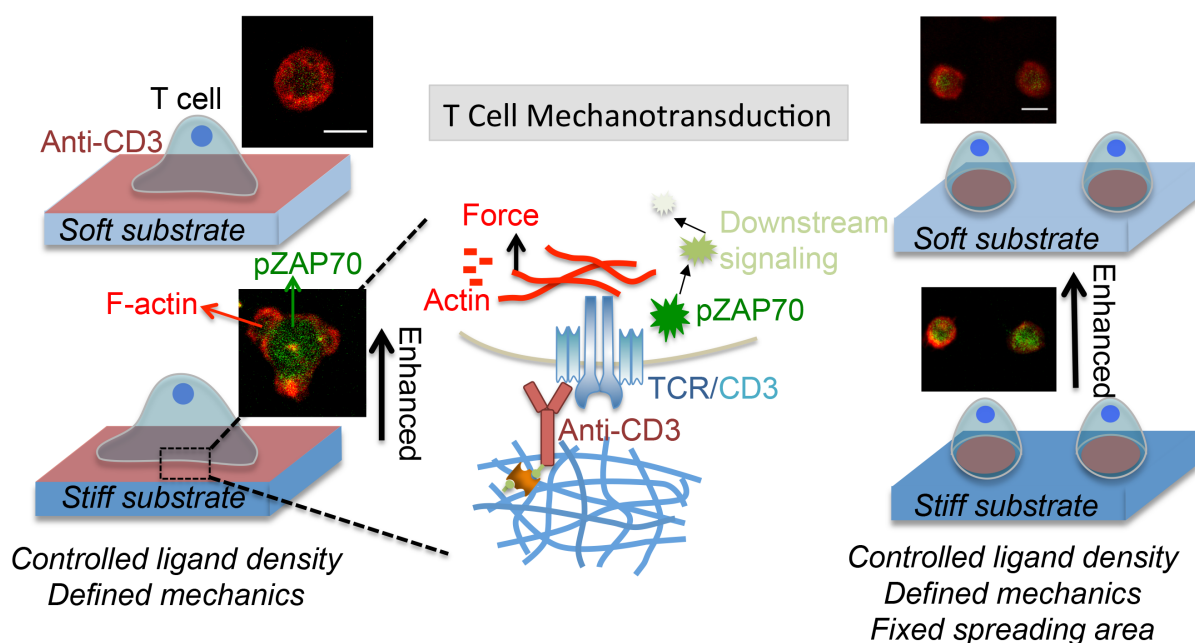
Figure 1. Schematic of the hydrogel-based mimics of the APC and formation of the artificial IS with a T cell. Both flat and micropatterned hydrogels were used for the characterization of T cell mechanotransduction by measuring pZAP70 expression.

3.2 Results and discussion

3.2.1 Fabrication of anti-CD3 with controlled and quantified ligand density on hydrogels

Anti-CD3 modified PAAm-co-AA hydrogels in patterned and non-patterned form were prepared for the study of T cell response and optimized to have the same ligand density independently of their Young's Modulus. For the non-patterned ones, PAAm-co-AA hydrogels were first functionalized with biotin-PEG$_8$-NH$_2$ and then incubated with streptavidin-488 (100 μg/mL) for increasing incubation time from 0.5 to 3 h. The mean fluorescence intensity of the streptavidin layer increased with incubation time and slightly decreased with substrate stiffness (Figure 2). The saturation level was achieved around 3 h after incubation in all hydrogels, and was

higher for the softer hydrogels. The larger mesh size in soft hydrogels might facilitate the diffusion of the protein.[24] Thus, 100 μg/mL streptavidin was incubated with 2 kPa hydrogel for 1-1.5 h and 12 and 50 kPa for 2.5-3 h, which resulted in a well-defined 3-4 μm fluorescent layer on the top of the swollen hydrogel imaged by confocal microscopy (Figure 2 and Figure 3A) and a comparable fluorescence distribution profiles and peak fluorescence intensities (Figure 3B,C). This result also indicates that streptavidin (ca. 10 nm in size) [25] diffuses only into the top 3-4 μm layer of the hydrogel within the given incubation time.
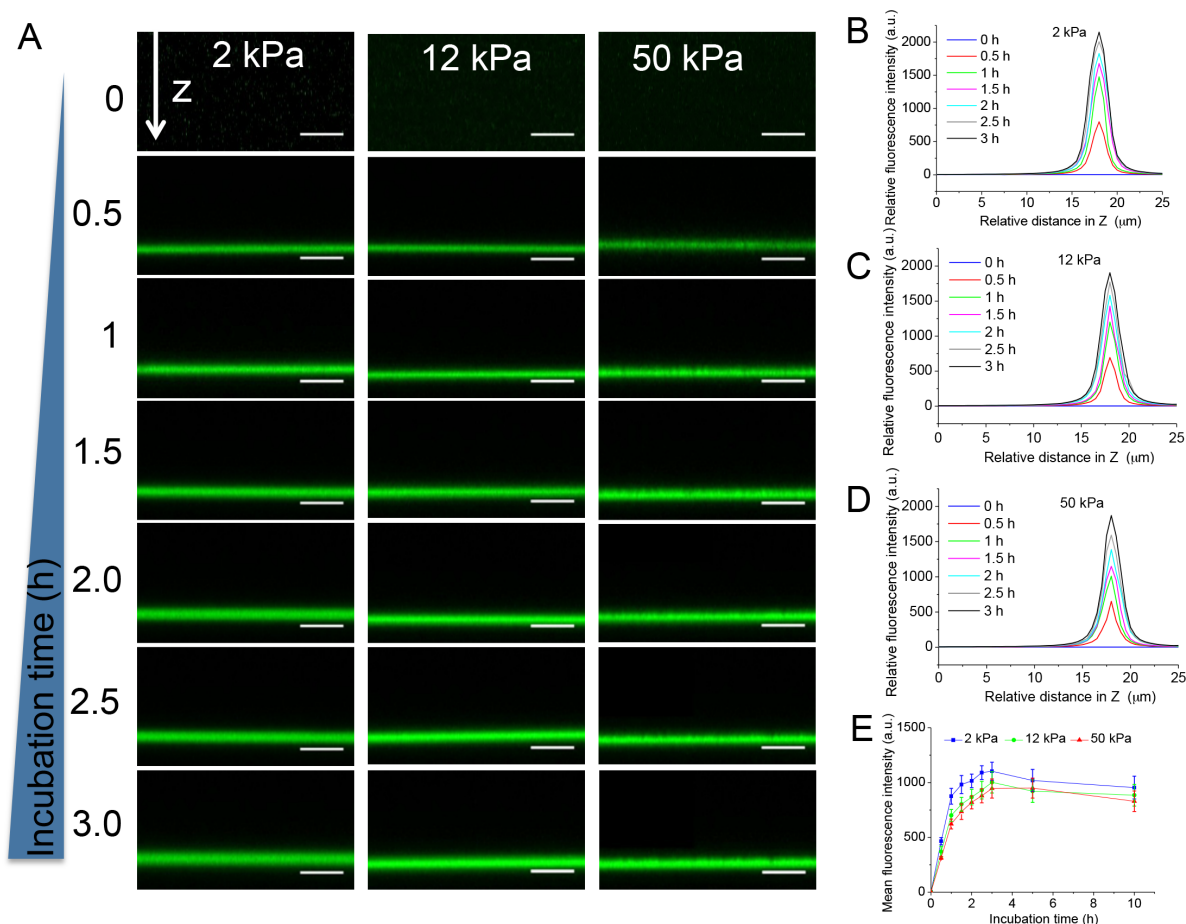

Figure 2. (A) Fluorescence image of the top layer of PAAm-co-AA hydrogel incubated with streptavidin-488 for different time after Z-stack images reconstruction. Scale bar, 10 μm. Relative fluorescence intensity profile of streptavidin-488 in 2 (B),

12 (C) and 50 kPa (D) hydrogel after different incubation time (0-3h). (E) Mean fluorescence intensity of streptavidin-488 as a function of incubation time. n=5.

In order to test if the immobilized streptavidin concentration can be further used to couple biotinylated ligands in a subsequent incubation steps, these hydrogels were then incubated with 10 μM Atto543-biotin and imaged by confocal microscope. No differences in the fluorescent intensity and distribution profiles of Atto543-biotin were observed among these three hydrogels (Figure 3D,E). These results indicate that the conjugation efficiency of biotin ligand to streptavidin-modified hydrogels is comparable in all substrates. Moreover, x-y fluorescence imaging of the hydrogel surface (Figure A5) confirmed homogeneous lateral distribution of the streptavidin and biotin and comparable fluorescence values for all the tested samples. These hydrogels with different stiffness but equivalent streptavidin density were used for further bio-functionalization to test with T cells in the next sections.
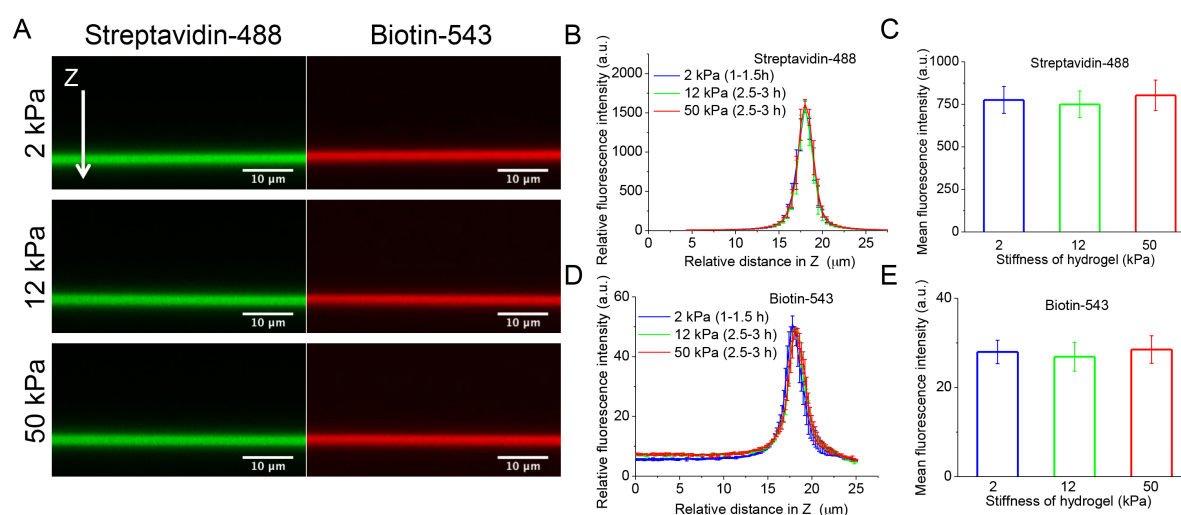

Figure 3. (A) Z-axis fluorescence imaging of the top layer (around 25 μm) of hydrogel functionalized with streptavidin-Alexa488 and biotin-Atto543. (B) Intensity profile of

streptavidin on hydrogel surface after different incubation time. (C) The mean fluorescence intensities of streptavidin-Alexa488 on hydrogels of different stiffness after specific incubation time. (D) Intensity profile of biotin-Atto543 on hydrogel functionalized with streptavidin-Alexa488. (E) The mean fluorescence intensities of biotin-Atto543 on hydrogels of different stiffness. Mean fluorescence intensity calculation: the fluorescence intensity sums within the top 4 μm hydrogel (n=10). Three independent experiments were used for analysis. Data are presented as mean ± SD.

The coupling of biotinylated anti-CD3 to the streptavidin-modified hydrogels was also tested. Streptavidin-modified hydrogels were incubated with biotinylated anti-CD3 (100 μg/mL) overnight and subsequently with phycoerithrin anti-mouse IgG (PE anti-IgG, 200 μg/mL) after washing with PBS. The PE labeled antibody is too big (around 60 nm) to penetrate deeply inside since the hydrogels as they have small mesh sizes (around 15 nm for 0.5 kPa), and therefore, it could be used to characterize the density of anti-CD3 on the hydrogel surface [24, 26]. Fluorescence imaging (x-y plane) of the hydrogel surface showed a homogeneous distribution of PE anti-IgG, indicating anti-CD3 was coated evenly on the hydrogel surface (Figure 4A). Z stack imaging across the top 25 μm hydrogel further confirmed that PE anti-IgG only accessed within the top 1-1.5 μm layer of the hydrogel (Figure 4B). The mean fluorescence intensity within the top 2 μm hydrogels of different stiffness was compared. The mean fluorescence intensity was found to be independent of substrates stiffness. The plain PAAm-co-AA hydrogel (50 kPa, without streptavidin) was also incubated with PE anti-IgG and then imaged as a control. The fluorescence was scarcely detected (Figure 4A, C), demonstrating that PE-anti-IgG is specifically captured by anti-CD3. We further quantified anti-CD3 density on the surfaces of

different substrates by counting the number of particles bound to the hydrogel surface after incubating with anti-IgG coated particles (diameter 0.6-0.7 μm). The tested hydrogels also showed a similar density of anti-IgG coated particles, further confirming a similar anti-CD3 density on all substrate surfaces (Figure A6).

These optimized hydrogels were used for investigating CD3-mediated T cell response to stiffness in the following cell experiments.
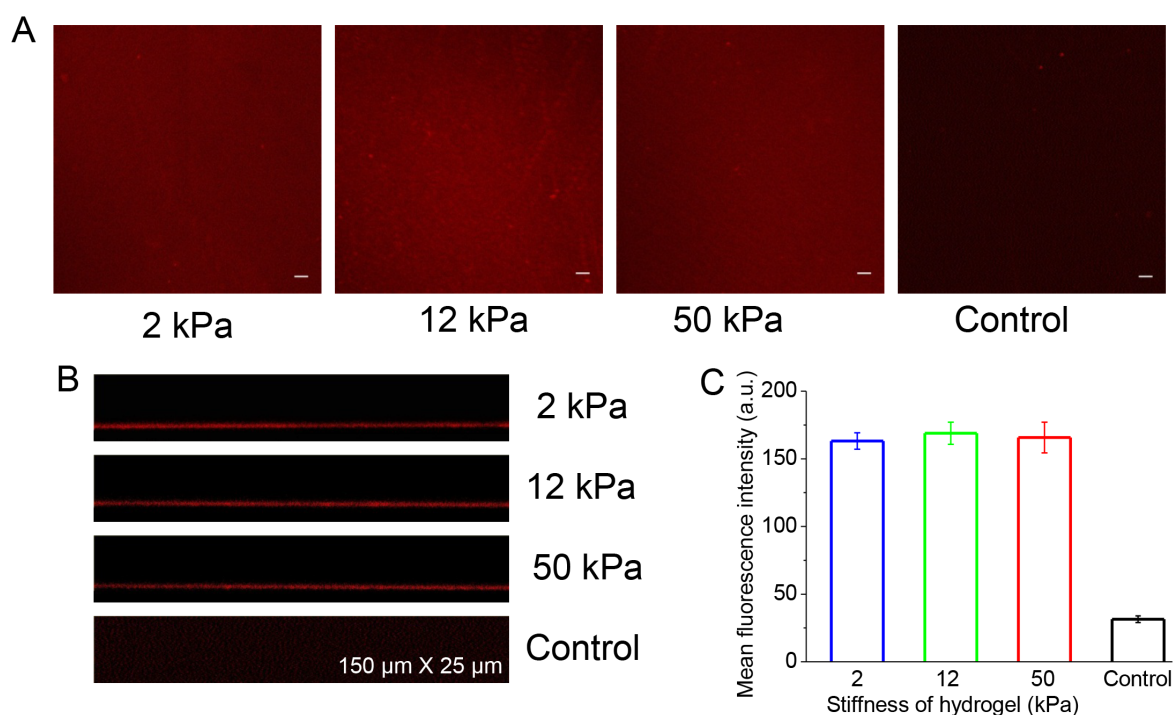
Figure 4. The XY-plane (A) and Z-stack (B) fluorescence images of anti-CD3 modified hydrogels after labeled by PE-anti-IgG antibody. Scale bars are 10 μm. (C) The mean fluorescence intensities of PE-anti-IgG antibody on hydrogels of different stiffness (n=10). Three independent experiments were used for analysis. Data are presented as mean ± SD.

For the patterned hydrogels, anti-CD3 (Alexa Fluor 555-labeled and biotinylated) areas were microcontactprinted on streptavidin-functionalized hydrogels of different

stiffness as described Chapter 2 (Figure A7). Regular and homogenous arrays of fluorescent dots of 8 µm diameter were obtained (Figure 5A-C). The micropatterned dots showed sharp edges and a high contrast between the dots and the background area on all substrates after washing with PBS, reflecting a high quality and lateral resolution of our method. Printing conditions were further optimized to achieve comparable fluorescence intensity of anti-CD3 micropatterns on the hydrogel with different stiffness (Figure 5D). The shape and fluorescence intensity of the micropatterned anti-CD3 remained stable during the immersion of hydrogels in PBS or cell culture medium even after for 24 h (Figure A8), demonstrating that the anti-CD3 antibody was stably conjugated to our hydrogels.
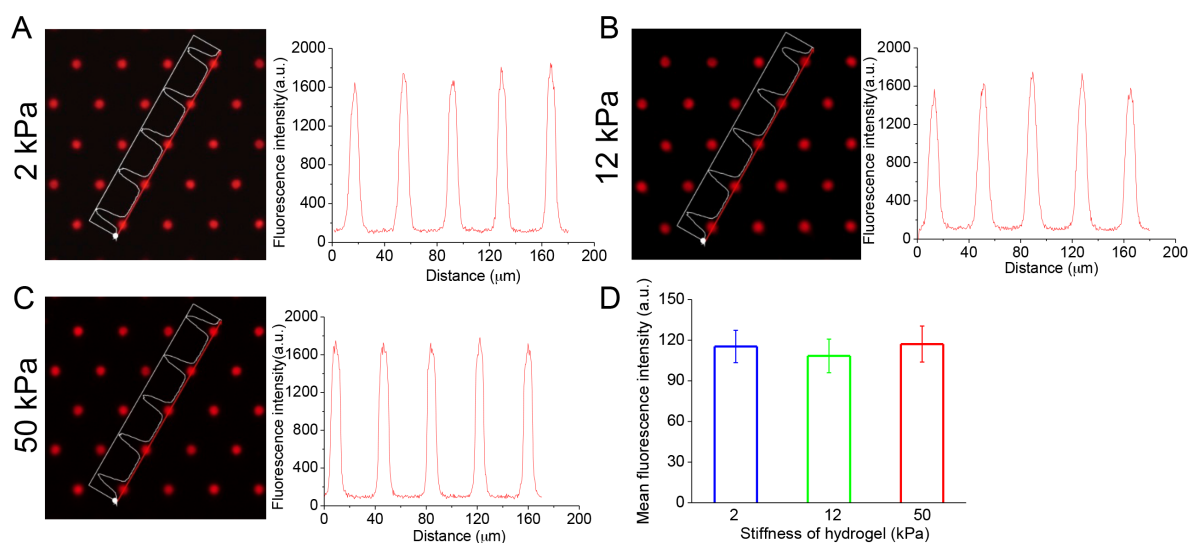

Figure 5. Examples of fluorescence images and intensity profiles of micropatterned anti-CD3 (8/30 µm) on hydrogels with stiffness 2 (A), 12 (B), and 50 kPa (C). (D) The mean fluorescence intensities of micropatterned anti-CD3 on hydrogels of different stiffness taken from A-C. Three independent experiments were used for analysis. Data are presented as mean ± SD.

3.2.2 ZAP70 phosphorylation on anti-CD3 functionalized hydrogels of different stiffness

The attachment and morphology of Jurkat T-cells on unpatterned 2, 12, and 50 kPa hydrogels with equal surface density of anti-CD3 ligand was analyzed. Cells were seeded for 30 min and then captured for analysis. Cells were able to recognize and attach to all hydrogels, but the number of the attached cells and the morphology adopted varied with the substrate stiffness. A 2-fold and 1.6-fold higher number of attached cells were found on 50 kPa and 12 kPa hydrogel, respectively, compared with that on 2 kPa hydrogel (Figure 6). Attached cells showed protrusions on stiffer hydrogels (Figure 6A-C). Cells seeded on 50 kPa streptavidin-functionalized hydrogels without anti-CD3 modification (biotin-anti-CD3 was replaced with biotin-PEG-OH as control experiment) showed negligible cell attachment (Fig. 6D), indicating that the interaction between cells and hydrogels was specifically mediated by the immobilized anti-CD3.

Our results are in agreement with Saitakis et al.,[7] who reported minimal T cell spreading on 0.5 and 6.4 kPa hydrogel and more pronounced spreading and cell extensions on 100 kPa hydrogels. Unfortunately, the quantification of spreading areas is not reported.[9, 15] Interestingly, Wahl et al. [18] reported that T cells respond to stiffness (0.5 kPa-40 MPa) in a biphasic fashion, reaching a maximal spreading on an optimal substrate stiffness (3-20 kPa) comparable to that of professional APCs. We did not find a biphasic behavior in our studies, only a steady increase in spreading with stiffness. Differences in the surface density of anti-CD3 as consequence of the different immobilization strategy could be the reason for the different results. Note that for adherent cells stiffness sensitivity can also be influenced by increasing the ligand density.[27]
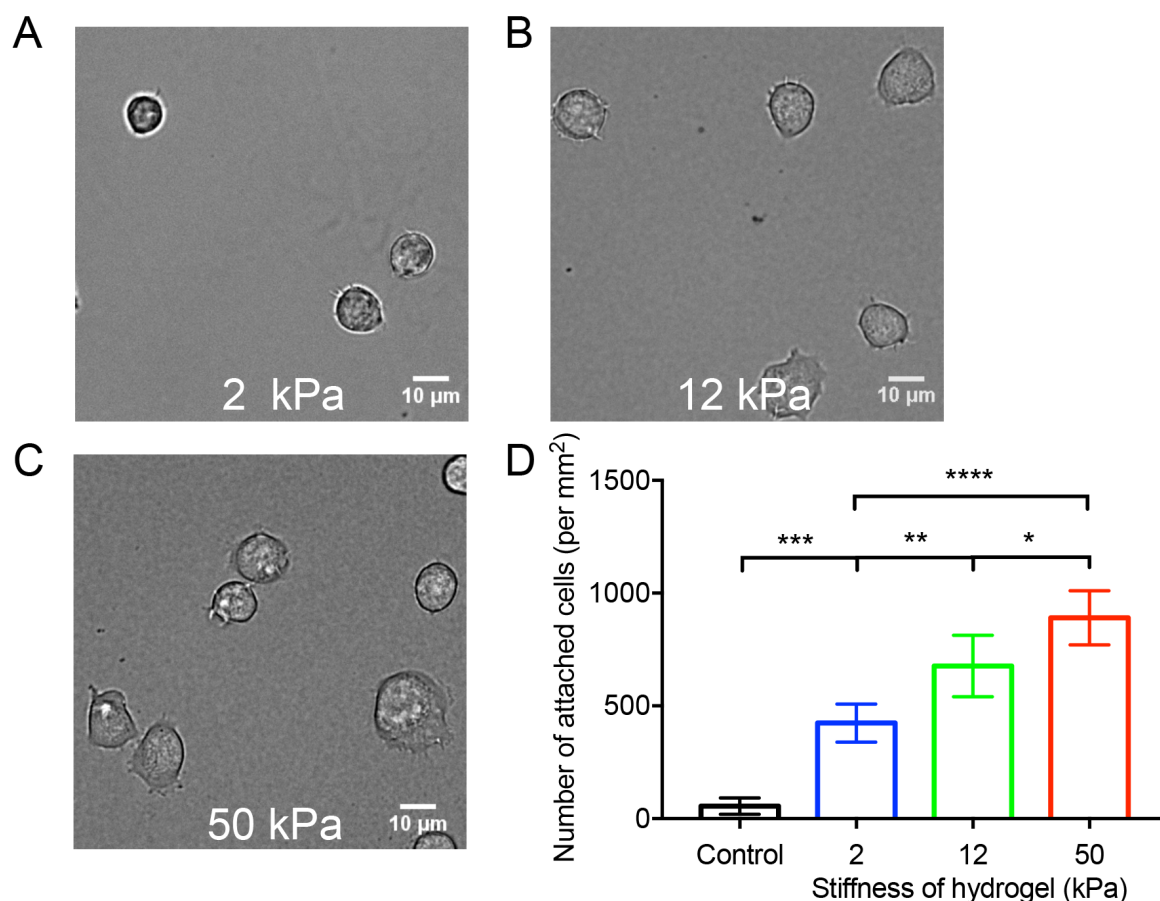
Figure 6. (A-C) Representative bright field images to show the morphology of Jurkat T-cells on anti-CD3 modified hydrogels of 2 (A), 12 (B), and 50 kPa (C) 30 min after cell seeding. Scale bar is 10 μm. (D) Quantitative analysis of the number of Jurkat T-cells attached to anti-CD3 modified hydrogels with different stiffness after gentle washing with PBS. Three independent experiments were used for statistical analysis. Bars represent means ± SD.

On stiff substrates like glass, plastic or glass-supported lipid bilayers coated with TCR-activators (Young's Modulus of tens of GPa), T cells have been reported to adopt a flat symmetrical round shape.[7, 28, 29] In our experiments, Jurkat T-cells on 50 and 12 kPa hydrogels did not display a flat symmetrical round shape. The higher number of attached cells on stiffer substrates modified with anti-CD3 alone agrees

with the findings on substrates modified with anti-CD3 plus anti-CD28, and or ICAM-1 from other authors.[7, 15] Thus, our findings confirm that CD3-dependent activation might play a leading role in the T cell mechanosensing, at least in terms of cell attachment.

To gain a further understanding of the stiffness-mediated modulation of T cell activation, we examined the induced level of phosphorylated ZAP70 (pY), which serves as an early T cell activation marker. ZAP70 is an inactive cytosolic tyrosine kinase that is recruited to a transmembrane receptor lacking intrinsic catalytic activity. Phosphorylation of ZAP70 on tyrosine residues (Tyr-315 and Tyr-319) upon TCR/CD3 stimulation is the initial step of TCR/CD3-mediated signal transduction. The pY signal was quantified 15 min after cell seeding. We found pY signal could be detected at all artificial IS interfaces formed between Jurkat T-cells and hydrogels (Figure 7A). A 1.9- and 1.6-fold higher pY level was observed on 50 kPa hydrogel than that on 2 and 12 kPa hydrogel, respectively (Figure 7B). It should be noted that the cell spreading area, as measured by measured by F-actin, also increased with stiffness: 173, 224 and 249 μm^2 on 2, 12 and 50 kPa hydrogels respectively (Figure 7A,C). These results suggest that the substrate stiffness can enhance T cell spreading and activation level, at least as measured by pY signal. In addition, it further confirms that the sensing of substrate rigidity probably occurs at least partly through the downstream of Zap70, which is consistent with findings from Judokusumo et al.'s research.[15] Tabdanov et al. [17] also demonstrated the early T cell activation (measured by the anti-phosphotyrosine antibody pY20) can be elevated on stiffer substrate coated with anti-CD3. Interestingly, Hui et al. [9] suggested that the early (2 min) pY signaling increases with substrate stiffness while the sustained (15 min) pY signaling decrease with substrate stiffness, which seems contradictory to our results. However, the authors used a poly-L-lysine coating to bind

anti-CD3 to the hydrogel, which might mediate ionic interactions with the cell membrane and thus trigger a faster T cell activation. Our trials to capture early burst of pY signal at 2 min were unsuccessful since cells could not stably attach to our anti-CD3 modified hydrogels within 2 min.
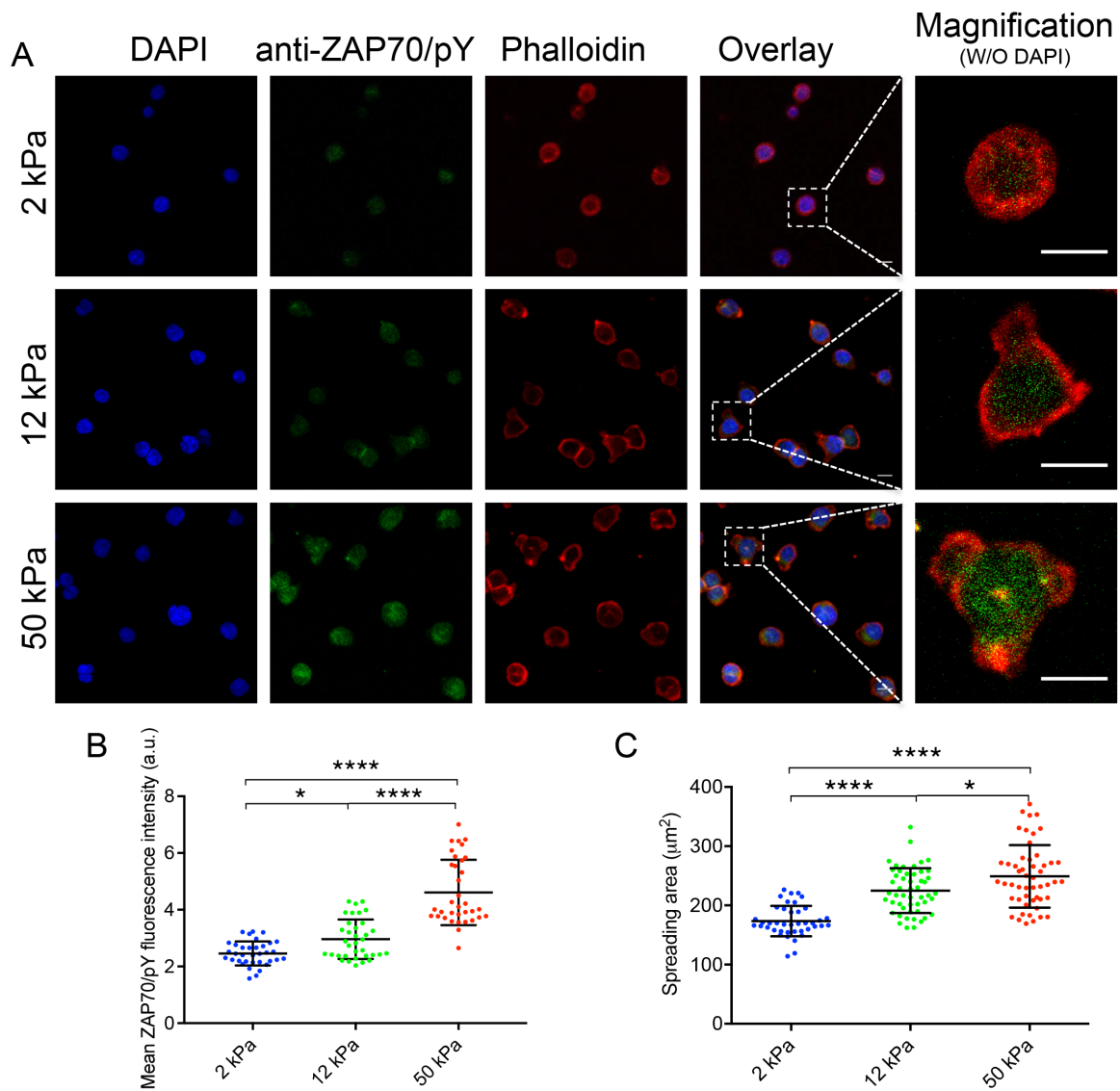

Figure 7. Representative immunofluorescence images of Jurkat T-cells on anti-CD3

modified hydrogels with different stiffness (2, 12, and 50 kPa). (A) Immunostaining of nuclei (blue), ZAP70/pY (green) and F-actin (red) at the interface between Jurkat T-cells and substrate. Dotted area shows the magnification image of single cell in the right column. Scale bar is 10 μm. (B) Statistical quantification of the mean fluorescence intensity of ZAP70/pY within the artificial IS between Jurkat T-cells and substrates with different stiffness. (C) Quantification of cell spreading area as measured by F-actin. Cells were seeded for 15 min before fixing and staining. Each dot represents one analyzed cell in three independent experiments. Bars represent means ± SD.

The clear dependence between cell attachment and activation, and the coupled effects of stiffness and spreading area in all these experiments hinder a conclusive statement whether the enhanced early T cell activation by stiffer substrate is a consequence of stiffness itself, or by stiffness-dependent cell spreading. Therefore, we designed experiments to clarify this issue.

3.2.3 ZAP70 phosphorylation on anti-CD3 patterned hydrogels

Jurkat T-cells were seeded on the micropatterned anti-CD3 hydrogels (substrates as shown in Figure 5) for 15 min and then fixed for analysis. The micropatterned anti-CD3 on hydrogels could limit cell spreading to a similar area, which allows studying how T cell activation is modulated by substrate stiffness independent of cell spreading.
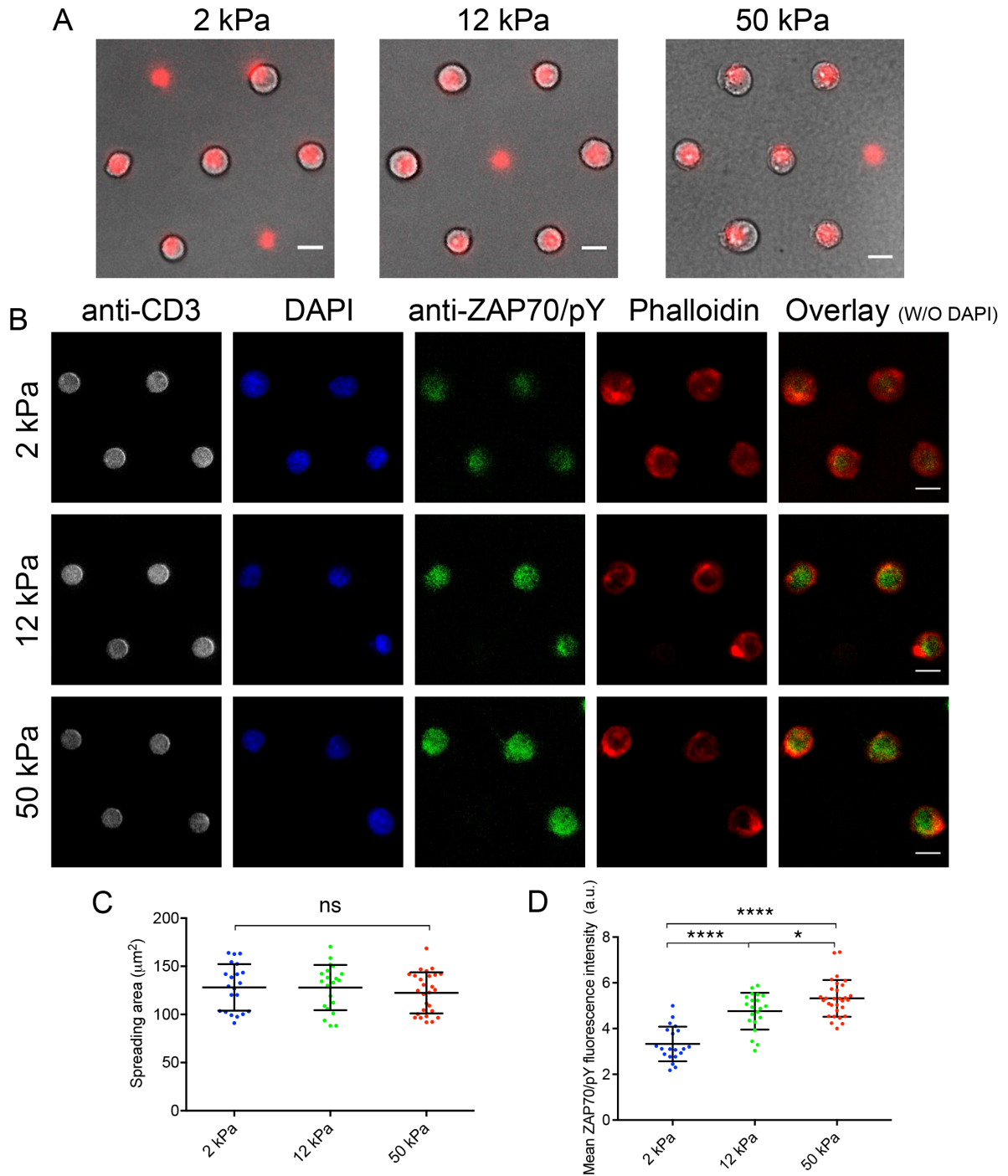
Figure 8. (A) Bright field imaging of Jurkat T-cells attached to micropatterned anti-CD3 arrays (8 μm diameter dots) on hydrogels of different stiffness (2, 12, and 50 kPa). (B) Representative images of stained nuclei (blue), ZAP70/pY (green), and F-actin (red) of Jurkat T-cells attached to anti-CD3 dots on hydrogels of different

stiffness. (C,D) Quantitative analysis of the spreading area (C) and mean fluorescence intensity of ZAP70/pY signal (D) at the interface between Jurkat T-cells and hydrogels of different stiffness. Cells were seeded for 15 min before fixing and staining. Each dot represents one analyzed cell in three independent experiments. Scale bar is 10 μm. Bars represent means ± SD.

Cells attached to the 8 μm (around 50 μm^2) anti-CD3 dots effectively, and remained on the micropatterned areas after gentle washing with PBS (Figure 8A), demonstrating that the micropatterned anti-CD3 still retained the bioactivity after printing. Dots of smaller size did not support stable adhesion and cells were easily washed away during fixing and staining. Larger dots (diameter > 11 μm) were not fully covered by Jurkat T-cells. Note that these cells have a diameter between 11 and 13 μm in suspension [30]. The stable attachment of Jurkat T- cells was determined by the anti-CD3 density on the 8 μm dots, which could be tuned by using different concentrations of the anti-CD3 ink. Jurkat T-cells attached well to 8 μm anti-CD3 dots generated with ink concentrations equal to or greater than 100 μg/mL (Figure 8A). Cells spreading area correlated with dot size on all substrates at anti-CD3 concentration of 100 μg/mL (Figure 8B). We further analyzed cell spreading area and pY signal of Jurkat T-cells immobilized on the micropatterned dots of the hydrogels with different stiffness. The spreading area was independent of substrate stiffness (Figure 8C). The pY signal was detectable on all cell-substrates interfaces 15 min after cell seeding, and showed an increase with substrate stiffness (Figure 8B, D). A 1.6- and 1.4-times higher pY level was observed on 50 kPa and 12 kPa hydrogels *vs.* 2 kPa hydrogels. Since the spreading area of individual cell on all micropatterned surfaces is similar, we can conclude that the early T cell activation, at least as measured by pY signal, responds to substrate stiffness rather than the effect of

stiffness on cell spreading. Bigger contact areas as observed in stiffer substrate may even strengthen the activation by engaging more CD3 molecules.

3.3 Conclusion

Studies of T cell activation using hydrogels as engineered cell-like interface have not been able to provide a conclusive demonstration on how stiffness influences T cell activation. The observed different spreading area on substrates with different stiffness, and the limited control of the ligand density on the hydrogel surface in most reported studies mask the contribution of mechanic parameters on IS formation and the immunological response. Here we present a simple and detailed experimental protocol to form artificial IS with defined area and similar ligand density on hydrogels of different stiffness. This system allowed a conclusive evaluation of receptor-specific T cell responses to APC mechanics and demonstrated that CD3 mediated early T cell activation, in terms of ZAP70 phosphorylation, is enhanced with increasing substrate stiffness.

3.4 Materials and methods

Reagents and materials

Solvents with p.a. purity were used as purchased unless specified. Acrylamide (AAm), acrylic acid (AA), N,N'-methylene-bis-acrylamide (bis-AAm), ammonium persulfate (APS, 10% w/v in PBS), tetramethylethylnediamine (TEMED), 3-acryloxypropyl-trimethoxysilane (3-APS), Sigmacote®, NaOH (5 M), NaCl (0.5 M), PBS buffer (1X, pH 7.0-7.4), 2-(N-morpho)-ethanesulfonic acid solution (MES buffer, 0.1 M, pH 4.5), ethanol (97%), bovine serum albumin (BSA), Biotin-PEG$_8$-NH$_2$, pararosaniline base, Atto 543 biotin, gold nanoparticles suspension (300 nm), N-hydroxysuccinimide (NHS), dimethylaminopropyl-3-ethylcarbodiimide

hydrochloride (EDC), were purchased from Sigma-Aldrich Chemie GmbH. Streptavidin, Alexa 488 streptavidin, Cy5 streptavidin, Alexa Fluor 555 NHS ester, Alexa Fluor 568 phalloidin were from Thermo Fisher Scientific. Biotin-PEG-OH (5 kDa) was from Nanocs. Inc. The following antibodies were purchased from Biolegend GmbH: biotinylated mouse anti human CD3 (anti-CD3), Alexa Fluor 488 anti-Zap70 (Y319)/Syk (Y352) antibody, PE anti-mouse IgG.

Preparation of PAAm-co-AA hydrogels with different stiffness

PAAm-co-AA hydrogels with different stiffness were prepared as indicated in section 2.4 (Materials and methods) of Chapter 2.

Characterization of the stiffness of hydrogels by AFM

The stiffness of glass supported hydrogel discs were characterized by AFM as indicated in section 2.4 (Materials and methods) of Chapter 2.

Functionalization of PAAm-co-AA hydrogels with

The biotinylation of PAAm-co-AA hydrogels was performed as mentioned in section 2.4 (Materials and methods) of Chapter 2.

Biofunctionalization of hydrogels of different stiffness with equal anti-CD3 density

Biotin-PEG$_8$-NH$_2$ functionalized PAAm-co-AA hydrogels with different stiffness were incubated with 100 μL of streptavidin solution (100 μg/mL) for different times between 0 to 3 h at 0.5 h interval. The concentration of immobilized streptavidin at the different incubation times was characterized by fluorescence imaging (see sections below). For cell studies, a streptavidin incubation time of 1-1.5 h was applied to 2 kPa

hydrogel and 2.5-3 h was applied to 12 and 50 kPa hydrogels. Under these conditions equal anti-CD3 densities were obtained on the hydrogels, independently of their mechanical properties. Streptavidin-functionalized hydrogels were further incubated with Atto 543 biotin (100 μg/mL, 100 μL) or biotinylated anti-CD3 (100 μg/mL, 100 μL) overnight at 4 °C.

Micropatterned anti-CD3 on hydrogels with different stiffness

Polydimethylsiloxane (PDMS, Sylgard 184 Silicone Elastomer Kit, Dow Corning) stamps were fabricated by double soft molding from a SU-8 photolithographic template [31, 32] as shown in Figure A7. The surface of the SU-8 template was previously passivated with a fluorosilane (1H,1H,2H,2H-Perfluorodecyltrichlorosilane) layer to avoid PDMS sticking by exposing the template to the fluorosilane in an evacuated oven for 30 min and baking at 90 °C for 1h. This step facilitates the peeling of the PDMS mold from the SU-8 template. A solution of PDMS Sylgard 184 A + B (elastomer: curing agent = 10:1 w/w) was mixed, degassed, and poured onto micropatterned SU-8 template followed by curing at 90°C for 1.5 h in oven. Patterned areas (5 x 5 mm^2) were cut from PDMS mold, washed in a 70% v/v ethanol solution and dried under a N$_2$ flow. The PDMS mold was treated with fluorosilane as described before for the SU-8 template. A second soft molding step was performed on it using the stamp casting station and frame from GeSiM μContact Printer. After curing at 90°C for 1.5 h, PDMS stamps with arrays of rounded pillars having a height around 5 μm and diameter about 8 μm were obtained.

In order to micropattern biotinylated anti-CD3 on the streptavidin-modified hydrogels, hydrogels were slowly dried within a chemical hood over 15 min. The PDMS stamps were cleaned in an ultrasound bath immersed in acetone and ethanol-MilliQ water for 5 min, followed by washing with water and dried with compressed nitrogen. The

surface of the PDMS stamps was hydrophilized by exposure to oxygen plasma (0.3 Mbar, 2 min). Biotinylated anti-CD3 solution (100 μg/mL, 10 μL) was applied on the stamp immediately after plasma treatment and incubated for 1 h. The solution was removed from the stamp and the stamp surface was gently dried with N_2. After moistening the anti-CD3 adsorbed stamp in humid box (95-98% humidity) for 5 min, microcontact printing was immediately performed with a GeSiM μContact Printer 4.1 (GeSiM, Germany) using a printing pressure of 12 kPa for 5 min at room temperature. The micropatterned substrate were left at ambient humidity for 30 min at 4°C after printing, followed by washing with PBS twice and blocking with biotin-PEG-OH (5K, 100 μg/mL, 100 μL) and BSA solution (100 μg/mL, 100 μL) for 1 h at room temperature. The obtained micropatterns were homogeneous and highly reproducible. Micropatterns were imaged by confocal fluorescence microscopy.

The reported conditions were obtained after a careful optimization of the experimental parameters. Higher printing pressures (14-15 kPa) resulted in the collapse of PDMS pillars and contamination of the background area with fluorescent protein (Figure A9). Shorter printing time (1 min) lead to a decrease in homogeneity and resolution (Figure A9A,B). Factors like the drying of the hydrogel and the PDMS after inking have an obvious influence on the quality of the microcontact printed features.

Characterization of the fluorescence intensity across the functionalized hydrogels

The distribution of streptavidin-488 or Atto-543-biotin molecules across the hydrogel was characterized by imaging the fluorescence intensity along the z-axis by confocal fluorescence microscopy. Gold nanoparticles (300 nm) were applied on the top of the hydrogels to facilitate identification of the top surface of the hydrogel in swollen state. The fluorescence signal was measured by scanning in z-axis from the top surface

(200 nm interval, 40 ×/W objective). Typical scanning depth was 25 μm. In order to visualize the concentration of anti-human CD3 in the hydrogel, hydrogels were also incubated with PE anti-mouse IgG antibody (0.2 mg/mL) overnight at 4°C and washed twice with PBS. The distribution of the mean fluorescence intensity of streptavidin-488 (4 μm depth), biotin-563 (4 μm depth) or PE anti-mouse IgG (1 μm depth) at the gel surface was analyzed by ImageJ software.

Fluorescence intensity determination on micropatterned hydrogels

Biotinylated anti-CD3 (0.5 mg/mL) was fluorescently labeled with Alexa Fluor 555 NHS ester (100 μg/mL) for 2 h at RT. 555-biotin-antiCD3 (100 μg/mL) was micropatterned on hydrogels of different stiffness. The distribution of the anti-CD3 across the gel thickness was imaged by confocal microscopy (scanning in z-axis with 200 nm interval, 40 ×/W objective). Surface profiles (within a depth of 2 μm) of the hydrogel were analyzed by image J software to compare the relative fluorescence intensity at the surface of micropatterned anti-CD3.

Cell culture

Jurkat T-cells, clone E6-1 (ATCC® TIB-152™) were cultured in RPMI-1640 Medium (Gibco) supplemented with 10% fetal bovine serum (Gibco), 100 units/mL penicillin, and 100 μg/mL streptomyocin at 37°C, 5% CO_2.

Immunochemistry

As for cell attachment experiment, Jurkat T-cells were seeded on hydrogels at a cell density of 200,000 cells/cm^2 for 0.5 h before fixing and imaging. As for T cell spreading and activation experiments, Jurkat T-cells were seeded on hydrogels at a similar cell density but only for 15 min before fixing and imaging. Cells were fixed and

permeabilized with a solution of 4% paraformaldehyde and 0.05% Triton X-100 (Sigma, Saint-Louis, MO) in PBS for 15 minutes at 37°C and washed with PBS for 3 times. Jurkat T-cells were stained with Alexa Fluor 568 Phalloidin and Alexa Fluor 488 anti-Zap70 (Y319)/Syk (Y352) antibody for 2 h at 37°C followed by being mounted (with DAPI).
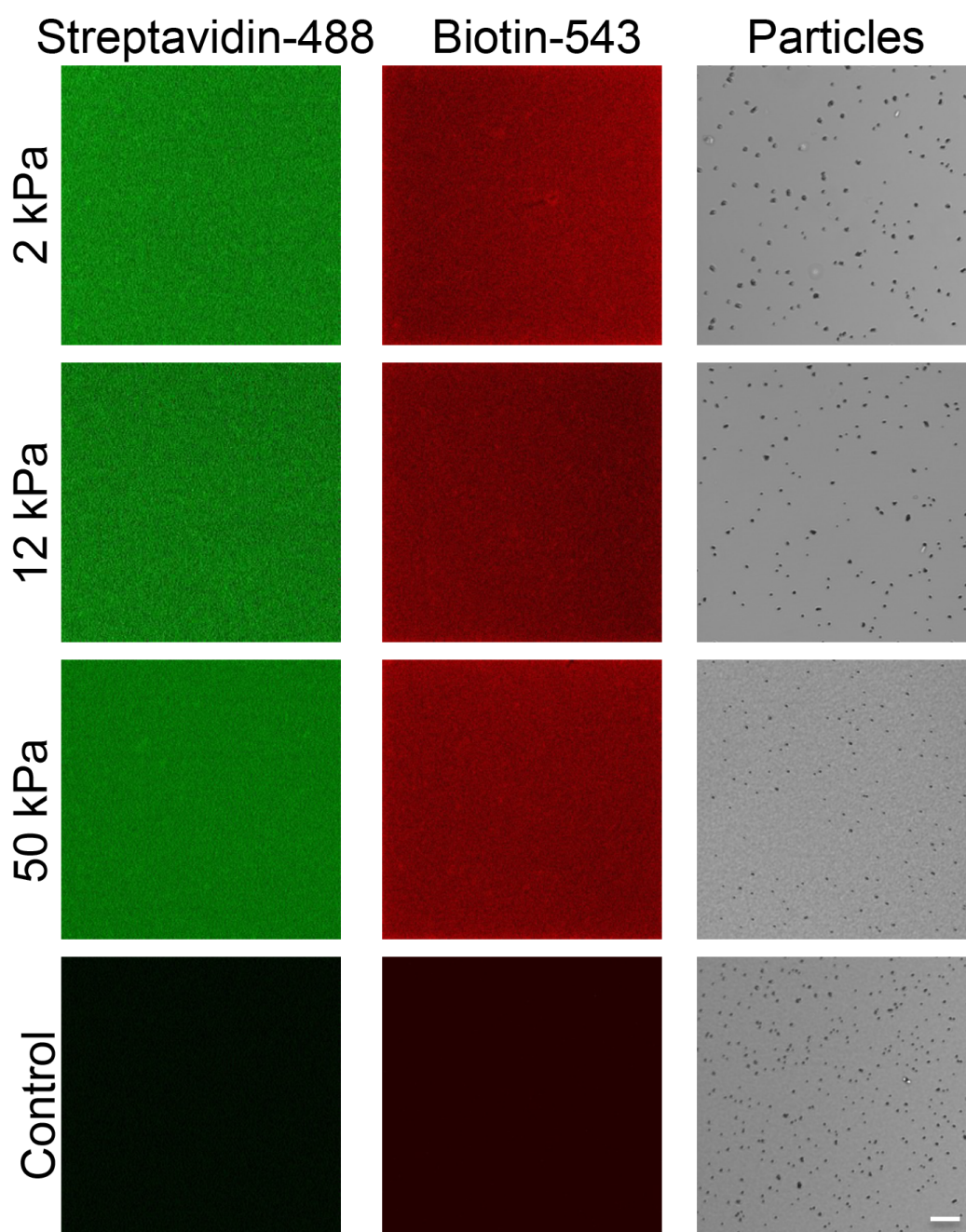
Appendix Chapter 3

Figure A5. Fluorescence images of the top surface of hydrogel functionalized with streptavidin-488 and biotin-543. Molecules are homogenously distributed on hydrogel surface. Scale bar 10 μm.
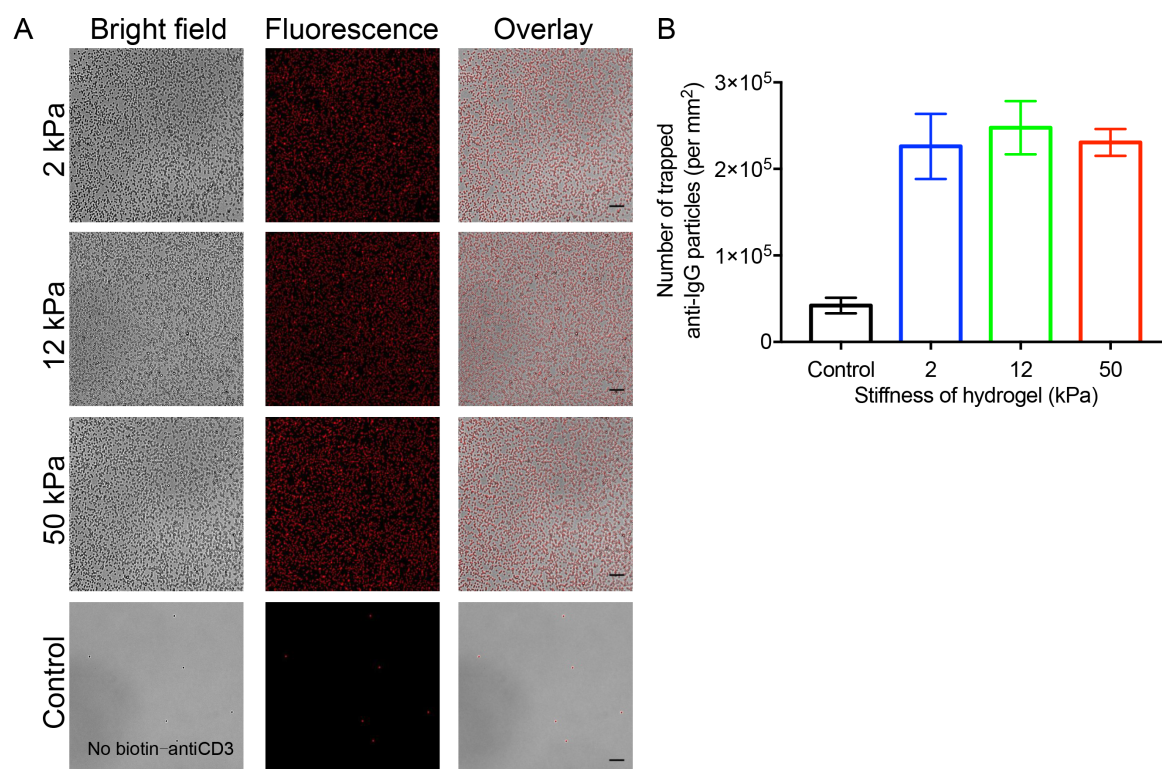
Figure A6. (A) Representative images to show anti-CD3 distribution after labeling by anti-IgG antibody coated particles (0.7 μm). Scale bar 10 μm. (B) The number of trapped anti-IgG antibody coated particles on substrate of different stiffness after washing gently with PBS. Three independent experiments were used for statistical analysis. Bars represent means ± SD.
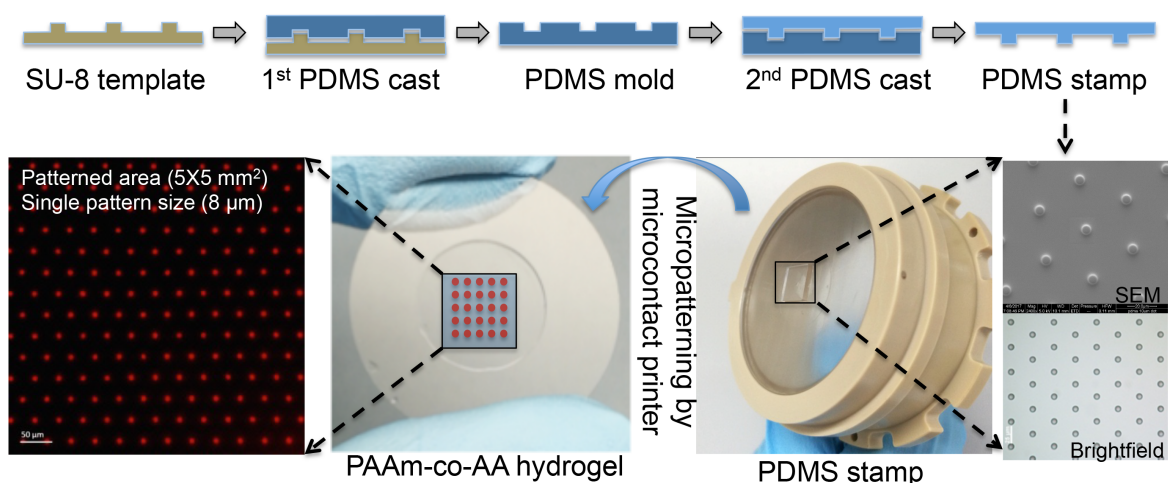
Figure A7. Schematic diagram to show the preparation of micropatterned molecules (streptavidin or biotinylated anti-CD3) on PAAm-co-AA hydrogel of different stiffness by microcontact printer.
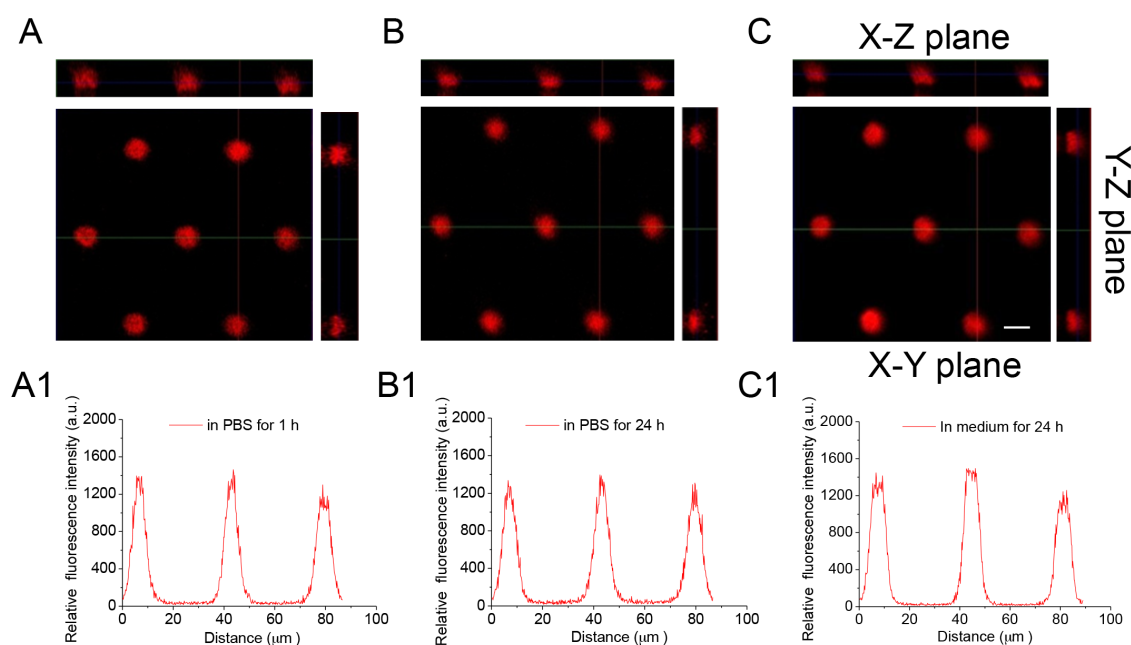
Figure A8. Fluorescence images and fluorescence intensity profiles of

micropatterned anti-CD3 (8/30 μm) on hydrogel (50 kPa) after keeping 1 h (A, A1), 24 h (B, B1) in PBS and 24 h (C, C1) in medium. Scale bar, 10 μm.

Figure A9. Fluorescence images of micropatterned streptavidin-488 (8/30 μm) on hydrogel (50 kPa) generated by 10-12 kPa N_2 pressure for 1 (A) and 5 min (B) or 14-15 kPa N_2 pressure for 1 (C) and 5 min (D).

References

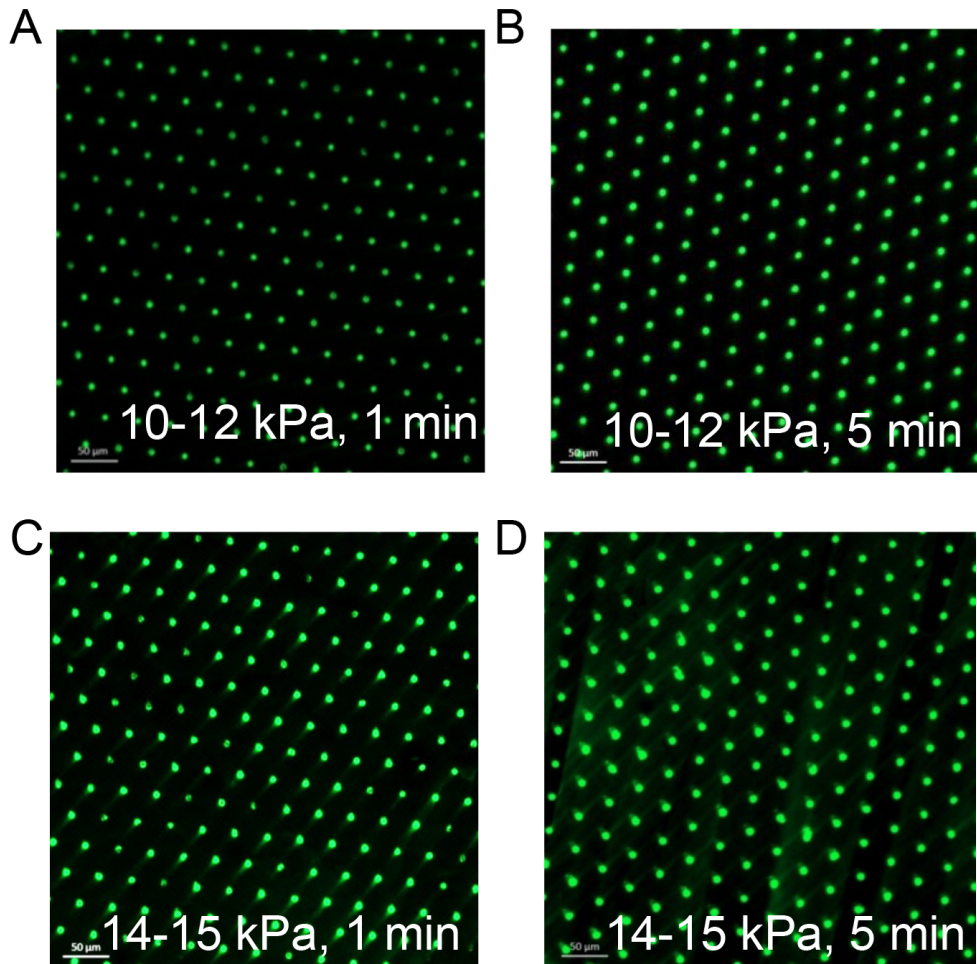[1] N. Bufi, M. Saitakis, S. Dogniaux, O. Buschinger, A. Bohineust, A. Richert, M. Maurin, C. Hivroz, A. Asnacios, Human Primary Immune Cells Exhibit Distinct Mechanical Properties that Are Modified by Inflammation, Biophys. J. 108(9) (2015) 2181-90.

[2] Y. Liu, L. Blanchfield, V.P. Ma, R. Andargachew, K. Galior, Z. Liu, B. Evavold, K. Salaita, DNA-based nanoparticle tension sensors reveal that T-cell receptors transmit defined pN forces to their antigens for enhanced fidelity, Proc. Natl. Acad. Sci .U. S. A. 113(20) (2016) 5610-5.

[3] V.P. Ma, Y. Liu, L. Blanchfield, H. Su, B.D. Evavold, K. Salaita, Ratiometric Tension Probes for Mapping Receptor Forces and Clustering at Intermembrane Junctions, Nano Lett. 16(7) (2016) 4552-9.

[4] R. Ma, A.V. Kellner, V.P. Ma, H. Su, B.R. Deal, J.M. Brockman, K. Salaita, DNA probes that store mechanical information reveal transient piconewton forces applied by T cells, Proc. Natl. Acad. Sci .U. S. A. 116(34) (2019) 16949-16954.

[5] C. Hivroz, M. Saitakis, Biophysical Aspects of T Lymphocyte Activation at the Immune Synapse, Front. Immunol. 7 (2016) 46.

[6] R. Basu, M. Huse, Mechanical Communication at the Immunological Synapse, Trends Cell Biol. 27(4) (2017) 241-254.

[7] M. Saitakis, S. Dogniaux, C. Goudot, N. Bufi, S. Asnacios, M. Maurin, C. Randriamampita, A. Asnacios, C. Hivroz, Different TCR-induced T lymphocyte responses are potentiated by stiffness with variable sensitivity, eLife 6 (2017).

[8] R. Basu, B.M. Whitlock, J. Husson, A. Le Floc'h, W. Jin, A. Oyler-Yaniv, F. Dotiwala, G. Giannone, C. Hivroz, N. Biais, J. Lieberman, L.C. Kam, M. Huse, Cytotoxic T Cells Use Mechanical Force to Potentiate Target Cell Killing, Cell 165(1)

(2016) 100-110.

[9] K.L. Hui, Balagopalan, L.L.E. Samelson, A. Upadhyaya, Cytoskeletal forces during signaling activation in Jurkat T-cells, Mol. Biol. Cell 26(4) (2015) 685-95.

[10] A. de la Zerda, M.J. Kratochvil, N.A. Suhar, S.C. Heilshorn, Review: Bioengineering strategies to probe T cell mechanobiology, APL Bioeng. 2(2) (2018) 021501.

[11] J.W. Hickey, Y. Dong, J.W. Chung, S.F. Salathe, H.C. Pruitt, X. Li, C. Chang, A.K. Fraser, C.A. Bessell, A.J. Ewald, S. Gerecht, H.Q. Mao, J.P. Schneck, Engineering an Artificial T-Cell Stimulating Matrix for Immunotherapy, Adv. Mater. 31(23) (2019) e1807359.

[12] A. Dang, S. De Leo, D.R. Bogdanowicz, D.J. Yuan, S.M. Fernandes, J.R. Brown, H.H. Lu, L.C. Kam, Enhanced activation and expansion of T cells using mechanically soft elastomer fibers, Adv. Biosyst. 2(2) (2018).

[13] L. MacQueen, Y. Sun, C.A. Simmons, Mesenchymal stem cell mechanobiology and emerging experimental platforms, J. R. Soc., Interface 10(84) (2013) 20130179.

[14] Y. Shao, J. Fu, Integrated micro/nanoengineered functional biomaterials for cell mechanics and mechanobiology: a materials perspective, Adv. Mater. 26(10) (2014) 1494-533.

[15] E. Judokusumo, E. Tabdanov, S. Kumari, M.L. Dustin, L.C. Kam, Mechanosensing in T lymphocyte activation, Biophys. J. 102(2) (2012) L5-7.

[16] R.S. O'Connor, X. Hao, K. Shen, K. Bashour, T. Akimova, W.W. Hancock, L.C. Kam, M.C. Milone, Substrate rigidity regulates human T cell activation and proliferation, J. Immunol. 189(3) (2012) 1330-9.

[17] E. Tabdanov, S. Gondarenko, S. Kumari, A. Liapis, M.L. Dustin, M.P. Sheetz, L.C. Kam, T. Iskratsch, Micropatterning of TCR and LFA-1 ligands reveals complementary effects on cytoskeleton mechanics in T cells, Integr. Biol. 7(10) (2015)

1272-84.

[18] A. Wahl, C. Dinet, P. Dillard, A. Nassereddine, P.H. Puech, L. Limozin, K. Sengupta, Biphasic mechanosensitivity of T cell receptor-mediated spreading of lymphocytes, Proc. Natl. Acad. Sci. U. S. A. 116(13) (2019) 5908-5913.

[19] K.H. Hu, M.J. Butte, T cell activation requires force generation, J. Cell Biol. 213(5) (2016) 535-42.

[20] K.T. Bashour, A. Gondarenko, H. Chen, K. Shen, X. Liu, M. Huse, J.C. Hone, L.C. Kam, CD28 and CD3 have complementary roles in T-cell traction forces, Proc. Natl. Acad. Sci. U. S. A. 111(6) (2014) 2241-6.

[21] K. Shen, V.K. Thomas, M.L. Dustin, L.C. Kam, Micropatterning of costimulatory ligands enhances CD4+ T cell function, Proc. Natl. Acad. Sci. U. S. A. 105(22) (2008) 7791-6.

[22] K.I. Jankowska, E.K. Williamson, N.H. Roy, D. Blumenthal, V. Chandra, T. Baumgart, J.K. Burkhardt, integrins Modulate T cell receptor signaling by constraining actin Flow at the immunological synapse, Front. Immunol. 9(25) (2018).

[23] J. Doh, D.J. Irvine, Immunological synapse arrays: patterned protein surfaces that modulate immunological synapse structure formation in T cells, Proc. Natl. Acad. Sci. U. S. A. 103(15) (2006) 5700-5.

[24] B. Trappmann, J.E. Gautrot, J.T. Connelly, D.G. Strange, Y. Li, M.L. Oyen, M.A. Cohen Stuart, H. Boehm, B. Li, V. Vogel, J.P. Spatz, F.M. Watt, W.T. Huck, Extracellular-matrix tethering regulates stem-cell fate, Nat. Mater. 11(7) (2012) 642-9.

[25] C.S. Neish, I.L. Martin, R.M. Henderson, J.M. Edwardson, Direct visualization of ligand-protein interactions using atomic force microscopy, Br. J. Pharmacol. 135 (2002) 1943-1950.

[26] Y. Chen, J. Cai, Q. Xu, Z.W. Chen, Atomic force bio-analytics of polymerization and aggregation of phycoerythrin-conjugated immunoglobulin G molecules, Mol.

Immunol. 41(12) (2004) 1247-52.

[27] A. Engler, L. Bacakova, C. Newman, A. Hategan, M. Griffin, D. Discher, Substrate compliance versus ligand density in cell on gel responses, Biophys. J. 86(1) (2004) 617-28.

[28] S.C. Bunnell, V. Kapoor, R.P. Trible, W. Zhang, L.E. Samelson, Dynamic actin polymerization drives T cell receptor-induced spreading: a role for the signal transduction adaptor LAT, Immunity 14(3) (2001) 315-29.

[29] A. Brodovitch, P. Bongrand, A. Pierres, T lymphocytes sense antigens within seconds and make a decision within one minute, J. Immunol. 191(5) (2013) 2064-71.

[30] M.J. Rosenbluth, W.A. Lam, D.A. Fletcher, Force microscopy of nonadherent cells: a comparison of leukemia cell deformability, Biophys. J. 90(8) (2006) 2994-3003.

[31] S. Alom Ruiz, C.S. Chen, Microcontact printing: A tool to pattern, Soft Matter 3(2) (2007) 168-177.

[32] A.d. Campo, C. Greiner, SU-8: a photoresist for high-aspect-ratio and 3D submicron lithography, J. Micromech. Microeng. 17(6) (2007) R81-R95.

Chapter 4

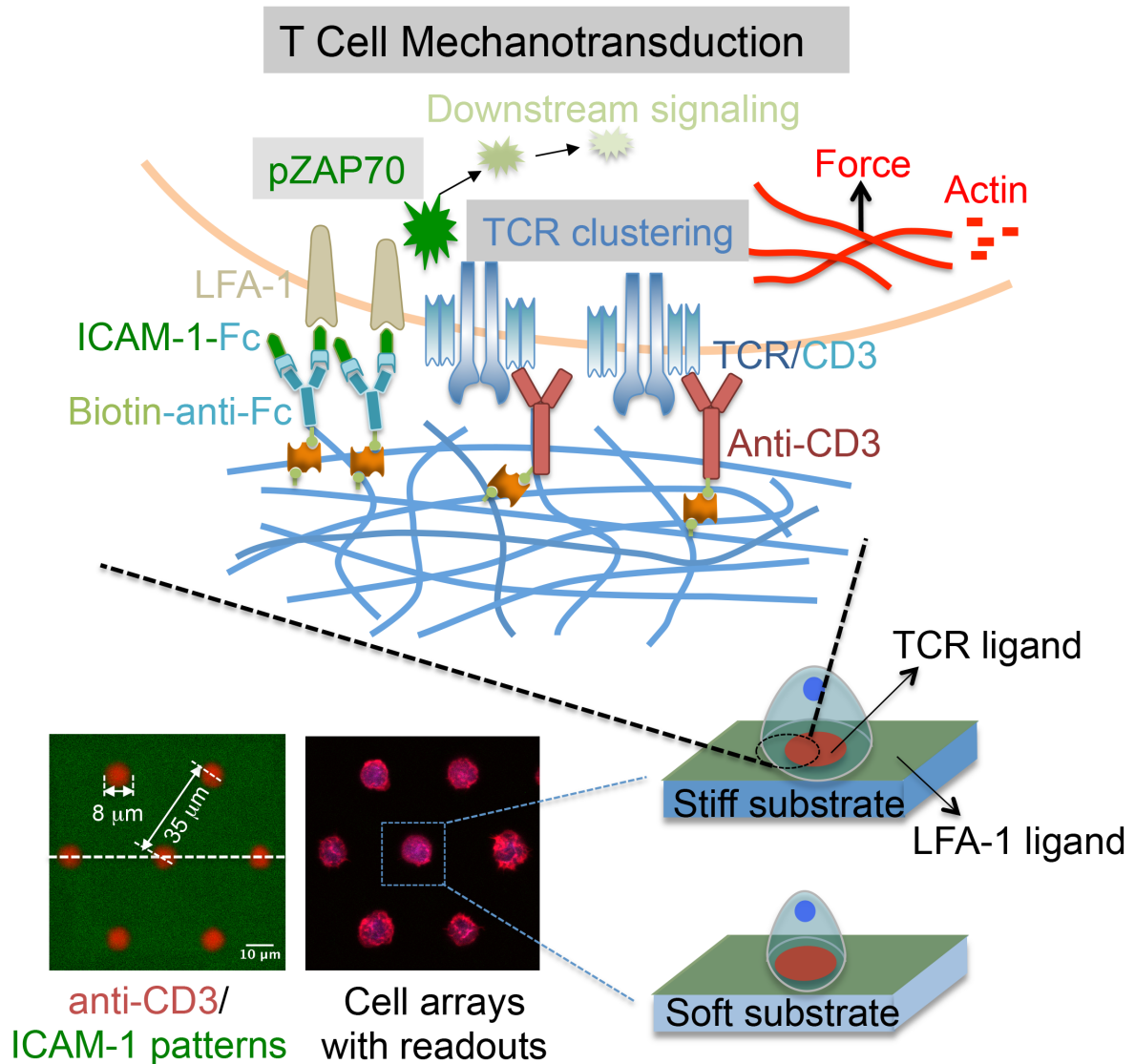# 4 T cell activation on anti-CD3/ICAM-1 patterned hydrogels

4.1 Introduction

T cell receptor (TCR) triggering is accompanied by the maturation of immunological synapse (IS), which involves the arrangement of the participating receptor-ligands pairs to finally form a concentric micron-scale structure at the T cell-APC interface.[1-4] Motivated by the segregated structure of the natural IS, microfabricated platforms with spatially segregated ligands have been developed to understand the role of assembly dynamics and geometry in T cell response.[5-10]

To directly figure out the role of TCR distribution during T cell activation, Doh and Irvine [5] fabricated multicomponent protein surfaces with micropatterned anti-CD3 surrounded by backfilled intercellular adhesion molecule-1 (ICAM-1), a ligand engaging with T cell integrin lymphocyte function-associated antigen 1 (LFA-1), to mimic T cell–APC interactions. Results showed that a full T activation was observed when anti-CD3 spots were surrounded by ICAM-1. This approach was further extended by Kam and Dustin [6] to create patterned surfaces with three components including anti-CD3, anti-CD28, and ICAM-1, by using multiple steps of microcontact printing. It was shown that the peripheral presenting of anti-CD28 to the cell, surrounding anti-CD3 spots on an ICAM-1 background, enhances cytokine (IL-2) secretion in naive $CD4^+$ T cells compared with integrating all these signals in the center of the IS. These studies highlight the importance of the APC ligands organization for the T cell activation.

In addition to the spatial organization of ligands, the role of mechanical force at the IS is actually more and more recognized as central in the process of T cell activation.[11-14] Many studies revealed that TCR-CD3 complex plays a crucial role in T cell mechanosensing,[12, 13, 15-18] but how LFA-1/ICAM-1 engagement contributes to the TCR mechanosensing is less studied. The first study to examine the effect of stiffness on T cell response in the context of LFA-1/ICAM-1 engagement was done by Kam and Iskratsch groups,[9] using polydimethylsiloxane (PDMS) of varying stiffness presenting anti-CD3 alone or together with ICAM-1 molecules. Results demonstrated that T cells on soft substrates (5 kPa) show less tyrosine phosphorylation (as early T cell activation marker measured at 30 min) than on rigid ones (2000 kPa) and engagement of LFA-1/ICAM-1 potentiates this response to stiff substrates. Also the LFA-1/ICAM-1-mediated adhesion was shown to potentiate actomyosin forces, which in turn regulate actin assembly downstream of the TCR. Another recent study reported biphasic mechanosensitivity of TCR-mediated spreading of T cells on PDMS/hydrogel substrates modified with different ligands.[19] When adhering solely via the TCR complex by using anti-CD3, T cell spreading first increased with substrate stiffness (0.5-5 kPa) and then decreased with increasing stiffness (5-7000 kPa). However, in the presence of ICAM-1, cell spreading increased with stiffness (0.5-2440 kPa) up to a saturation value. Thus ICAM-1 seems to abrogate biphasic mechanoresponse of TCR-mediated spreading. Saitakis et al.[20] also evaluated how matrix stiffness regulates various T cell responses within the context of co-stimulator, anti-CD28 and ICAM-1, however, the contribution of ICAM-1/LFA-1 engagement to T cell response was not expounded in their study.

In this chapter the role of LFA-1/ICAM-1 engagement in T cell mechanosensing was further studied. To this end, the anti-CD3 arrays on hydrogels described in chapter 3, were further developed to contain a second ligand, ICAM-1, surrounding the anti-CD3

dots, to recapitulate key features of a physiological IS to study how the mechanical regulations of anti-CD3-mediated zeta-chain-associated protein kinase 70 (ZAP70) phosphorylation and TCR accumulation/clustering are affected by the surrounding presence of ICAM-1 (Scheme 1).

Scheme 1. Engineered hydrogels with spatially patterned IS arrays containing micropatterned anti-CD3 and backfilled ICAM-1 (ICAM-1-Fc) to study T cell mechanotransduction.

4.2   Results and discussion

4.2.1 Fabrication of anti-CD3/ICAM-1 patterned hydrogels with different stiffness

To mimic an IS structure with a segregated receptor complex arrangement, we first microcontact printed anti-CD3 dots on PAAm hydrogels of different stiffness. The anti-CD3 dots target the CD3 co-receptor and are expected to activate T cells. The hydrogel with anti-CD3 dots was further back-filled with LFA-1 targeting ICAM-1 adhesive protein to achieve anti-CD3/ICAM-1 surface (Figure 1).[21, 22] This spatial arrangement of the ligands at the hydrogel surface mimics the natural concentric receptor distribution at the mature IS interface.[5-7, 23] Dot arrays with 8 μm diameter and 35 μm gaps were used as this geometry was proven optimum for attachment of single Jukart T-cell on microarrays. Note that the diameter of a single Jurkat T-cell in suspension is 11-13 μm.[24]

The streptavidin-functionalized PAAm hydrogels had a stiffness of around 1, 12, and 50 kPa at given bis-AAm/AAm ratios before and after microcontact printing as measured by AFM (Figure A10). Anti-CD3/ICAM-1 patterns were obtained by first microcontactprinting biotinylated anti-CD3 on streptavidin-functionalized PAAm hydrogels, and then back-filling with ICAM-1-Fc as specified in section 2.4 (Figure A11). In order to visualize the ligands distribution on hydrogel surface, biotinylated anti-CD3 was fluorescently labeled with Alexa Fluor 555 and ICAM-1-Fc was fluorescently labeled with Alexa Fluor 488. Homogenous and highly reproducible arrays of anti-CD3 dots with diameter of 8 μm, separated by 35 μm and surrounded by ICAM-1 background were obtained on hydrogels of different stiffness (Figure 1A, B). At optimized conditions, patterns with sharp edges and high contrast between were observed (Figure 1B). The uniformity and dimensions of the protein patterns

was maintained on the swollen hydrogels, corroborating the efficient and stable transfer and binding of the proteins to the hydrogel surface. The printing conditions, especially incubation time and concentration of the biotinylated anti-CD3, printing pressure, and contact time were adjusted to obtain a similar fluorescence intensity of anti-CD3 (i.e. the same protein density) on hydrogels of different stiffness (Figure 1C).[25] The fluorescence intensity of ICAM-1-Fc was also kept similar on all hydrogel surfaces (Figure 1D).
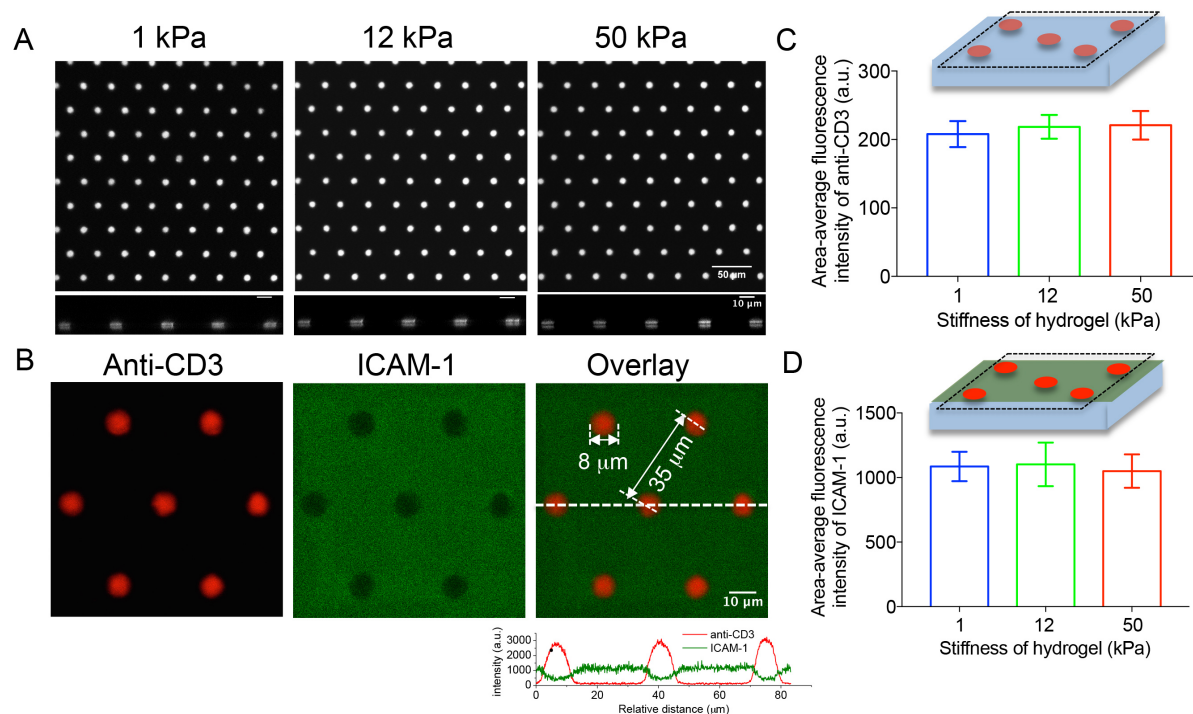
Figure 1. Preparation and characterization of micropatterned surface on hydrogels of different stiffness (1, 12, 50 kPa). A) Fluorescence images of anti-CD3 patterns (Alexa Fluor 555) on hydrogels of different stiffness. Anti-CD3 dots have a diameter of 8 μm and are separated by 35 μm gaps. Scale bar is 50 μm. The lower figures show corresponding fluorescence images of micropatterns after reconstructing Z stack images. Scale bar is 10 μm. B) Fluorescence images of anti-CD3/ICAM-1 arrays on hydrogel, which contain both anti-CD3 patterns (Alexa Fluor 555, red) and

backfilled ICAM-1 (Alexa Fluor 488, green). Lower graph shows the fluorescence intensity profile corresponding to the dotted line of the fluorescence image, showing the uniformity of the anti-CD3 and ICAM-1 on hydrogel surface. Scale bar is 10 μm. C, D) Area-average fluorescent intensity of anti-CD3 pattern (C) and ICAM-1 (D) on hydrogels with different stiffness. Comparable protein density was observed on all substrate surfaces. Values presented average ± SD from three independent experiments.

Antigens accessibility on hydrogel of different stiffness was also further determined by PE-anti-IgG (for anti-CD3) and PE-anti-CD54 (for ICAM-1-Fc). Comparable fluorescence intensities were observed on all hydrogels (Figure 2), indicating that the accessibility of the surface immobilized anti-CD3 and ICAM-1-Fc was independent of the hydrogel stiffness. These quantifications are important for the following cell studies in order to unequivocally differentiate between cell responses to mechanical properties and ligand density.
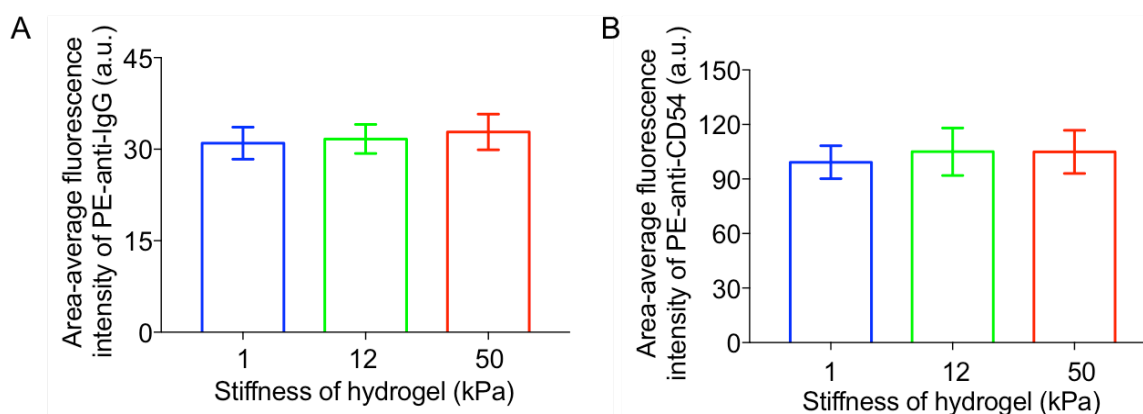

Figure 2. Semi-quantification of antigens density on hydrogel of different stiffness. A) Anti-CD3 coating on the hydrogel as labeled by PE-anti-IgG. B) ICAM-1 coating on the hydrogel as labeled by PE-anti-CD54.

In summary, homogeneous anti-CD3 patterns surrounding by ICAM-1 background with comparable protein densities and accessibility were obtained on hydrogels with different stiffness. These APC model surfaces will be used to reconstruct the cell-cell interface at the IS and to study T cell activation in response to mechanical engagement and spatial distribution of the ACP ligands in the subsequent studies.

4.2.2 Jurkat T-cell spreading on micropatterned hydrogels

Jurkat T-cells were seeded on hydrogels (1, 12, and 50 kPa) surface with anti-CD3 patterns alone (no ICAM-1) or anti-CD3/ICAM-1 for increasing time. We optimized the cell density number in order to cover the surface patterns with cells in time of minutes. Theoretically, ca. 7.0×10^5 cells are required to cover 1×1 cm^2 surface area in a close-packed arrangement. In the praxis, a seeding density of 4.5×10^5 cells/cm^2 enabled most dots to be covered by cells within 10 min after seeding (Figure 3).

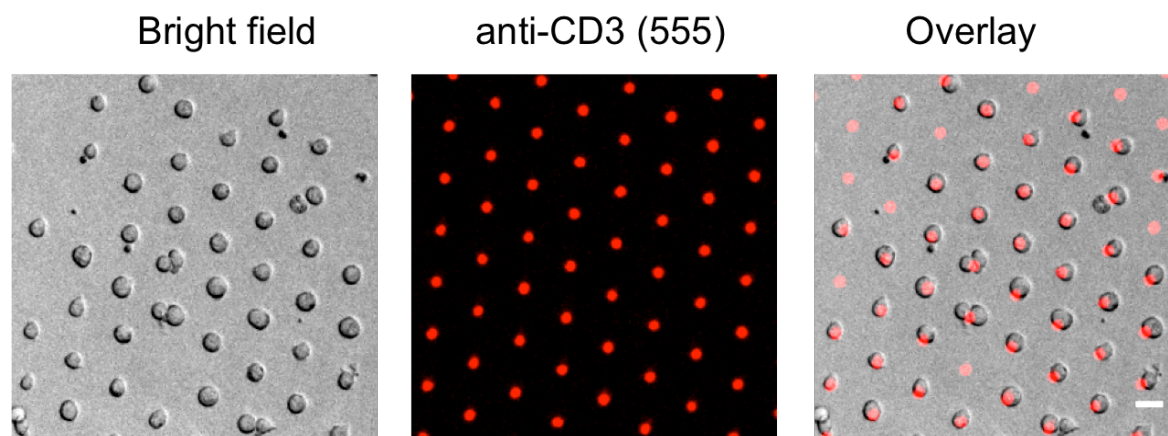| Bright field	anti-CD3 (555)	Overlay

Figure 3. Jurkat T-cell cultured on micropatterned surface. Most of anti-CD3 patterns could be recognized by Jurkat T-cell within 10 min after cell seeding. Scale bar is 20 μm.

The substrates were gently washed with PBS at this time point and cells were fixed subsequently. Cell spreading (characterized by actin outline) on the anti-CD3 pattern alone or anti-CD3/ICAM-1 surface was observed over the whole dot area, and the cell spreading area was independent of substrate stiffness in both cases at 10 min (Figure A12). Interestingly, cell spreading hardly changed when ICAM-1 was introduced to 1 and 12 kPa substrates, whereas a slight increase was found on 50 kPa substrate, which might be explained in that ICAM-1 began to facilitate cell spreading on stiff substrate (50 kPa) 10 min after cell seeding. Since ICAM-1 is an adhesive receptor responsible for T cell spreading and immobilized ICAM-1 could increase cell spreading compared with anti-CD3 alone surface,[19, 26] we further increased the cell seeding time to allow ICAM-1 to engage with LFA-1 for longer time to further study how the cell spreading behavior was influenced by substrate stiffness. To this end, we prolonged cell-seeding time from 10 min to 20 min. Cell spreading area remained unchanged on anti-CD3 pattern alone surface (Figure 4A, C). However, spread largely beyond the anti-CD3 area was observed on anti-CD3/ICAM-1 surface, especially on 50 kPa (Figure 4B). A 26% increase in spreading area was observed on 50 kPa when ICAM-1 was introduced, and a slight larger spreading area was also found on 50 kPa than on 1 or 12 kPa substrates with anti-CD3/ICAM-1 arrays (Figure 4C). It should be noted that ICAM-1 alone did not support Jurkat T-cell adhesion and spreading, even at high surface concentration on stiff substrates (data are not shown), consistent with previous observations that LFA-1 has a low affinity for ICAM-1 unless it is activated by TCR/CD3 stimulation.[22] Taken together, Jurkat T-cell attachment and spreading on our micropatterned hydrogels is driven by the presence of anti-CD3 and is initially (10 min) confined to a similar area on all substrates with anti-CD3 pattern alone or anti-CD3/ICAM-1 arrays. At longer time scale (20 min), cell spreading does not change on substrates with

anti-CD3 pattern alone, but increases in the presence of ICAM-1, especially on 50 kPa substrate. This suggests the ICAM-1 can facilitate Jurkat T-cell spreading on stiff substrate surface.
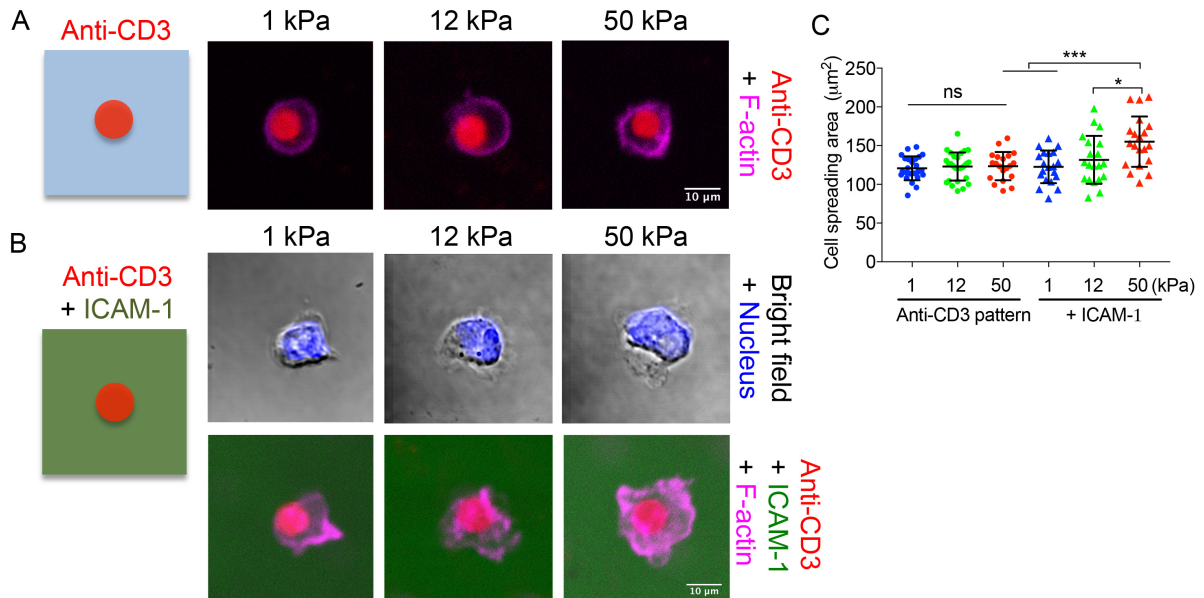

Figure 4. Jurkat T-cells cultured on micropatterned hydrogels with different stiffness. A) Fluorescence images of F-actin to show cell spreading on anti-CD3 pattern alone surface with different stiffness 20 min after cell seeding. Scale bar is 10 μm. B) Bright field and F-actin fluorescence images to show cell spreading on anti-CD3/ICAM-1 surface with different stiffness 20 min after cell seeding. F-actin and nucleus of Jurkat T-cells were stained by Alexa Fluor 594 Phalloidin (pink) and DAPI (blue). Scale bar is 10 μm. C) Characterization of cell spreading on micropatterned hydrogels 20 min after cell seeding. Values presented average ± SD from three independent experiments. *$p < 0.05$, **$p < 0.01$, ***$p < 0.001$.

4.2.3 ZAP70 phosphorylation induced by micropatterned hydrogels

ZAP70 phosphorylation, which is essential for TCR/CD3-mediated signaling

transduction, is usually taken as an early marker to quantify T cell activation.[27, 28] Phosphospecific antibodies can be used to detect phosphorylated ZAP70 (pZAP70), though the available antibodies are unable to distinguish between pZAP70 (Tyr319) and phosphorylated Syk (Tyr352), the two major Syk family of tyrosine kinases involved in T cell signaling. Tyrosine phosphorylation was then captured for Jurkat T-cells 20 min after cell seeding on different substrates. Both the total ZAP70 and pZAP70 were detected to better quantify ZAP70 phosphorylation level at IS by calculating pZAP70/Total ZAP70 ratio. The total ZAP70 signal was observed at all anti-CD3/T cell interfaces, whereas pZAP70 was only obviously detected on the stiffer substrates (12 and 50 kPa) (Figure 5A). Quantification data confirmed that the pZAP70/Total ZAP70 ratio increases with hydrogel stiffness on the anti-CD3 patterns alone surface (Figure 5C). The fluorescent total ZAP70 and pZAP70 antibodies revealed microclusters of proteins at the central part of the anti-CD3/T cell interface on 12 and 50 kPa substrates. On 50 kPa substrate, total ZAP70 and pZAP70 clusters largely co-localized. In contrast, no obvious colocalization was observed on 1 and 12 kPa substrates (Figure 5A). These results indicate that pZAP70 might be the major component of ZAP70 clusters on stiff substrates. The clustering of pZAP70 was also enhanced by stiffer substrates (Figure 5D), which is consistent with the results calculated by pZAP70/Total ZAP70 ratio. These results together suggest that CD3-mediated T cell activation, at least as measured by ZAP70 phosphorylation level, is potentiated on stiffer substrates.

When anti-CD3 patterns were surrounded by ICAM-1, the total ZAP70 signal was also clearly detected on all substrates, but clustering was more visible on 12 kPa substrate rather than on 1 and 50 kPa substrates (Figure 5B, D). Accumulation of pZAP70 was obviously observed on 12 and 50 kPa substrates, but not on 1 kPa substrate (Figure 5B). By comparing the pZAP70/total ZAP70 ratio, the highest

ZAP70 phosphorylation level was found on 12 kPa substrate rather than on softer (1 kPa) or stiffer (50 kPa) substrates (Figure 5C). Also, pZAP70 clusters co-localized well with total ZAP70 clusters on 12 kPa substrate rather than on 1 and 50 kPa substrates, on which clusters formation was not evident (Figure 5B, D). Therefore, the engagement of ICAM-1 surrounding anti-CD3 patterns seems to enhance ZAP70 phosphorylation level on intermediate substrate stiffness (12 kPa) but fails to increase pZAP70 accumulation (as measured by pZAP70/total ZAP70 ratio) on softer or stiffer substrates, and even decreases pZAP70 clustering (as measured by pZAP70 cluster number) on stiffer substrate (50 kPa).

In a previous study, Tabdanov et al.[9] reported lower tyrosine phosphorylation levels of primary human CD4$^+$ T cells was found on anti-CD3 and ICAM-1-modified PDMS substrates with stiffness of 5 kPa than on 2000 kPa substrate. Authors observed that ICAM-1 engagement even enhanced the response on the 2000 kPa substrate, whereas we did not observe this trend in our study. Jankowska et al. suggested that forces exerted by the cytoskeleton can lead to integrin affinity maturation during IS maturation, which enables integrin (ICAM-1) to engage with their ligands (LFA-1) to suppress tyrosine phosphorylation through a negative feedback loop.[29] This suggestion strongly supports our observation that pZAP70 accumulation (as measured by pZAP70/total ZAP70 ratio) was not enhanced on 50 kPa substrates in the presence of ICAM-1, and even the pZAP70 clustering (as measured by pZAP70 cluster number) was largely reduced. We can explain in that the higher cell spreading area on 50 kPa substrate (Figure 5B,C) enables ICAM-1 to engage more LFA-1, which finally dampen ZAP70 phosphorylation through a negative feedback loop. On softer substrates (1, 12 kPa), the engagement of ICAM-1 with LFA-1 does not suppress ZAP70 phosphorylation, but facilitates ZAP70 phosphorylation on 12 kPa substrate. Nevertheless, more experiments are required to prove it.

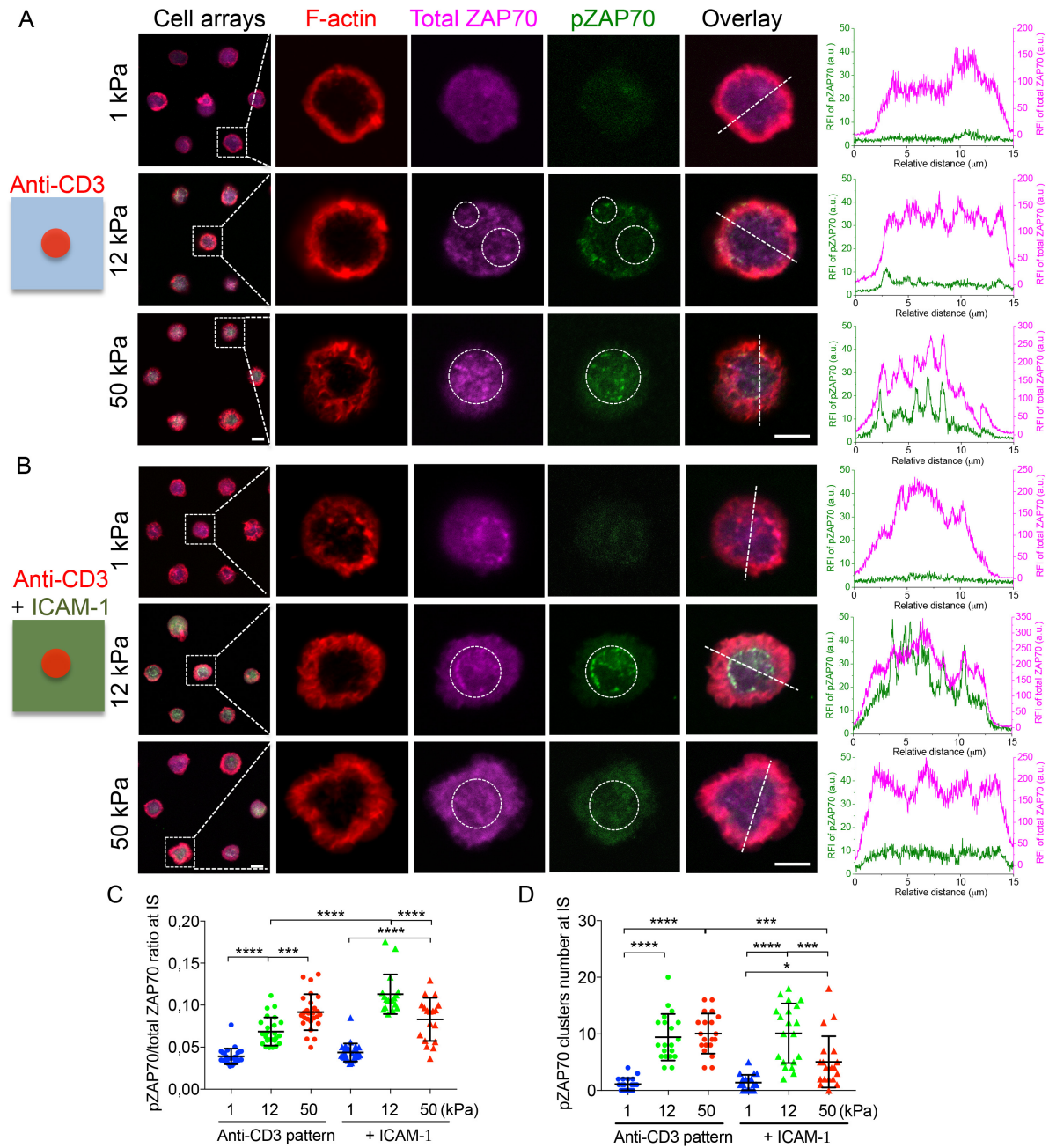**Figure 5.** ZAP70 phosphorylation on micropatterned hydrogels 20 min after cell seeding. A, B) Immunofluorescence images to show stained F-actin, total ZAP70, and pZAP70 of Jurkat T-cells on the substrates surface with anti-CD3 patterns alone (A) and anti-CD3/ICAM-1 arrays (B). Right graphs show intensity profile of total ZAP70 (pink) and pZAP70 (green) corresponding to the dotted line of the

fluorescence images. The dotted square indicates the cell magnification image on the corresponding right side and the dotted circle is to compare how pZAP70 clusters co-localize with total ZAP70 clusters. Scale bar is 10 μm. C, D) Quantification of ZAP70 phosphorylation level (pZAP70/total ZAP70 ratio, C) and pZAP70 clusters number (D) at the cell-substrate interface. Values presented average ± SD from independent experiments. *$p < 0.05$, **$p < 0.01$, ***$p < 0.001$, ****$p < 0.0001$.

4.2.4 The early ZAP70 phosphorylation on micropatterned hydrogels

To further study the modulatory role of ICAM-1 in stiffness-regulated activation of T cells, we detected the early ZAP70 phosphorylation 10 min after cell seeding. At this early time point, results suggest that ICAM-1 does not obviously facilitate cell spreading, especially on 1 and 12 kPa substrates (Figure A12). Also the spreading area of cells on all substrates was similar in the presence of ICAM-1, so we assumed that the early ZAP70 phosphorylation was only determined by substrate stiffness here. Note that 10 min is the earliest possible time point at which cells recognized the anti-CD3 patterns well and the cell attachment was strong enough to resist the washing step during immunostaining process.

ZAP70 phosphorylation on anti-CD3/ICAM-1 surface was clearly detected on 12 and 50 kPa substrates, and a higher pZAP70 accumulation (as measured by pZAP70/total ZAP70 ratio) was observed with increasing substrate stiffness (Figure 6A, B). A larger number of pZAP70 clusters was found on stiff substrates (12 and 50 kPa) than on soft one (1 kPa), though no difference was observed between 12 and 50 kPa substrates (Figure 6A, C), which could be attributed to the fact that only clusters larger than 0.01 μm^2 are analyzed by our method. These results were different to what we observed at 20 min, at which time pZAP70 phosphorylation showed a declined trend from 12 kPa to 50 kPa substrate (Figure 5C, D). These results also

highlight the importance of the time scale in the study of T cell activation mechanosensitivity, which can be linked to the sequential activation of the receptors at the IS. Our data are supported by a previous report, in which the temporal evolution of early signaling in Jurkat T-cells is demonstrated to be sensitive to substrate stiffness.[30] It should be also noted pZAP70 accumulation level increased with cell seeding time on 12 kPa substrate but remained unchanged on 50 kPa substrate (Figure 6D), whereas the number of pZAP70 clusters reduced after longer cell seeding time on both 12 and 50 kPa substrates (Figure 6E).
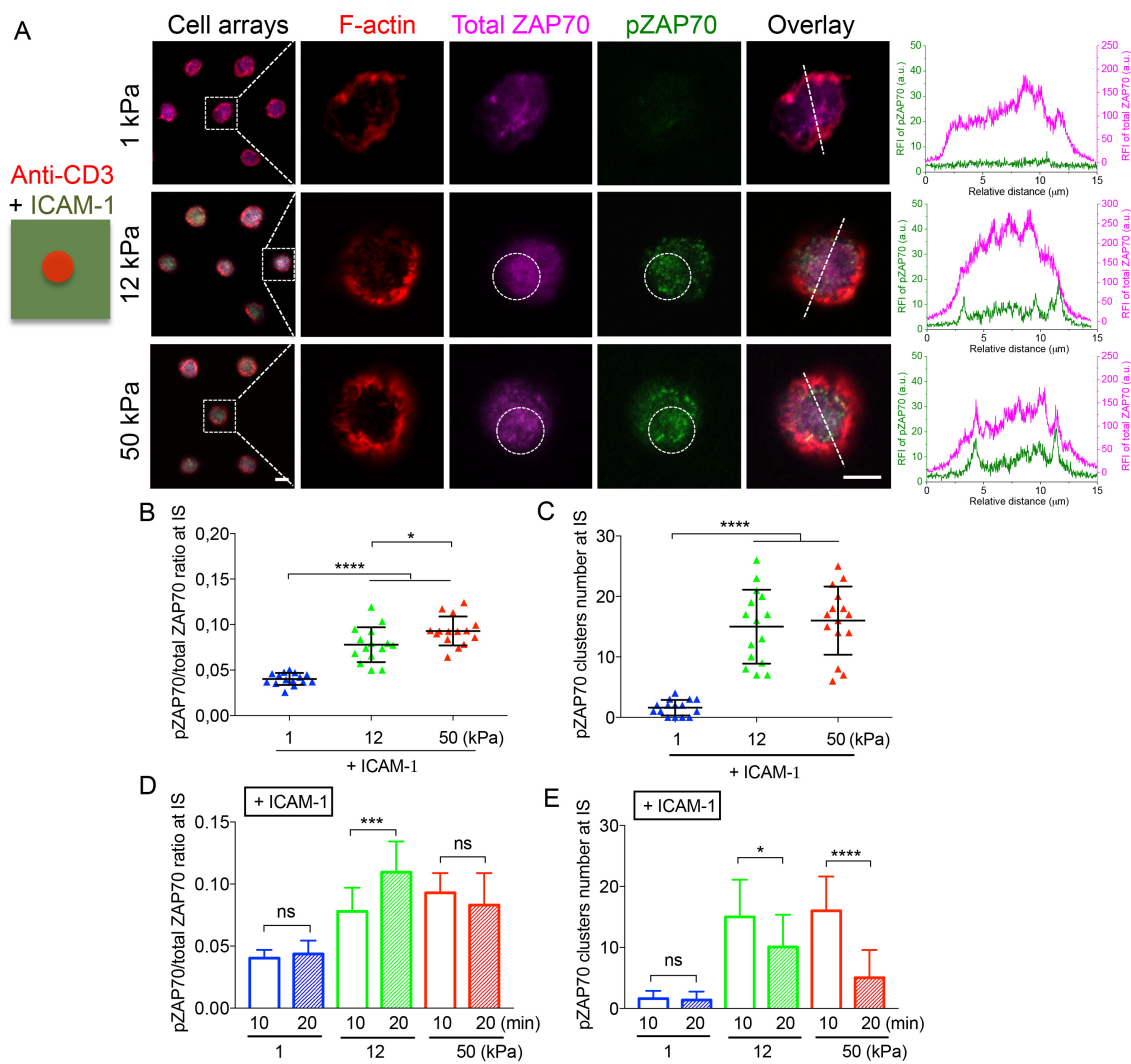

Figure 6. ZAP70 phosphorylation on anti-CD3/ICAM-1 surface with different stiffness

10 min after cell seeding. A) Immunofluorescence images to show stained F-actin, total ZAP70, and pZAP70 of Jurkat T-cells on anti-CD3/ICAM-1 surface. On the right column are intensity profiles of total ZAP70 (pink) and pZAP70 (green) at the cell-substrate interface. Scale bar is 10 μm. B, C) Characterization of pZAP70/total ZAP70 ratio (B) and pZAP70 clusters number (C) at the cell-substrate interface. D, E) Comparison of pZAP70/total ZAP70 ratio (D) and pZAP70 cluster number (E) at the cell-substrate interface at different cell seeding time. Values presented average ± SD from three independent experiments. *$p < 0.05$, **$p < 0.01$, ***$p < 0.001$, ****$p < 0.0001$.

The results observed on 50 kPa hydrogel are consistent with reported data indicating that CD3-mediated tyrosine kinase signaling, including ZAP70 phosphorylation, occurs early and largely before the mature IS is formed, and reaches a peak less than 20 min. [31] In addition, ZAP70 signaling clusters were also proved to gradually disappear when they are transported toward the center of IS, which is probably mediated by an endocytosis process, consistent with what we observed on 50 kPa substrate. [32] On 12 kPa substrate, the elevated pZAP70 accumulation with increased cell seeding time may be attributed to that it needs a longer time for pZAP70 to accumulate at IS to reach a peak on such a soft substrate.

In summary, in the context of the mechanosignalling processes involved in T cell activation by APCs, our results suggest that: (i) CD3-mediated early T cell activation, as measured by ZAP70 phosphorylation level, is potentiated by a stiffer engagement of the CD3 ligand of the APC. (ii) Engagement of ICAM-1 can either enhance or dampen the ZAP70 phosphorylation level on substrate with different stiffness. (iii) Mechanoresponsive receptors during T cell activation play different roles and the temporal evolution of early signaling in Jurkat T-cells is demonstrated to be sensitive

to substrate stiffness.

4.2.5 TCR accumulation/clustering at IS on micropatterned hydrogels

TCRs are evenly distributed in quiescent T cells and accumulate at the T cell-APC interface upon antigen recognition to mature IS formation. [33] The strength of T cell activation can also be characterized, at least partly by the TCR density at the IS interface. It has been demonstrated that artificial substrates presenting antibodies against TCR/CD3 (i.e. anti-CD3) induce a similar behavior.[5, 6, 34] Using our micropatterned hydrogels platform, we investigated how the TCR accumulation is influenced by substrate stiffness on our platform.

The TCR (αβ), F-actin and LFA-1 of T cells on the micropatterned hydrogels were co-stained 30 min after cell seeding. An actin ring at the periphery of the cell was found on all substrates. LFA-1 colocalized with F-actin on all substrates surface, even in the absence of ICAM-1 (Figure 7A, B). This suggests that anti-CD3 recognition by Jurkat T-cell induces LFA-1 accumulation at the periphery of the IS, independently of the ICAM-1 engagement. Interestingly, TCR accumulated at the periphery of IS on substrates with anti-CD3 pattern alone (Figure 7A), but largely accumulated in the actin-depleted center of the IS in the presence of ICAM-1 (Figure 7B). This was observed on both 12 and 50 kPa substrates, but not on 1 kPa. The interaction between LFA-1 and ICAM-1 seems to facilitate the transport of TCR to the center of the IS and then support IS maturation, during which a minimum stiffness (> 1 kPa) may be required.
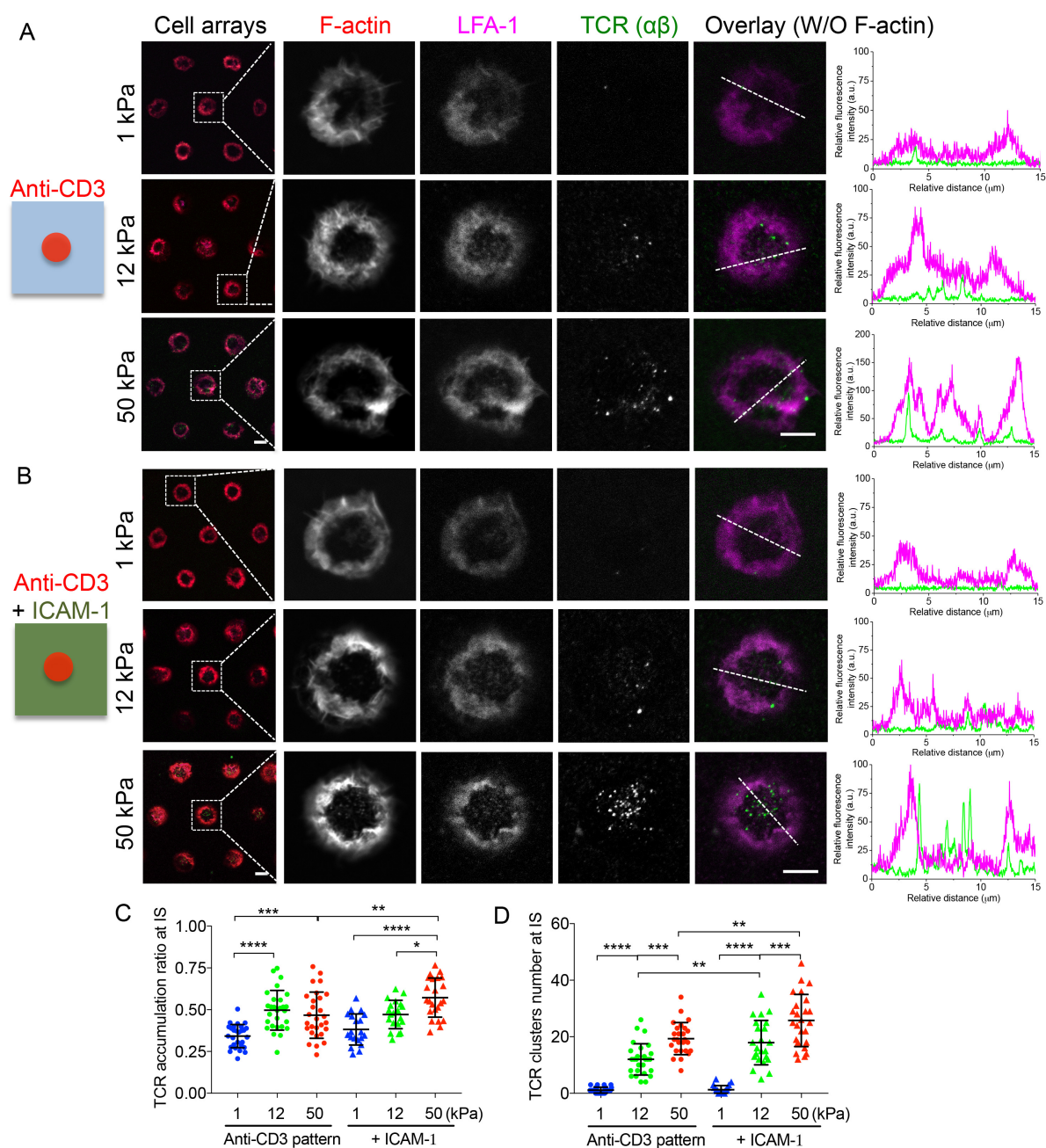
Figure 7. TCR accumulation on micropatterned surface with different stiffness. A, B) Immunostaining of F-actin, LFA-1, and TCR (αβ) on substrates with anti-CD3 patterns alone (A) and anti-CD3/ICAM-1 arrays (B). Left graphs show intensity profile of LFA-1 and TCR (αβ) corresponding to the dotted line in the fluorescence images. Cells were fixed and stained after seeding for 30 min. Scale bar is 10 μm. C, D) Quantification analysis of TCR accumulation ratio (C) and TCR clusters number (D)

at IS interface. Values presented average ± SD from three independent experiments. *p < 0.05, **p < 0.01, ***p < 0.001, ****p < 0.0001.

We further quantified TCR accumulation ratio at IS on the substrates with different stiffness. As for the quantification, we defined the TCR accumulation ratio at IS as the value of the fluorescence intensity of TCR within IS (1/3 of cell body close to the cell-substrate interface) divided by the total fluorescence intensity of TCR across the whole cell. On substrate with anti-CD3 patterns alone, TCR accumulation ratio was higher on 12 and 50 kPa substrates than on 1 kPa. No significant difference was detected in the accumulation ratio between 12 and 50 kPa substrates (Figure 7C). In contrast, TCR accumulation ratio increased across the whole range of stiffness tested here on anti-CD3/ICAM-1 surface (Figure 7C). Interestingly, a significantly higher value of TCR accumulation ratio was found on 50 kPa substrate when ICAM-1 was present, but the presence of ICAM-1 did not make any obvious difference on 1 or 12 kPa substrates. These results indicate that LFA-1/ICAM-1 engagement may promote TCR accumulation at IS only when substrate reach a stiffness around 50 kPa.

TCR clustering plays a dominant role in effective T cell activation, so it was also quantified here.[18, 35] TCR clusters were observed on all substrates, and the number of clusters followed the same trends observed for TCR accumulation (Figure 7D). More TCR clusters were found on stiffer substrates and the presence of ICAM-1 can further enhanced that, especially on 12 and 50 kPa substrate. Taken together, TCR accumulation and clustering can be potentiated by substrate stiffness and the engagement of LFA-1/ICAM-1 can further enhance this CD3-mediated response.
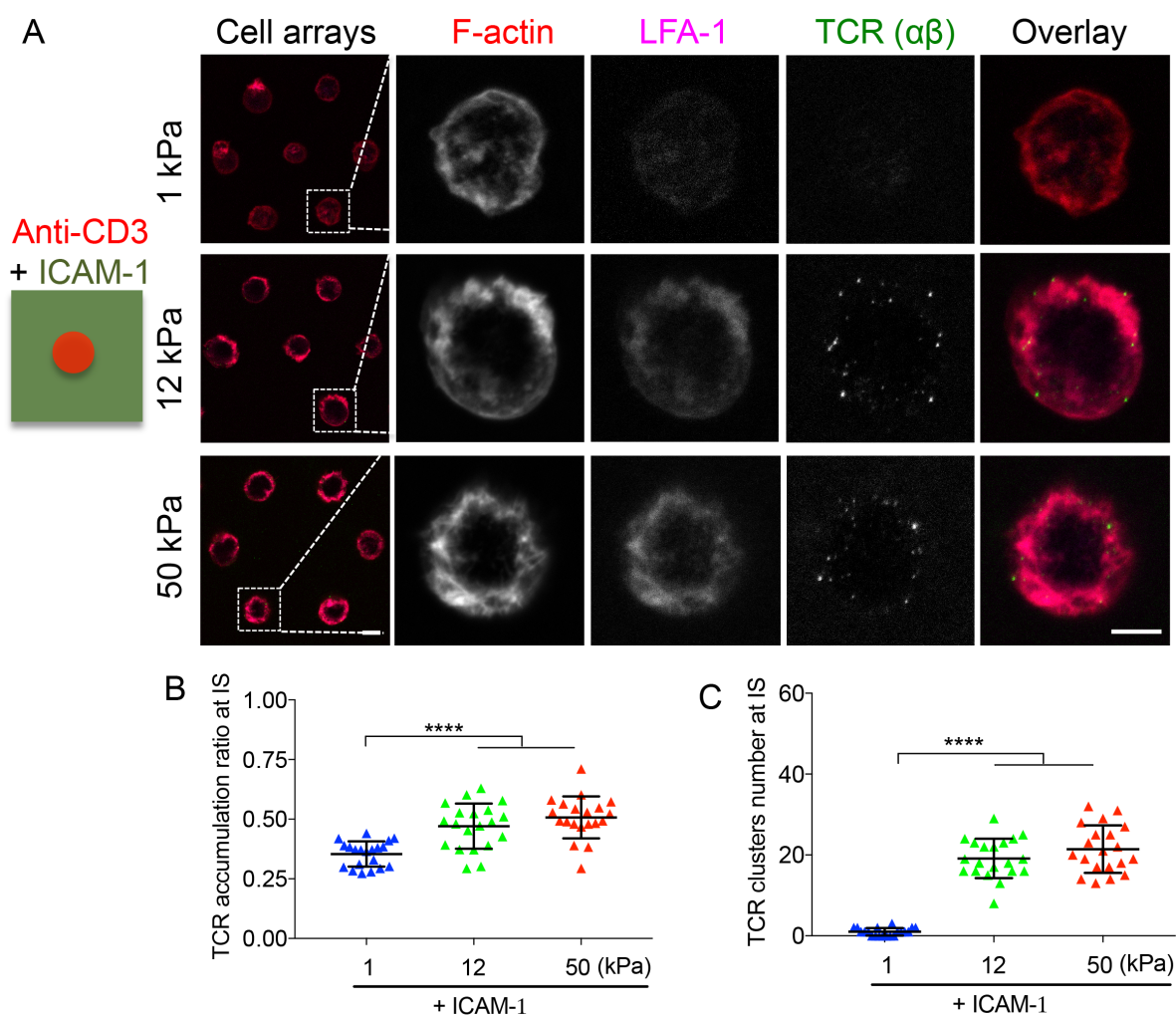
Figure 8. TCR microclusters accumulation induced by micropatterned surface. A) Immunostaining of F-actin, LFA-1, and TCR (αβ) on anti-CD3/ICAM-1 arrays supported by hydrogels of different stiffness. Jurkat T-cells were fixed and stained after seeding for 10 min. Scale bar is 10 μm. B, C) Quantification analysis of TCR accumulation ratio and clusters number at IS interface. Values presented average ± SD from three independent experiments. *p < 0.05, **p < 0.01, ***p < 0.001, ****p < 0.0001.

Similarly, we also studied how TCR accumulation at IS responses to substrate stiffness at an early stage. To this end, we detected the early TCR accumulation 10

min after cell seeding substrates with anti-CD3/ICAM-1 arrays. TCR clusters were clearly observed on 12 and 50 kPa substrates, but largely accumulate at the periphery of IS (Figure 8A). A higher TCR accumulation ratio and TCR cluster number were found on stiff substrates (12 and 50 kPa) than on soft one (1 kPa), but no significant difference was found between 12 and 50 kPa substrates (Figure 8B, C). These results demonstrate a little bit longer time (>10 min) may be required for TCR to accumulate in the actin-depleted center of the IS on anti-CD3/ICAM-1 surface. In addition, the capability of Jurkat T-cells to distinguish between 12 kPa and 50 kPa substrates, at least in term of TCR accumulation and clustering, is also time-dependent. This further verifies the temporal evolution of early signaling in Jurkat T-cells is sensitive to substrate stiffness.

4.3   Conclusion

A schematic graph is used to illustrate the delicate Jurkat T-cell mechanotransduction on our platform as measured by ZAP70 phosphorylation and TCR accumulation in different time scales (Figure 9). Specifically, as for anti-CD3 pattern alone surface, both ZAP70 phosphorylation and TCR accumulation level increased with substrate stiffness, suggesting T cell activation induced through TCR/CD3 complex is mechanosensitive, even without integrin (ICAM-1) engagement. On anti-CD3/ICAM-1 surfaces, Jurkat T-cell exhibited a more delicate mechanosensitivity. On the one hand, TCR accumulation could be potentiated by stiff substrates in the presence of ICAM-1 engagement after seeding cell for 10 and 30 min, though no significant different was found between 12 and 50 kPa at 30 min. On the other hand, T cell activation, as measured by ZAP70 phosphorylation, showed different trends with stiffness at different detected time. At 10 min, ZAP70 phosphorylation level increased with substrate stiffness. At 20 min however, ZAP70 phosphorylation level first

increased when substrate stiffness increased from 1 kPa to 12 kPa, and then declined when substrate stiffness further increased from 12 kPa to 50 kPa. This suggests the mechanosensitivity of Jurkat T-cell may be also time-dependent during the early T cell activation as measured by ZAP70 phosphorylation level on our anti-CD3/ICAM-1 surface.

In addition, ICAM-1 engagement generated different effects on T cell signaling when the substrates presented different stiffness: an increased ZAP70 phosphorylation level was induced on soft substrate (12 kPa), but not on stiff substrate (50 kPa), which even showed a declined trend of ZAP70 phosphorylation. This suggests the mechanosensitivity of Jurakt T-cell can also be tightly associated with integrin engagement. To conclude, a new understanding to unravel the role of ICAM-1 in TCR-mediated mechanotransduction within IS is realized by using our platform.
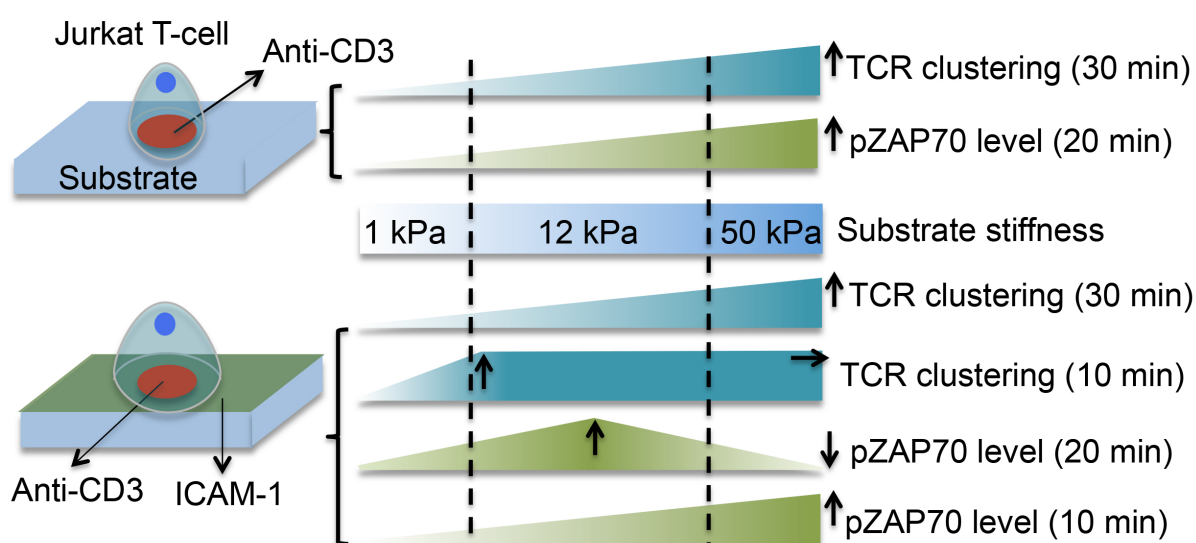

Figure 9. Schematic graph to illustrate the T-cell mechanotransduction on our platforms as measured by ZAP70 phosphorylation and TCR accumulation/clustering in different time scales.

4.4 Materials and methods

Reagents

Solvents with p.a. purity were used as purchased unless specified. Acrylamide (AAm), N,N'-methylene-bis-acrylamide (bis-AAm), acrylic acid (AA), ammonium persulfate (APS, 10% w/v in PBS), tetramethylethylnediamine (TEMED), 3-acryloxypropyl-trimethoxysilane (3-APS), Sigmacote, NaOH (5 M), NaCl (0.5 M), PBS buffer (1X, pH 7.0-7.4), 2-(N-morpho)-ethanesulfonic acid solution (MES buffer, 0.1 M, pH 4.5), ethanol (97%), bovine serum albumin (BSA), Biotin-PEG$_8$-NH2, gold nanoparticles suspension (300 nm), N-hydroxysuccinimide (NHS), dimethylaminopropyl-3-ethylcarbodiimide hydrochloride (EDC), were purchased from Sigma-Aldrich Chemie GmbH. Streptavidin, Alexa-Fluor 488 NHS ester, Alexa-Fluor 555 NHS ester, Alexa Fluor 546 phalloidin, Alexa Fluor 594 phalloidin, and secondary antibody Alexa Fluor 647 Goat anti-Rabbit IgG were purchased from Thermo Fisher Scientific. Biotin-PEG-OH (5 kDa) was from Nanocs. Inc. The following antibodies were purchased from Biolegend GmbH: biotin anti-human CD3 (OKT3), biotin anti-human IgG Fc, human ICAM-1-Fc, PE anti-mouse IgG, PE anti-human CD54, Alexa Fluor 488 anti-human TCR α/β, Alexa Fluor 647 anti-human CD11a/CD18 (LFA-1), and Alexa Fluor 488 anti-Zap70 (Y319)/Syk (Y352) antibodies. Rabbit anti-human Zap70 antibody was purchased from MyBioSource.

Preparation and characterization of the micropatterned PAAm hydrogel

PAAm hydrogel with desired stiffness was prepared in a similar way as mentioned in section 2.4 (Materials and methods) of Chapter 2. Hydrogels with expected stiffness around 1, 12, and 50 kPa were prepared by using monomer solution (pH 8.0) consisting of 0.03% bis-AAm, 0.11% bis-AAm, and 0.5% bis-AAm, respectively, together with 12% AAm and 0.6% AA after passing through a 0.22 μm (pore size)

filter.

Prepared PAAm hydrogels were chemically modified to facilitate protein conjugation onto its surface. Here, PAAm hydrogels were firstly biotinylated as mentioned in section 2.4 (Materials and methods) of Chapter 2.

The biotinylated hydrogels were further coupled with streptavidin (0.1 mg/mL) for next micropatterning procedure. Protein micropatterning on hydrogel was obtained by using a commercialized microcontact printer (4.1 μCP, GeSiM, Germany). For microcontact printing, topological masters (8/35 μm circular patterns) were made by photolithography with a 5 μm thickness of Su-8 photoresist layer, which was achieved by spin-coating on silicon wafers. PDMS stamps were fabricated by casting from these masters in a casting station, by which it enables them to be manipulated by microcontact printer. In order to print anti-CD3 (biotinylated) on the streptavidin-modified hydrogels, hydrogels were previously dried in chemical hood for 15 min. Plasma-treated PMDS stamp was incubated with anti-CD3 (100 μg/mL, 10 μL) for 1 h and then dried with N_2 to remove extra anti-CD3. After moistening the anti-CD3 absorbed stamp in humid box (95-98% humidity) for 5 min, microcontact printing was immediately performed with our μCP using a printing pressure of 12 kPa for 5 min at room temperature. The micropatterned hydrogels could be used for cell experiments after blocking with Biotin-PEG-OH (100 μg/mL, 100 μL) and BSA solution (100 μg/mL, 100 μL) for 1 h at room temperature. The mimetic IS arrays on hydrogel was achieved by further incubating micropatterned hydrogel with anti-human Fc (biotinylated, 50 μg/mL, 100 μL) and ICAM-1-Fc (50 μg/mL, 100 μL) for 1 h respectively at room temperature before blocking. After extensive washing, the micropatterned substrates were ready for use. The obtained micropatterns were stable throughout these experiments.

To compare the surface densities of these proteins, anti-CD3 and ICAM-1-Fc were

also labeled with Alexa Fluor 555 and Alexa Fluor 488 respectively before patterning. Micropatterns were imaged with confocal fluorescence microscopy. To determine the antibodies accessibility to cells, PE anti-mouse IgG (100 μg/mL, 100 μL) and PE anti-human CD54 antibody (100 μg/mL, 100 μL) was used to label mouse anti-CD3 and human ICAM-1-Fc antibodies. All the substrates were imaged using a Zeiss LSM 880 laser-scanning confocal microscope (Carl Zeiss Microscopy, Germany). The mean fluorescence intensity of the coupled antibodies on the surfaces of the PAAm hydrogel was quantified by ImageJ (INM-Leibniz Institute for New Materials, Germany) software.

Mechanical characterization of hydrogels

The stiffness of glass supported hydrogel discs were characterized by AFM as indicated in section 2.4 (Materials and methods) of Chapter 2.

All hydrogels (streptavidin-functionalized hydrogels before and after microcontact printing) were measured in PBS at room temperature. Young's modulus (stiffness) was calculated by fitting force vs. indentation depth data to a linearized Hertz model derived for a spherical indenter by using JPK image processing software (a poisson ratio of 0.5 was used here). Each stiffness value was calculated from data analysis of three samples.

Cell culture

Jurkat T-cells, clone E6-1 (ATCC® TIB-152™) were cultured in RPMI-1640 Medium (Gibco) supplemented with 10% fetal bovine serum (Gibco), 100 units/mL penicillin, and 100 μg/mL streptomyocin at 37°C, 5% CO_2.

Immunochemistry

Jurkat T-cells were seeded on micropatterned substrates at a cell density around 4.5 $\times$ 10^5 cells/cm^2 and were allowed to incubate for specified time before fixing. Jurkat T-cells were fixed with 4% paraformaldehyde solution for 15 min at 37°C, followed by permeabilizing with 0.5% Triton X-100 (Sigma, Saint-Louis, MO) in PBS for another 15 minutes at 37°C after washing 3 times with PBS. After further blocking with 1% BSA for 0.5 h, F-actin was labeled with Alexa Fluor 594 phalloidin or Alexa Fluor 546 phalloidin as required. Alexa Fluor 488 anti-Zap70 (Y319)/Syk (Y352) antibody was used to stain pZAP70 and rabbit anti-human Zap70 antibody was used to stain total ZAP70 followed by further labeling with secondary antibody Alexa Fluor 647 Goat anti-Rabbit IgG. TCR and LFA-1 on cell surface was stained with Alexa Fluor 488 anti-human TCR α/β and Alexa Fluor 647 anti-human CD11a/CD18 (LFA-1), respectively. All the coverslips were finally mounted with mounting medium (with DAPI) for image acquiring.

PE anti-mouse IgG and PE anti-human CD54 was used to compare the surface accessibility of anti-human CD3 and ICAM-1-Fc, respectively, on substrates of different stiffness.

Image analysis

To analyze anti-CD3 and ICAM-1 densities on different substrates, a z-series with 0.25 μm interval was captured to cover the top 25 μm thickness of hydrogel (The gold nanoparticles layer was used to label the top of hydrogel). For fluorescently labeled anti-CD3 and ICAM-1, the z-series within the top 4 μm thickness of hydrogel was summed up into one reconstructed image by Image J software, whereas for secondary antibody that used to quantify the accessibility of anti-CD3 and ICAM-1 on substrates, the z-series within the top 2 μm thickness of hydrogel was summed up into one reconstructed image. The integrated signal intensity from the reconstructed

stack image was analyzed by Image J software.

To measure ZAP70 phosphorylation and TCR accumulation, the relative amounts of total ZAP70, pZAP70, and TCR were detected by labeling with related fluorescent antibodies, and then the fluorescence intensity at the IS was measured. Five fields were imaged for each immunostained coverslip containing several patterned cells. A z-series with 0.25 μm interval was captured to cover the whole cell body in each case. For images of total ZAP70 and pZAP70, only the 1/3 of z-series close to the cell-substrate interface was summed up into one reconstructed image by Image J software, whereas for TCR images, both the total z-series and 1/3 of z-series close to the cell-substrate interface were summed up into reconstructed images. The integrated signal intensity from the reconstructed stack image was measured by drawing a ROI around each cell according to the F-actin staining with Image J software. The fluorescence intensity of total ZAP70 divided by the fluorescence intensity of pZAP70 (pZAP70/total ZAP70 ratio) was used to characterize ZAP70 phosphorylation level at IS. The fluorescence intensity of TCR within IS (1/3 of cell body close to the cell-substrate interface, 1/3 of z-series) divided by the total fluorescence intensity of TCR across the whole cell (total z-series) was used to represent TCR accumulation ratio at IS.

The cluster number analysis of pZAP70 and TCR was done by Image J software with a setting of 1% threshold and only the cluster size larger than 0.01 μm^2 was counted.

Statistical analysis

Microsoft Excel, Origin and Prism software were used for statistical analysis here. Student's t-test was used to calculate statistical significance for unpaired samples, and data are shown as mean ± SD.
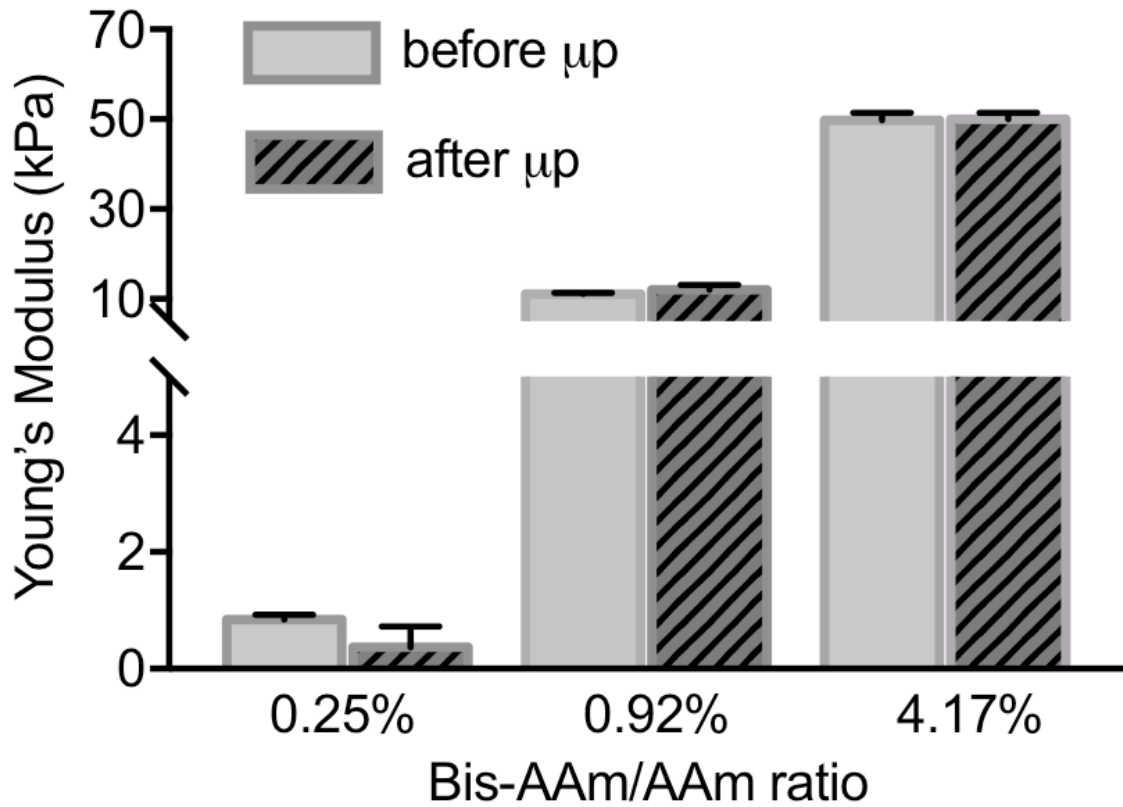
Appendix Chapter 4

Figure A10. Stiffness (1, 12 and 50 kPa) of PAAm hydrogel as measured by AFM indentation before and after microcontact printing.
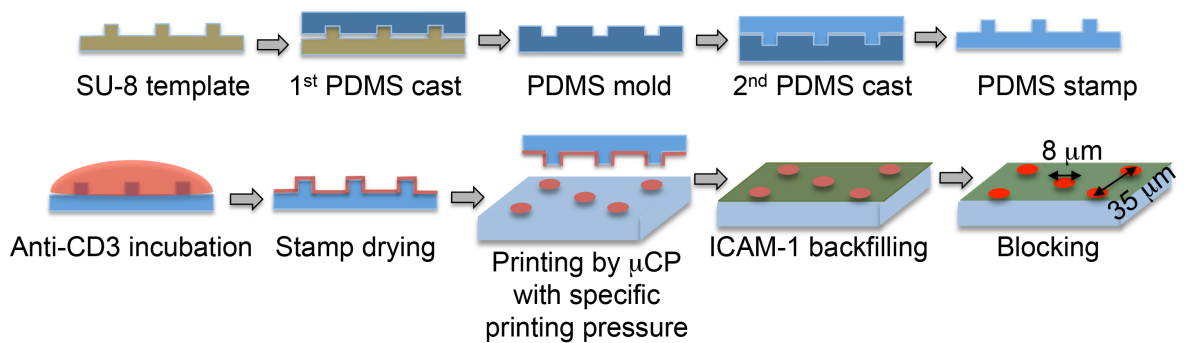
Figure A11. Preparation scheme to show micropatterned surface generated by soft lithography. The microcontact printing process was accomplished by a commercialized microcontact printer (mCP, GeSiM).
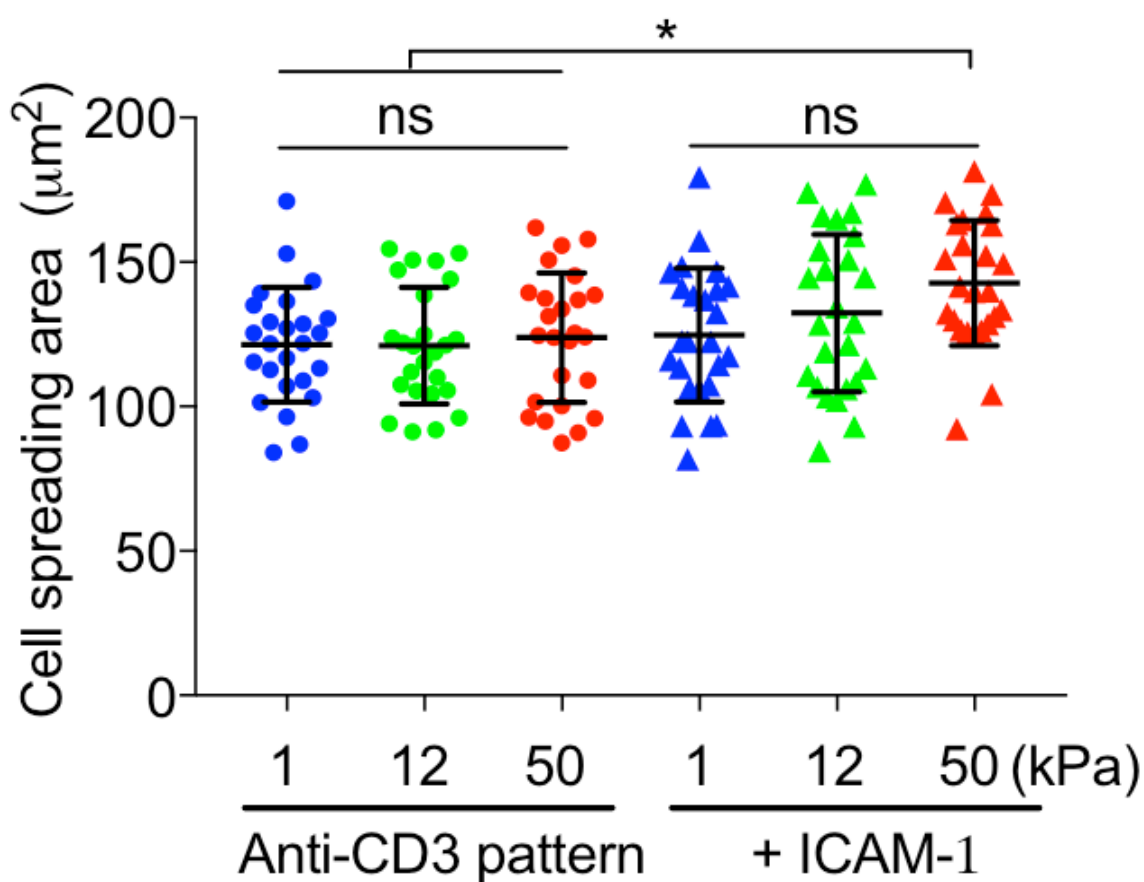

Figure A12. Quantification analysis of cell spreading area after seeding cells for 10 min. Values presented average ± SD from three independent experiments. *p < 0.05, **p < 0.01, ***p < 0.001, ****p < 0.0001.

References

[1] M.M. Davis, J.J. Boniface, Z. Reich, D. Lyons, J. Hampl, B. Arden, Y. Chien, Ligand recognition by alpha beta T cell receptors, Annu. Rev. Immunol. 16 (1998) 523-44.

[2] C.R.F. Monks, B.A. Freiberg, H. Kupfer, N. Sciaky, A. Kupfer, Three-dimensional segregation of supramolecular activation clusters in T cells, Nature 395(6697) (1998) 82-86.

[3] F. Kong, A.J. Garcia, A.P. Mould, M.J. Humphries, C. Zhu, Demonstration of catch bonds between an integrin and its ligand, J Cell Biol 185(7) (2009) 1275-84.

[4] J.B. Huppa, M.M. Davis, T-cell-antigen recognition and the immunological synapse, Nat. Rev. Immunol. 3(12) (2003) 973-83.

[5] J. Doh, D.J. Irvine, Immunological synapse arrays: patterned protein surfaces that modulate immunological synapse structure formation in T cells, Proc. Natl. Acad. Sci. U. S. A. 103(15) (2006) 5700-5.

[6] K. Shen, V.K. Thomas, M.L. Dustin, L.C. Kam, Micropatterning of costimulatory ligands enhances CD4+ T cell function, Proc. Natl. Acad. Sci. U. S. A. 105(22) (2008) 7791-6.

[7] H.R. Jung, J.C. Choi, W. Cho, J. Doh, Microfabricated platforms to modulate and monitor T cell synapse assembly, Wiley Interdiscip. Rev.: Nanomed. Nanobiotechnol. 5(1) (2013) 67-74.

[8] H.R. Jung, K.H. Song, J.T. Chang, J. Doh, Geometrically controlled asymmetric division of CD4+ T cells studied by immunological synapse arrays, PLoS One 9(3) (2014) e91926.

[9] E. Tabdanov, S. Gondarenko, S. Kumari, A. Liapis, M.L. Dustin, M.P. Sheetz, L.C. Kam, T. Iskratsch, Micropatterning of TCR and LFA-1 ligands reveals complementary

effects on cytoskeleton mechanics in T cells, Integr. Biol. 7(10) (2015) 1272-84.

[10] E. Benard, J.A. Nunes, L. Limozin, K. Sengupta, T Cells on Engineered Substrates: The Impact of TCR Clustering Is Enhanced by LFA-1 Engagement, Front. Immunol. 9 (2018) 2085.

[11] C. Hivroz, M. Saitakis, Biophysical Aspects of T Lymphocyte Activation at the Immune Synapse, Front. Immunol. 7 (2016) 46.

[12] K.H. Hu, M.J. Butte, T cell activation requires force generation, J. Cell Biol. 213(5) (2016) 535-42.

[13] E. Judokusumo, E. Tabdanov, S. Kumari, M.L. Dustin, L.C. Kam, Mechanosensing in T lymphocyte activation, Biophys. J. 102(2) (2012) L5-7.

[14] M.L. Previtera, Mechanotransduction in the Immune System, Cell. Mol. Bioeng. 7(3) (2014) 473-481.

[15] R.S. O'Connor, X. Hao, K. Shen, K. Bashour, T. Akimova, W.W. Hancock, L.C. Kam, M.C. Milone, Substrate rigidity regulates human T cell activation and proliferation, J. Immunol. 189(3) (2012) 1330-9.

[16] R. Basu, B.M. Whitlock, J. Husson, A. Le Floc'h, W. Jin, A. Oyler-Yaniv, F. Dotiwala, G. Giannone, C. Hivroz, N. Biais, J. Lieberman, L.C. Kam, M. Huse, Cytotoxic T Cells Use Mechanical Force to Potentiate Target Cell Killing, Cell 165(1) (2016) 100-110.

[17] A. de la Zerda, M.J. Kratochvil, N.A. Suhar, S.C. Heilshorn, Review: Bioengineering strategies to probe T cell mechanobiology, APL Bioeng. 2(2) (2018) 021501.

[18] J.W. Hickey, Y. Dong, J.W. Chung, S.F. Salathe, H.C. Pruitt, X. Li, C. Chang, A.K. Fraser, C.A. Bessell, A.J. Ewald, S. Gerecht, H.Q. Mao, J.P. Schneck, Engineering an Artificial T-Cell Stimulating Matrix for Immunotherapy, Adv. Mater. 31(23) (2019) e1807359.

[19] A. Wahl, C. Dinet, P. Dillard, A. Nassereddine, P.H. Puech, L. Limozin, K. Sengupta, Biphasic mechanosensitivity of T cell receptor-mediated spreading of lymphocytes, Proc. Natl. Acad. Sci. U. S. A. 116(13) (2019) 5908-5913.

[20] M. Saitakis, S. Dogniaux, C. Goudot, N. Bufi, S. Asnacios, M. Maurin, C. Randriamampita, A. Asnacios, C. Hivroz, Different TCR-induced T lymphocyte responses are potentiated by stiffness with variable sensitivity, eLife 6 (2017).

[21] M. Raab, H. Wang, Y. Lu, X. Smith, Z. Wu, K. Strebhardt, J.E. Ladbury, C.E. Rudd, T cell receptor "inside-out" pathway via signaling module SKAP1-RapL regulates T cell motility and interactions in lymph nodes, Immunity 32(4) (2010) 541-56.

[22] B.L. Walling, M. Kim, LFA-1 in T Cell Migration and Differentiation, Front. Immunol. 9 (2018) 952.

[23] D.J. Irvine, J. Doh, B. Huang, Patterned surfaces as tools to study ligand recognition and synapse formation by T cells, Curr. Opin. Immunol. 19(4) (2007) 463-9.

[24] M.J. Rosenbluth, W.A. Lam, D.A. Fletcher, Force microscopy of nonadherent cells: a comparison of leukemia cell deformability, Biophys. J. 90(8) (2006) 2994-3003.

[25] A. Farrukh, J.I. Paez, M. Salierno, A. del Campo, Bioconjugating Thiols to Poly(acrylamide) Gels for Cell Culture Using Methylsulfonyl Co-monomers, Angew. Chem., Int. Ed. Engl. 55(6) (2016) 2092-6.

[26] W.A. Comrie, A. Babich, J.K. Burkhardt, F-actin flow drives affinity maturation and spatial organization of LFA-1 at the immunological synapse, J Cell Biol 208(4) (2015) 475-91.

[27] H. Wang, T.A. Kadlecek, B.B. Au-Yeung, H.E. Goodfellow, L.Y. Hsu, T.S. Freedman, A. Weiss, ZAP-70: an essential kinase in T-cell signaling, Cold Spring

Harbor Perspect. Biol. 2(5) (2010) a002279.

[28] M.L. Dustin, The immunological synapse, Cancer Immunol. Res. 2(11) (2014) 1023-33.

[29] K.I. Jankowska, E.K. Williamson, N.H. Roy, D. Blumenthal, V. Chandra, T. Baumgart, J.K. Burkhardt, integrins Modulate T cell receptor signaling by constraining actin Flow at the immunological synapse, Front. Immunol. 9(25) (2018).

[30] K.L. Hui, Balagopalan, L.L.E. Samelson, A. Upadhyaya, Cytoskeletal forces during signaling activation in Jurkat T-cells, Mol. Biol. Cell 26(4) (2015) 685-95.

[31] K. Lee, A.D. Holdorf, M.L. Dustin, A.C. Chan, P.M. Allen, A.S. Shaw, T cell receptor signaling precedes immunological synapse formation, Science 295(5559) (2002).

[32] A. Hashimoto-Tane, T. Saito, Dynamic Regulation of TCR-Microclusters and the Microsynapse for T Cell Activation, Front. Immunol. 7 (2016) 255.

[33] V. Das, B. Nal, A. Dujeancourt, M. Thoulouze, T. Galli, P. Roux, A. Dautry-Varsat, A. Alcover, Activation-Induced Polarized Recycling Targets T Cell Antigen Receptors to the Immunological Synapse: Involvement of SNARE Complexes, Immunity 20(5) (2004).

[34] M.B.M. Meddens, S.F.B. Mennens, F.B. Celikkol, J. Te Riet, J.S. Kanger, B. Joosten, J.J. Witsenburg, R. Brock, C.G. Figdor, A. Cambi, Biophysical Characterization of CD6-TCR/CD3 Interplay in T Cells, Front. Immunol. 9 (2018) 2333.

[35] J.W. Hickey, F.P. Vicente, G.P. Howard, H.Q. Mao, J.P. Schneck, Biologically Inspired Design of Nanoparticle Artificial Antigen-Presenting Cells for Immunomodulation, Nano Lett. 17(11) (2017) 7045-7054.

Chapter 5

5 Conclusion and outlook

In this PhD thesis novel, APC ligands-patterned hydrogels have been developed and applied to study how the mechanical engagements of T cell ligands contribute to the early T cell signaling in Jurkat T-cell. The patterned APC ligands (anti-CD3 and/or ICAM-1) on PAAm hydrogels (1, 12, and 50 kPa) at defined geometries and densities were fabricated by an automated microcontact printing system. The early response of T cells was studied on the anti-CD3 and anti-CD3/ICAM-1 patterned hydrogels.

The following are the major conclusions of this work:

1) A robust experimental protocol for independent control of substrate stiffness, APC ligands spatial arrangement, ligand type and density was successfully developed. This biomaterial model enables accurate experimentation to decipher the causal relationships between substrate stiffness and T cell early signaling.

2) Anti-CD3 patterned hydrogels with defined IS area and similar ligand density provided a conclusive evaluation of receptor-specific T cell responses to APC mechanics. This platform demonstrates that CD3 mediated early T cell activation, in terms of ZAP70 phosphorylation, can be elevated by increasing substrate stiffness. These results confirm that T cell activation induced through TCR/CD3 complex is mechanosensitive, even without the engagement of the integrin (ICAM-1).

3) On anti-CD3/ICAM-1 patterned hydrogels, Jurkat T-cell exhibited a stiffness-regulated activation response. On the one hand, TCR accumulation

154

/clustering was potentiated by stiff substrates in the presence of ICAM-1 engagement. On the other hand, T cell activation, as measured by ZAP70 phosphorylation, behaved differently on substrates with different stiffness depending on the time scale at which they were measured. At 10 min after seeding cell, ZAP70 phosphorylation level increased with substrate stiffness. At 20 min however, ZAP70 phosphorylation level increased with substrate stiffness on soft substrates (1 kPa to 12 kPa) but declined on stiffer ones (50 kPa). This suggests the mechanosensitivity of Jurkat T-cell may be also time-dependent during the early T cell activation as measured by ZAP70 phosphorylation level on anti-CD3/ICAM-1 patterned hydrogel surface.

4) ICAM-1 engagement has different effects on T cell signaling depending on the stiffness of the hydrogel, which suggests the mechanosensitivity of Jurakt T-cell can be tightly regulated by integrin engagement.

The methodology presented in this work provides a valuable methodological contribution to the immunobiology community studying T cell mechanotranduction. Work remains to be done to exploit the full potential of this platform, both in aspects of biological application and platform development. Studies with primary T cell such as CD8^{+} should be carried out to validate this model for primary cells.

In the near future, more advanced platforms that can be used to better mimic a real T cell-APC interaction will be developed. To this end, the concentric patterning of more APC ligands, which includes anti-CD3, anti-CD28, ICAM-1 and maybe other ligands, will be established on hydrogel surface by a multistep printing technique based on our microcontact printing system. These advanced platforms will finally provide a comprehensive understanding of the complicated and tangled molecular interactions between T cells and APCs.

List of scientific contributions

Articles

1) Cell-Cell-like interfaces: synthetic hydrogels as APC mimics for study of T cell mechanotransduction.

Jingnan Zhang, Renping Zhao, Bin Li, Aleeza Farrukh, Markus Hoth, Bin Qu, Aránzazu del Campo* (*Under review*)

2) Engineered T cell ligands arrays on hydrogel as artificial antigen presenting cells to study TCR-mediated mechanotransduction.

Jingnan Zhang, Renping Zhao, Bin Li, Markus Hoth, Bin Qu, Aránzazu del Campo* (*Manuscript completed, to be submitted*)

3) Surface micropatterning of hydrogels by a pneumatically-controlled microcontact printer：applications to T cell mechanotransduction studies.

Jingnan Zhang, Aránzazu del Campo* (*Manuscript completed, to be submitted*)

4) Optoregulated force application to individual cellular receptors using molecular motors.

Yijun Zheng, Mitchell Han, Renping Zhao, Johanna Blass, **Jingnan Zhang**, Jean-Rémy Colard-Itté, Damien Dattler, Markus Hoth, Andrés J. García, Nicolas Giuseppone, Roland Bennewitz, Bin Qu, Aránzazu del Campo* (*Manuscript completed, to be submitted*)

Conference and seminar

1) Engineered antigen-presenting interfaces: model platforms for studies of T cell mechanotransduction. SFB1027 Summer Camp, Jun 17-19. 2019, Annweiler am Trifels, Germany (Talk)

2) Cell-cell like interface. INM Colloquium Biointerfaces, March 26. 2019, INM–

Leibniz Institute for New Materials, Saarbrücken, Germany (Talk)

3) Stiffness to modulate the early T cell signaling through micropatterned TCR/CD3 and LFA-1 ligands. SFB Summer Camp 2018, Jun 26-29. 2018, Ebernburg, Germany (Talk)

4) Hydrogels mimicking antigen presenting cells: new platforms to study T lymphocyte activation. Bioinspired and Biomimetic Hydrogels, April 15-18. 2018, Bergisch-Gladbach, Germany (Poster presentation)

5) A Platform to study the role of forces in T lymphocyte activation. Febs-international summer school on immunology, Sep 23-30. 2017, Hvar, Croatia (Poster presentation)

6) A platform to study the mechanosensitivity of different receptors in early T cell activation. SFB1027 Summer Camp, Jun 07-09. 2017, Pforzheim, Germany (Talk)

7) A platform to study the role of forces in T lymphocyte activation. Cell Physics 2017, October 11-13. 2017, Saarbrüken, Germany (Poster presentation)

8) Model platforms for studying mechanical factors involved in T cell activation. Cellular Dynamics, Sept 04-07. 2016, Bad Honnef, Germany (Poster presentation)

9) Model platforms for studying mechanical factors involved in T cell activation. Cell Physics 2016, June 22-24. 2016, Saarbrüken, Germany (Poster presentation)

(Collected credit points: 30)

Curriculum Vitae
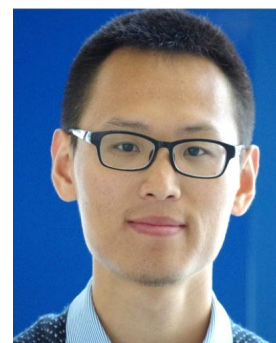
Jingnan Zhang

PERSONAL PROFILE

Nationality: Chinese (Linyi, Shandong) Birth Date: 13/08/1989

E-mail: jingnan.zhang@leibniz-inm.de; willzjn@hotmail.com

Tel: +49 17628360015; +86 17660561068

Address: INM-Leibniz Institute for New Materials, Campus D22, 66123 Saarbrücken, Germany

Supervisor: Prof. Aránzazu del Campo Bécares: INM-Leibniz Institute for New Materials

RESEARCH FOCUS

Immune Cell Mechanobiology; Micropatterned Hydrogels;

Engineered Cellular Microenvironment; Biomaterials for Cancer Research

WORKING & EDUCATIONAL BACKGROUND

► Dynamic Biomaterials, INM-Leibniz Institute for New Materials, Germany (PhD student, Jan. 2016 to Dec. 2019)

Thesis title: Engineered antigen-presenting hydrogels: model platforms for studies of T cell mechanotransduction

► Institute of Biomedicine and Biotechnology, Chinese Academy of Sciences, Shenzhen (RA, Jul. 2014 to Dec. 2015)

Research project: Smart biomaterial for theranostic studies including multimodal imaging, diagnosis, and targeted therapy

► Department of Chemistry, Jinan University (Master in Biochemistry & Molecular Biology, Sep. 2011 to Jun. 2014)

Thesis title: The synthesis of multifunctional selenium nanoparticle and its potential use as an inhibitor in Alzheimer's disease

RESEARCH EXPERIENCE

► As PhD student in INM-Leibniz Institute for New Materials, Saarbrücken, Germany (Jan. 2016 to Dec.2019)

Research summary: Application of different micropatterning techniques, either by microcontact printing (with automatic microcontact printer) of different proteins on hydrogel surface or by photochemical activation of molecules at hydrogel surface through photomask or scanning laser, to spatially control cell behaviors (attachment, spreading, migration, activation) on micropatterned substrates. The micropatterned substrates (with varying mechanical properties) could be further used as artificial antigen presenting cells to study how mechanical engagement of receptors regulate the early T cell signaling events.

► Cardiac Development and Remodelling, Max Planck Institute for Heart and Lung Research (Sep. 2017)

Research project: Substrate rigidities influence muscle stem cell quiescence and differentiation

► Dynamic Biointerface, Max Planck Institute for Polymer Research, Germany (Oct. 2016)

Research training: Photolithography based on SU-8 photoresist and surface micropatterning by microcontact printing

► As research assistant in Chinese Academy of Sciences, Shenzhen, China (Jul. 2014 to Dec. 2015)

Project 1: Human H-ferritin based nanoprobes crossing BBB for multimodal imaging-guided therapy of brain tumor

Project 2: Smart indocyanine green-based biomaterial for dual-modal imaging-guided

phototherapy of breast cancer

► As master student in Jinan University, Guangzhou, China (Sep. 2011 to Jun. 2014)

Project 1: Ruthenium complexes inhibit bFGF-mediated angiogenesis and target G-quadruplex of telomere and bcl-2 for cancer therapy

Project 2: Inhibition of amyloid-β peptide aggregation by functionalized selenium nanoparticles

HONORS＆AWARDS＆CERTIFICATES

Certificate for been chosen in a competition among young scientists worldwide for participation in 19th international summer school on Immunology (2017)

Certificate for the "Histology Crash Course" in IMB Mainz (2017)

Certificate for the "Modern Laser-Microscopy in Cellbiology" course training in Saarbrüken (2016)

Excellent Postgraduate Dissertation of Jinan University (2014)

Chinese National Scholarship for Postgraduate (2013)

Excellent Graduate Cadre of Jinan University (The First Prize) (2012)